WHZ Westsächsische Hochschule Zwickau
University of Applied Sciences

# Influence of hydrothermal treatment on the expansion behaviour of PLGA-Mineral filler mixtures foamed with supercritical $CO_2$


Marco Pelaez

Student Number: 48652

FACULTY OF PHYSICAL ENGINEERING/COMPUTER SCIENCES


Submitted in Fulfilment of the Requirements for the Degree of

Master of Science

(Advance green engineering and sustainable management)

31 January 2026

| | |
|---|---|
| **1st Examiner:** | Prof. Dr. Stefan Zigan |
| **2nd Examiner:** | Prof. Dr. Philip Kitschke |
| **Industry Supervisor:** | Prof. Dr. Pablo García Triñanes |

This work would never have been possible without the support of Carlos, Jesus Santiago, and David. Thank you for making this reality; this thesis is dedicated to you for trusting me and giving me the opportunity to prove myself far from home. Gentlemen, you have my eternal gratitude.

I also dedicate this to my mother Gloria, my father Manny, and my siblings Ricardo and Giovanna, for their unconditional support. And to you, Allisson, a special mention for being the witness to this process day after day.

**Abstract**

The growing demand for sustainable and biodegradable materials for biomedical and environmental applications have driven significant research into polymer foams. This study investigates the impact of hydrothermal pretreatment on the expansion behaviour of poly(D,L-lactide-co-glycolide) (PLGA, 75:25) composites foamed using supercritical carbon dioxide ($scCO_2$) with the addition of three mineral fillers Wollastonite, Rice husk ash and Bentonite at concentrations of 25 and 33.3 wt.%.

PLGA composites underwent two processing routes: direct foaming and hydrothermal pretreatment followed by foaming. The expansion efficiency, pore morphology, and structural stability were systematically evaluated through volumetric analysis and scanning electron microscopy.

Results indicated a notable improvement in foam expansion and pore uniformity for composites subjected to hydrothermal treatment + foaming, particularly with wollastonite and bentonite as additives. Hydrothermal pretreatment facilitated $CO_2$ diffusion and enhanced nucleation, generating more uniform and interconnected porous structures. However, samples containing rice husk ash exhibited variable responses, achieving the highest overall expansion factor without HT pretreatment, suggesting complex filler-polymer interactions.

This study demonstrates that hydrothermal pretreatment, combined with carefully selected mineral additives, significantly influences the structural and expansion characteristics of PLGA foams. These findings advance the design and fabrication of biodegradable porous materials with tailored properties for targeted biomedical and environmental applications.

**Keywords:**

PLGA foams, Supercritical $CO_2$ foaming, Hydrothermal treatment, Biodegradable composites, Mineral fillers (Wollastonite, RHA, Bentonite)

# TABLE OF CONTENTS

## TABLE OF FIGURES

## TABLE INDEX

# 1 CHAPTER ONE

## 1.1 Introduction

The growing demand for sustainable materials has driven the development of biodegradable polymers as viable alternatives to conventional petroleum-based plastics (Álvarez et al., 2020). Derived from renewable feedstocks, these polymers offer essential properties such as biocompatibility and biodegradability, making them highly suitable for biomedical applications, including tissue engineering scaffolds, drug delivery systems, and implantable devices (Valor et al., 2021).

Despite these advantages, the practical use of biodegradable polymers often requires precise control of their microstructural features, like, porosity, interconnectivity, and mechanical integrity. High porosity enables cell migration and proliferation within scaffolds, which is essential for new tissue formation. Furthermore, interconnected pores facilitate the diffusion of nutrients, oxygen, and metabolic waste, sustaining cell viability. However, excessive porosity can reduce mechanical strength, while insufficient interconnectivity limits biological performance. Therefore, achieving an optimal balance between these parameters is critical for biomedical applications (Mukasheva et al., 2024). Unfortunately, conventional fabrication techniques such as solvent casting or phase separation typically involve toxic organic solvents and often yield non-uniform pore architectures (Carrascosa et al., 2024).

Supercritical carbon dioxide ($scCO_2$) foaming has emerged as a promising, solvent-free alternative to produce porous polymeric structures. Under supercritical conditions, $CO_2$ acts as a plasticising agent, diffusing into the polymer matrix and lowering its glass transition temperature. Upon depressurisation, the system becomes thermodynamically unstable, triggering nucleation and bubble growth that led to pore formation (Liao et al., 2012; Tai et al., 2010). However, controlling pore morphology and achieving uniform structures remains challenging due to the complex physicochemical interactions governing $CO_2$ diffusion, nucleation, and bubble growth (Zhou et al., 2024).

To overcome these limitations, hydrothermal pretreatment (HT) has been proposed as a pre-foaming strategy to modify the polymer's microstructure. This method, which exposes polymers to heated water under moderate pressure, can promote chain mobility, local plasticisation, or mild hydrolysis, thereby improving gas diffusion and bubble nucleation. Studies on semicrystalline biopolymers such as polycaprolactone (PCL) and polybutylene succinate (PBS) have shown that HT enhances porosity and pore connectivity (García-Jarana et al., 2025). However, its effects on amorphous copolymers such as PLGA, especially when combined with inorganic fillers that may act as nucleating and reinforcing agents, remain underexplored.

The present study addresses this gap by investigating the influence of hydrothermal pretreatment on the foaming behaviour of PLGA 75:25 composites containing three mineral additives: Wollastonite (WLS), Rice Husk Ash (RHA), and Bentonite (BT). It compares two processing routes, direct foaming (F) and hydrothermal pretreatment followed by foaming (HT+F),

using volumetric measurements, scanning electron microscopy (SEM to analyse expansion behaviour and microstructural evolution. By advancing solvent-free and structurally optimised fabrication strategies, this work contributes to the development of biodegradable porous materials for biomedical and environmental applications.

## 1.2 Current state of knowledge and research goals

The development of porous scaffolds for biomedical applications, particularly tissue engineering and orthopaedics, relies heavily on biodegradable polymers such as poly(lactic-co-glycolic acid) (PLGA). This is widely recognised for its biocompatibility, adaptative biodegradability, and extensive use in medical devices (Nifant'ev et al., 2024). Among fabrication techniques, $scCO_2$ foaming has gained attention as an efficient, environmentally friendly process that eliminates the need for toxic organic solvents (Carrascosa et al., 2024). During foaming, $scCO_2$ diffuses into the polymer matrix and lowers its glass transition temperature ($T_g$). Rapid depressurisation then creates thermodynamic instability, causing bubble nucleation and pore formation. Parameters such as saturation pressure, temperature, and depressurisation rate determine pore size, distribution, and interconnectivity (Tai et al., 2010).

Although $scCO_2$ foaming provides a clean and controllable processing route, achieving precise control of pore morphology and interconnectivity remains difficult. Cellular architecture strongly influences nutrient transport, mechanical properties, and biological performance in scaffolds (Mathieu et al., 2005). To address these challenges, mineral fillers such as hydroxyapatite (HAp) and magnesium hydroxide [$Mg(OH)_2$] are frequently incorporated into polymer matrixes to act as heterogeneous nucleation sites and mechanical reinforcements. These fillers improve cell structure uniformity and strength, with compressive properties comparable to trabecular bone (Carrascosa et al., 2024). Moreover, they can modify $CO_2$ diffusion pathways and influence expansion behaviour.

The combined effects of hydrothermal pretreatment and supercritical $CO_2$ foaming on PLGA, particularly in the presence of inorganic mineral fillers, have not been systematically investigated. This represents a crucial research goal, as the interplay between polymer hydration, filler-induced nucleation, and $CO_2$ diffusion could critically determine foam morphology and stability. A detailed understanding of these mechanisms is essential to optimise solvent-free, reproducible scaffold fabrication methods capable of achieving targeted mechanical and morphological properties for advanced biomedical applications (Carrascosa et al., 2024).

The primary aim of this study is to investigate the influence of hydrothermal pretreatment on the expansion behaviour, pore morphology, and structural integrity of PLGA 75:25 composites foamed with supercritical $CO_2$ in combination with mineral fillers.

**Specific objectives are:**

1. To evaluate the effect of hydrothermal pretreatment on the expansion factor and pore morphology of PLGA-based foams.

2. To compare the influence of three mineral fillers (wollastonite, rice husk ash, and bentonite) at two loadings (25 wt.% and 33.3 wt.%) on foaming behaviour.
3. To characterise the resulting microstructures using SEM.

## 1.3 Research hypothesis and questions

Hypothesis:
Hydrothermal pretreatment modifies the molecular and microstructural characteristics of PLGA, enhancing $CO_2$ solubility and nucleation efficiency during foaming. This leads to improved expansion and more uniform pore architectures. The extent of these improvements depends on the type and concentration of the mineral filler.

Research Questions:

1. How does hydrothermal pretreatment affect the foaming efficiency and pore morphology of PLGA composites?
2. What roles do different mineral fillers play in controlling expansion and pore uniformity?
3. Does the combination of HT with specific fillers yield synergistic improvements in foam structure?

## 1.4 Thesis Structure

This thesis is structured into six chapters**. Chapter 1** introduces the research background, current state of knowledge, aims, and hypothesis. **Chapter 2** presents a detailed literature review on biodegradable polymers, hydrothermal treatment, and supercritical $CO_2$ foaming mechanisms, with emphasis on the role of mineral fillers. **Chapter 3** describes the materials, sample preparation procedures, and experimental methods used for hydrothermal and foaming treatments. **Chapter 4** reports the experimental results, discusses these findings in the context of existing literature and proposes possible interpretations. Finally, **Chapter 5** summarizes the main conclusions and provides recommendations for future research.

# 2 THEORETICAL FRAMEWORK

## 2.1 Biodegradable polymers and PLGA systems

### 2.1.1 Overview of Biodegradable Polymers

The growing interest in biodegradable polymer systems is driven by global environmental concerns and the increasing demands of biomedical engineering, particularly for materials intended for temporary implantation. Biodegradable materials are defined as those capable of degrading naturally through enzymatic or non-enzymatic processes, producing biocompatible and non-toxic by-products that are subsequently eliminated by the body (Makadia & Siegel, 2011). These materials are commonly classified according to their origin (Nifant'ev et al., 2024). Natural biodegradable polymers include polysaccharides such as cellulose, starch, alginate, chitosan, and hyaluronic acid, as well as proteins like collagen, while synthetic biodegradable

polymers predominantly consist of aliphatic polyesters and polycarbonates, particularly α-hydroxy acid-based polymers such as polylactic acid (PLA), polyglycolic acid (PGA), and their copolymers (Anderson & Shive, 1997; Makadia & Siegel, 2011)

The biodegradability of synthetic polyesters is governed primarily by hydrolytic degradation of the polymer backbone, involving the non-enzymatic cleavage of ester linkages, which progressively reduces molecular weight through the formation of oligomers and ultimately monomers (García-Jarana et al., 2025; Makadia & Siegel, 2011). In biologically inert polymers such as PLGA, hydrolysis constitutes the dominant degradation mechanism. The rate of this process is strongly influenced by polymer chemistry, including the presence of hydrolytically labile functional groups such as esters, amides, anhydrides, and carbonates, as well as morphological factors like crystallinity and hydrophilicity (García-Jarana et al., 2025). In bulk-degrading systems, the accumulation of carboxylic acid end groups further accelerates degradation through autocatalytic effects (Makadia & Siegel, 2011).

Importantly, the hydrolytic degradation behaviour of aliphatic polyesters is frequently quantified using degradation half-times, defined as the time required for a material to lose approximately 50% of its initial molecular weight or mass. Experimental studies have demonstrated that these half-times vary widely depending on polymer composition and hydrophilicity. For instance, PGA exhibits relatively short degradation half-times, typically ranging from weeks to a few months, whereas PLA degrades more slowly, with reported half-times extending from several months to over one year due to its higher hydrophobicity and crystallinity (Anderson & Shive, 1997; Makadia & Siegel, 2011). Early in-vivo investigations further reported degradation half-lives of approximately 5 months for PGA and around 6 months for PLA, highlighting the slower resorption behaviour of lactide-rich systems (Heller et al., 2000).

From an environmental perspective, the development of biodegradable polymers is strongly motivated by the need to mitigate waste accumulation and sustainability challenges associated with conventional petroleum-based plastics (de Macedo Rooweder Lima, 2024; Nifant'ev et al., 2024). Increasing emphasis is placed on materials derived from renewable feedstocks, aligning polymer production with the principles of the green economy and responsible lifecycle management. By degrading into metabolizable products, biodegradable polymers significantly reduce the persistence of environmental pollutants, offering lower-impact alternatives for a wide range of applications (de Macedo Rooweder Lima, 2024).

Among synthetic biodegradable polyesters, poly(lactic-co-glycolic acid) (PLGA) stands out as one of the most extensively characterized and widely utilized biomaterials (Makadia & Siegel, 2011). As a copolymer of lactic acid (LA) and glycolic acid (GA), PLGA is typically amorphous and has achieved widespread adoption due to its well-established biocompatibility and approval by the U.S. Food and Drug Administration (FDA) (Carrascosa et al., 2024; Makadia & Siegel, 2011). A major advantage of PLGA lies in its highly tuneable degradation kinetics, which are primarily governed by the LA:GA ratio. Increasing the hydrophilic glycolide content generally accelerates degradation, with PLGA 50:50 exhibiting the fastest degradation among PLGA compositions, characterized by half-times ranging from approximately one week to one month. Conversely,

increasing the lactic acid fraction progressively extends degradation into the range of several months (Makadia & Siegel, 2011). These quantitative differences in degradation half-times are critical for biomedical design, as they enable precise temporal matching between material resorption and tissue healing or controlled drug release requirements. The glass transition temperature ($T_g$) of PLGA is typically above physiological temperature *(≈37°C*), maintaining a glassy structure that evolves as hydrolysis proceeds and molecular weight decreases (Makadia & Siegel, 2011).

Other aliphatic polyesters, such as polycaprolactone (PCL), exhibit significantly slower degradation kinetics due to their semi-crystalline nature, rendering them suitable for long-term implants and sustained drug delivery systems requiring stability over several months or even years (García-Jarana et al., 2025; Wang et al., 2024). PCL is characterized by a low melting temperature (*329K-334K*) and a glass transition temperature around *213K* (García-Jarana et al., 2025). In contrast, while PLA offers high intrinsic biocompatibility and excellent thermal processability, its inherent hydrophobicity and relatively slow degradation rate may limit its applicability in scenarios requiring rapid scaffold resorption. The combined use of PLGA, PLA, PCL, and other biodegradable polyesters such as polyhydroxybutyrate (PHB) enables the design of composite systems with tailored mechanical properties and degradation profiles suited to diverse biomedical applications (Nifant'ev et al., 2024).

Overall, the principal advantages of biodegradable polymer systems in biomedical applications stem from their proven biocompatibility, safety, and functional versatility. Their degradation kinetics and mechanical properties can be precisely controlled through molecular architecture and compositional design, allowing structural support and resorption timelines to be matched with tissue regeneration processes (Makadia & Siegel, 2011). In parallel, their adoption contributes to a reduced environmental footprint, positioning biodegradable polymers as key materials in future sustainable healthcare and manufacturing strategies (Nifant'ev et al., 2024).

### 2.1.2 Chemistry and Structure of PLGA

The architecture of PLGA forms the foundation of its utility in biomedical applications, particularly as a scaffold and drug delivery vehicle approved by the FDA (Makadia & Siegel, 2011). Chemically, PLGA is a synthetic aliphatic polyester synthesized primarily through the ring-opening polymerization (ROP) of its corresponding cyclic diesters, glycolide (GL) and lactides (LA), derived from glycolic acid (GA) and lactic acid (LA) monomers (Nifant'ev et al., 2024). The resulting copolymer features random copolymer architecture linked predominantly by ester linkages within the backbone (Figure 1). This ester structure is crucial, as the primary degradation mechanism of PLGA in biological or aqueous environments is non-enzymatic hydrolysis of these bonds, yielding biocompatible monomers (lactic and glycolic acids) that are subsequently metabolized by the body (Makadia & Siegel, 2011).

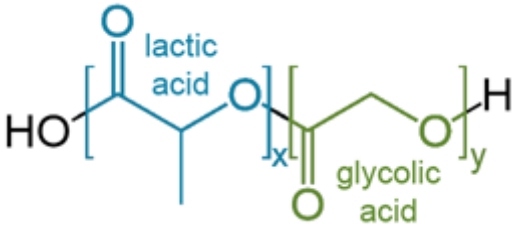


Figure 1. PLGA structure (Nifant'ev et al., 2024)

The lactic to glycolic (L:G) ratio is the primary structural determinant controlling the degradation rate and subsequent material properties of PLGA (Makadia & Siegel, 2011; Nifant'ev et al., 2024). Glycolide units are inherently more hydrophilic due to the absence of the methyl side group found in lactide units (Makadia & Siegel, 2011). Consequently, increasing the percentage of the more reactive and hydrophilic glycolate (G) comonomer unit accelerates the rate of hydration and subsequent hydrolytic degradation (Makadia & Siegel, 2011; Nifant'ev et al., 2024). A significant finding in polymer science is that PLGA 50:50 (equimolar LA:GA) typically exhibits the fastest degradation kinetics. Degradation proceeds via an autocatalytic process, wherein the carboxylic acid end groups generated during hydrolysis lower the local pH within the polymer matrix, further enhancing the rate of ester bond cleavage (Makadia & Siegel, 2011).

This ratio profoundly influences the polymer's phase characteristics, primarily dictating its glass transition temperature ($T_g$) and overall crystallinity. PLGA is classified as amorphous when the glycolate content falls within the (25-75)% mol range. Generally, increasing the content of GA tends to decrease the $T_g$ of the resulting copolymer. Since the $T_g$ of most PLGA compositions lies above physiological temperature (*37°C*), the material exists in a glassy and rigid state (Makadia & Siegel, 2011). Degradation preferentially targets the looser, more penetrable amorphous regions first, leading to initial chain scission. This process initially enhances polymer chain mobility as molecular weight is lost, temporarily causing the remaining segments to reorganize into more ordered, crystalline domains, highlighting the direct link between chemical composition and structural mobility (Anderson & Shive, 1997). This phenomenon is best explained by the mechanisms described in Figure 2.

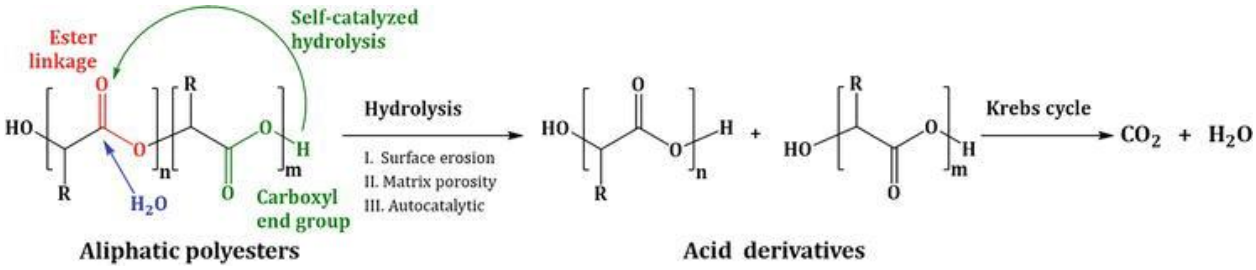


Figure 2. Hydrolytic degradation of aliphatic polyesters (Kreua-ongarjnukool et al., 2021).

The molecular weight ($M_\omega$) and molecular weight distribution (MWD) are equally critical in defining the polymer's mechanical performance, thermal behaviour, and degradation kinetics. Polymers with higher $M_\omega$ possess longer chains, leading to higher mechanical strength and, typically, slower initial degradation rates because more ester linkages must be cleaved for the polymer to solubilize. Furthermore, $T_g$ exhibits a direct dependence on $M_\omega$, declining as the chains

shorten (Makadia & Siegel, 2011). The degradation process follows a biphasic pattern: an initial stage of rapid $M_\omega$ loss via random chain scission (due to internal hydrolysis) with no appreciable mass loss, followed by a slower stage characterized by bulk erosion and substantial mass loss (Makadia & Siegel, 2011; Pakeyangkoon et al., 2009). A wider MWD exacerbates this effect, introducing a greater number of chains ends that function as acidic catalysts, thereby accelerating the onset of autocatalytic degradation (Anderson & Shive, 1997).

The relationship between $T_g$ and polymer chain mobility is paramount, especially when considering melt processing or $scCO_2$ application. In its native state, PLGA maintains structural integrity at physiological temperatures because the glassy state severely restricts macromolecular chain motion (Makadia & Siegel, 2011). However, operating temperatures during manufacturing (e.g., melt moulding or extrusion) must often exceed the $T_g$, entering the rubbery state where mobility is high. This high mobility dramatically increases the susceptibility to thermal degradation ($T_g$) during melt processing, causing irreversible chain scission and $M_\omega$ reduction (Tai et al., 2010). Such molecular weight loss directly compromises the final mechanical integrity and alters the planned degradation kinetics.

The amorphous character of PLGA 75:25 (LA:GA) is particularly salient for processing via $scCO_2$ foaming. This ratio falls within the widely accepted range for amorphous (25-75)% mol GL and features a reported ambient $T_g$ of approximately *43°C* (Valor et al., 2021). The presence of carbonyl groups in the polyester structure promotes a strong Lewis acid-base interaction with the electron-deficient carbon atom of $CO_2$ (Tai et al., 2010). This strong affinity leads to enhanced $CO_2$ solubility and gas plasticisation. This plasticization drastically lowers the polymer's $T_g$ and significantly increases chain mobility and free volume, reducing the melt viscosity and surface tension (Liao et al., 2012).

For $scCO_2$ foaming applications, the amorphous, highly plasticizable nature of PLGA 75:25 is critical, as the material readily accepts large concentrations of $CO_2$. This enhanced plasticization allows processing at milder temperatures, which is advantageous for incorporating temperature-sensitive bioactive molecules (Tai et al., 2010). However, this high susceptibility also dictates the foaming behaviour and limits process control: during the rapid depressurization stage, the material transitions quickly from a highly mobile, rubbery state back to its glassy, rigid state (vitrification). Achieving a durable and stable cellular foam architecture relies entirely on the successful and uniform occurrence of this rapid vitrification, preventing destructive phenomena such as bubble collapse or coalescence before the cellular structure is mechanically stabilized (Makadia & Siegel, 2011).

However, this amorphous character presents a specific paradox in supercritical fluid applications. While the amorphous nature of PLGA facilitates homogeneous $CO_2$ dissolution due to accessible free volume, it simultaneously limits foam stability. The absence of crystalline domains, which typically mechanically stabilize expanding cells, makes the structure prone to collapse during the rubbery-to-glassy transition, necessitating precise control strategies.

### 2.1.3 Degradation Mechanisms and Kinetics

The overall performance and biological longevity of PLGA implants are governed by their degradation characteristics, primarily through a hydrolytic mechanism. This is predominantly a non-enzymatic process, whereby water penetration initiates the cleavage of the polymer's ester linkages (Anderson & Shive, 1997; Makadia & Siegel, 2011). Hydrolysis proceeds via random chain scission, resulting in the progressive formation of lactic acid and glycolic acid monomers and oligomers. In most physiological environments, including neutral or mildly acidic media. PLGA undergoes bulk degradation as its shown in Figure 3, this phenomenon is defined by the rate of water diffusion into the matrix significantly outpacing the rate of polymer mass loss or erosion from the surface (Makadia & Siegel, 2011; Mathieu et al., 2005).

The kinetics of this bulk erosion are dramatically accelerated by autocatalysis, a process intrinsic to the degradation of these polyesters. As ester bonds are cleaved, free carboxylic acid end groups are generated. Because these acidic oligomers are initially physically confined within the polymer matrix, they lower the local pH (Makadia & Siegel, 2011; Mathieu et al., 2005). This localized acidic microclimate effectively catalyses further ester bond hydrolysis in the polymer's interior, leading to a faster degradation rate in the core compared to the surface, particularly evident in larger devices (Anderson & Shive, 1997; Mathieu et al., 2005). This buildup of acidic products also generates osmotic pressure, which draws more water into the structure and promotes swelling and subsequent morphological failure (Makadia & Siegel, 2011; Mathieu et al., 2005).

The rate of degradation is fundamentally tuned by the polymer's chemical composition, specifically the ratio of LA to GA units. GA units lack the hydrophobic methyl side group present in LA units, rendering them more hydrophilic and more susceptible to hydrolytic attack (Anderson & Shive, 1997). Consequently, increasing the glycolide content generally accelerates water uptake and ester bond cleavage, leading to faster biodegradation kinetics (Anderson & Shive, 1997; Makadia & Siegel, 2011; Tai et al., 2010). This compositional effect is reflected quantitatively in the degradation half-times reported for PLGA systems. Experimental studies indicate that PLGA 50:50 exhibits the shortest degradation half-times, typically on the order of one week to approximately one month, making it suitable for applications requiring rapid resorption, such as short-term drug delivery or temporary scaffolding (Anderson & Shive, 1997; Makadia & Siegel, 2011).

However, this relationship is non-linear, as copolymers with either higher lactide or higher glycolide contents degrade more slowly than the equimolar composition. Lactide-rich formulations, such as PLGA 85:15, display significantly extended degradation half-times, commonly ranging from several months, due to increased hydrophobicity, reduced water diffusion, and higher glass transition temperatures that limit chain mobility (Anderson & Shive, 1997; Makadia & Siegel, 2011). As a result, these compositions are better suited for applications requiring prolonged structural integrity or sustained release profiles. Overall, the dependence of degradation half-times on the LA:GA ratio provides a quantitative framework for tailoring PLGA degradation kinetics to match specific biomedical time scales.

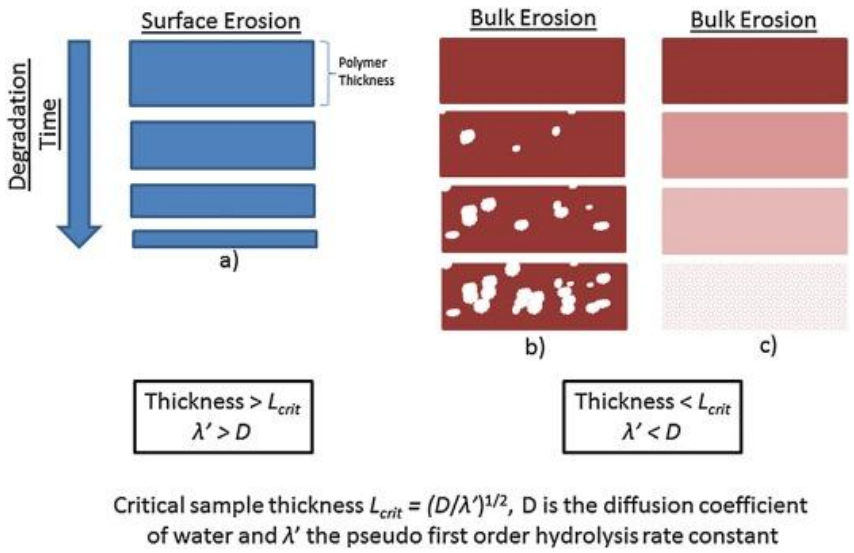


Figure 3. Schematic illustration of three types of erosion phenomena: (a) surface erosion with a growing hydrolysis front, (b) bulk erosion with autocatalysis due to retained degradation products (e.g. PLA), (c) bulk erosion without autocatalysis (e.g. PLA-co-PCL) where water diffusion and catalyst are faster than the reaction rate. $L_{crit}$ is the critical sample thickness, $\lambda'$ is the pseudo first order rate of hydrolysis and $D$ is the diffusion coefficient (Nifant'ev et al., 2024).

Beyond composition, other molecular factors influence degradation. Polymers possessing a higher molecular weight ($M_\omega$) degrade more slowly, as more chain scission events are required to reach an easily soluble chain length (Anderson & Shive, 1997; Makadia & Siegel, 2011). Since the typical glass transition temperature ($T_g$) of PLGA copolymers generally sits above the physiological temperature ($\theta = 37° C$), the material exists primarily in a glassy state initially, restricting water access and slowing the onset of bulk erosion (Makadia & Siegel, 2011). Furthermore, degradation occurs preferentially within amorphous domains (Makadia & Siegel, 2011). Given that many common PLGA grades are inherently amorphous, this facilitates initial water penetration and promotes bulk hydrolysis (Makadia & Siegel, 2011). Lastly, degradation rates are sensitive to the microenvironmental pH and temperature, accelerating exponentially with increasing temperature, and highly pronounced under alkaline or strongly acidic conditions due to catalytic effects (Anderson & Shive, 1997; Makadia & Siegel, 2011; Mathieu et al., 2005; Wang et al., 2024).

The initial stage of degradation depends critically on water diffusion. For amorphous PLGA, water sorption into the matrix is immediate, softening the material and dramatically enhancing the flexibility of the polymer chains, corresponding to the material's plasticization (Álvarez et al., 2020). This plasticization induces swelling, followed by substantial morphological changes (Makadia & Siegel, 2011; Mathieu et al., 2005). As the bulk molecular weight decreases, the structure loses integrity, generating internal porosity and microcracks. The eventual loss of water-soluble monomers and oligomers results in observable mass loss, often leaving behind more slowly degrading oligomers that may crystallize briefly, contributing to heterogeneous breakdown (Anderson & Shive, 1997; Makadia & Siegel, 2011; Mathieu et al., 2005).

The mechanical stability and degradation profile of PLGA can be deliberately modulated through the incorporation of inorganic additives (Carrascosa et al., 2024). Basic fillers, notably

magnesium hydroxide [$Mg(OH)_2$], function as pH buffering agents (Carrascosa et al., 2024; Jang et al., 2018). By reacting with the acidic degradation products (lactic and glycolic acid), $Mg(OH)_2$ effectively neutralizes the local microenvironment, thereby suppressing the autocatalytic acceleration of bulk hydrolysis and mitigating the acid-induced inflammatory response. However, careful control is required, as the filler itself can also promote chain scission via a base-catalyzed ester hydrolysis mechanism, as shown in Figure 4B. Optimized reinforcement, sometimes utilizing specific morphologies such as fibrous $Mg(OH)_2$, ensures maximum beneficial surface area for interaction while providing improved mechanical strength (Carrascosa et al., 2024; Jang et al., 2018).

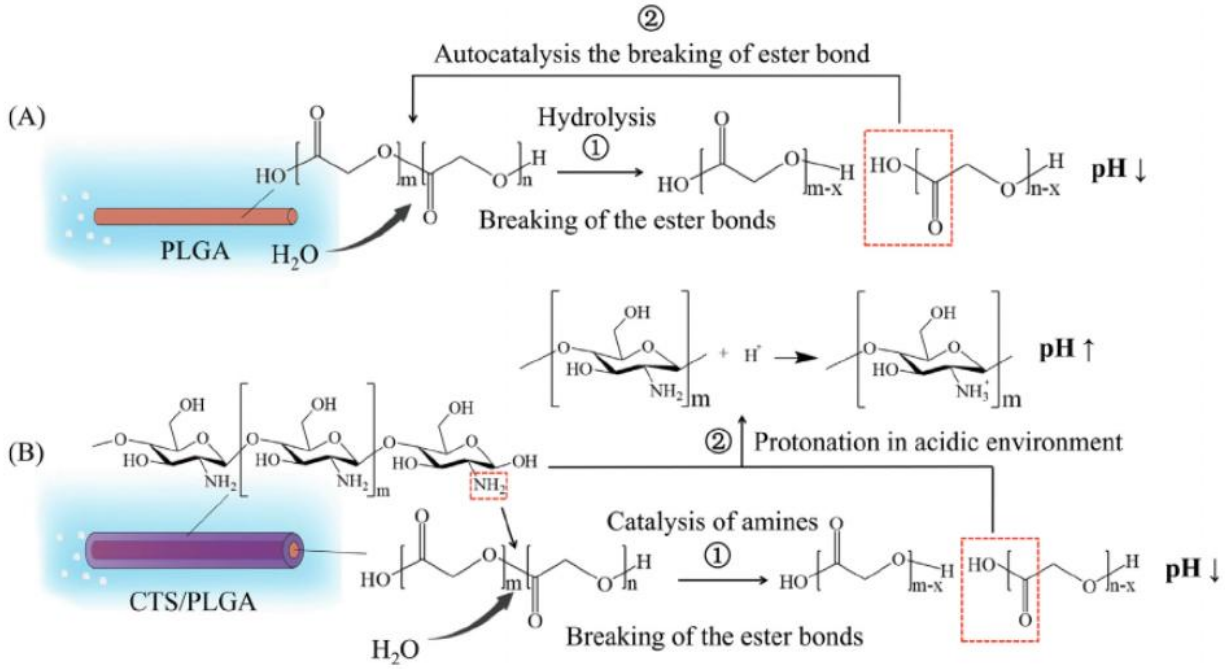


Figure 4. Proposed degradation mechanisms for the PLGA fibres (A) and the shell-core structured CTS/PLGA fibres (Shen et al., 2019).

Other mineral fillers, such as rice husk ash (RHA) and wollastonite, influence degradation indirectly by modifying the matrix characteristics. RHA contains porous amorphous silica, contributing high specific surface area and internal porosity. When incorporated into polymer compositions, RHA can reduce the interdiffusion coefficients, suggesting that the filler's porous structure helps to partially retain the plasticizer within the matrix (Sadykova et al., 2024). Wollastonite (calcium silicate) is favoured for its acicular (needle-like) structure (Hadal et al., 2004). This high aspect ratio filler is incorporated to increase mechanical performance, which also helps maintain structural integrity as the surrounding polymer matrix begins to hydrolyse and weaken (Chan et al., 2020).

Finally, post-processing techniques like hydrothermal treatment involve controlled exposure to water at high temperatures and pressures, directly influencing polymer chains. Applying this treatment before supercritical $CO_2$ foaming (pre-treatment) has been shown to enhance scaffold properties, specifically increasing final porosity and interconnectivity. This is due to internal structural modification that favours better pore formation kinetics during the subsequent

depressurization step. In contrast, applying hydrothermal treatment after the foaming process compromises the achieved architecture, leading to undesirable pore collapse, loss of interconnectivity, and reduced mechanical integrity (García-Jarana et al., 2025). These findings highlight the potential for precise structural tuning when combining supercritical processing with selective pre-treatment methods.

### 2.1.4 Biomedical Relevance of PLGA

Poly(lactic-co-glycolic acid) occupies a preeminent position in the field of biomedical materials due to its fundamental characteristics of biocompatibility and controllable biodegradation, attributes which have secured its fundamental approval by the FDA. PLGA is a versatile synthetic polymer that degrades through hydrolysis of its ester linkages into lactic acid and glycolic acid, which are natural metabolites safely eliminated by the body via normal metabolic pathways. The polymer's degradation characteristics and subsequent physical properties can be precisely tuned through control over its initial molecular weight and the mole ratio of its constituent monomers (L:G ratio) (Makadia & Siegel, 2011).

This tunability allows PLGA to be engineered for a wide array of clinical applications demanding bioresorbable properties. Historically, PLGA has been utilized in the manufacturing of temporary surgical devices, including absorbable sutures and wound closure systems, as well as for fixation implants in orthopaedic, craniofacial, and maxillofacial surgeries. Its capacity for predictable mechanical decay and eventual resorption minimizes the need for secondary surgical removal, simplifying clinical management (Makadia & Siegel, 2011).

However, the most impactful application of PLGA lies in its extensive development as a carrier for controlled and sustained drug delivery systems. PLGA matrices are widely employed in the formulation of micro and nano-sized particles (microcapsules, microspheres, and nanospheres) capable of encapsulating a broad spectrum of pharmaceutical agents, including small molecule drugs, peptides, proteins, and macromolecules. By manipulating the polymer composition and geometry, these devices can be designed to release their payload at desired doses over extended intervals, ranging from days to years (Makadia & Siegel, 2011).

Beyond drug delivery, PLGA serves as a primary material in Tissue Engineering, where it is utilized to create porous three-dimensional temporary matrices, or scaffolds, intended to act as an analogue to the native extracellular matrix, this is best exemplified by Figure 5. The ultimate goal is for these scaffolds to provide structural support while simultaneously promoting cell integration and guiding the formation of new, functional tissue as the scaffold gradually degrades (Du et al., 2024; Liao et al., 2012).

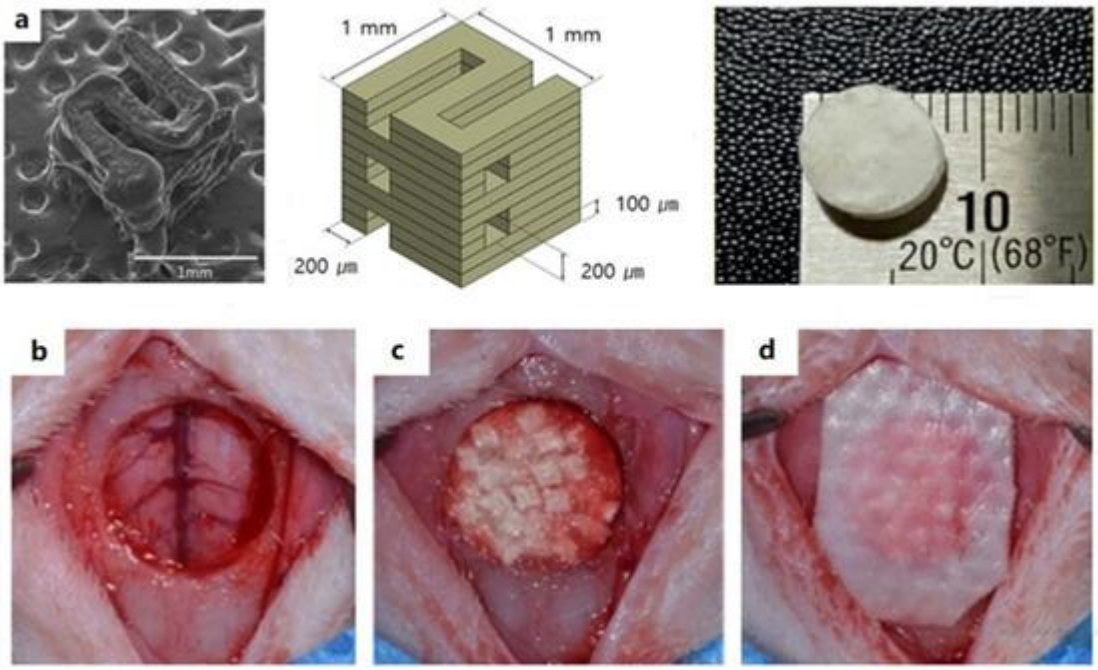


Figure 5. Bone defect repair model based on PCL/PLGA/β-TCP scaffolds: (a) SEM image and PCL/PLGA/β-TCP scaffold simulation structure; (b) porous bone defect structure (8 mm-diameter); (c) defect area filled with PCL/PLGA/β-TCP composite bone graft; (d) defect area filled with collagen membrane (Sun et al., 2022).

The success of PLGA scaffolds in promoting tissue regeneration hinges upon meeting a stringent set of structural and functional criteria (Liao et al., 2012). Functionally, the material must maintain biocompatibility throughout its lifecycle, avoiding adverse immune reactions as it degrades (Liao et al., 2012; Mathieu et al., 2005). Structurally, scaffolds must feature sufficiently high porosity, frequently necessitating values exceeding 75% for applications like bone regeneration, to ensure adequate void volume. This high void volume is essential for facilitating vascularization (blood vessel formation) and the unhindered diffusion of essential nutrients, oxygen, and the efficient removal of metabolic waste products throughout the matrix (Mathieu et al., 2005).

Crucially, the internal structure must possess ubiquitous interconnectivity, allowing cells to migrate freely into the structure's interior rather than simply adhering to its external surface (Liao et al., 2012). Furthermore, the pore size itself must be carefully regulated to match the physiological requirements of the target tissue. For bone tissue engineering, optimal pore diameters are generally advocated within the *200-400μm* range to maximize osteogenesis, angiogenesis, and cell infiltration while retaining necessary mechanical strength (Mathieu et al., 2005).

Despite the clear structural requirements for ideal scaffolds, conventional fabrication methods, including solvent casting/particulate leaching, emulsion freeze-drying, and thermally induced phase separation present significant methodological limitations (Liao et al., 2012; Mathieu et al., 2005). These traditional techniques typically necessitate the heavy use of potentially harmful organic solvents, such as dichloromethane, tetrahydrofuran, or ethyl acetate (Mathieu et al., 2005).

The critical drawback of this solvent dependency is the inherent difficulty in removing solvent residues completely, even after extensive purification and post-processing steps (Mathieu et al., 2005). The remaining traces of organic solvent pose a severe risk, potentially leading to material biocompatibility problems and localized toxicity upon implantation (Carrascosa et al., 2024; Mathieu et al., 2005). Furthermore, many of these methods often employ high processing temperatures, either during melt processes (like extrusion) or during the subsequent stages required for solvent evaporation, which can severely degrade or totally inactivate sensitive thermolabile bioactive agents, such as proteins or growth factors, intended for scaffold encapsulation (Liao et al., 2012).

From a morphological perspective, conventional techniques frequently struggle to achieve the complex, regular, and highly interconnected porous structures required for optimal cell function (Liao et al., 2012; Zhou et al., 2024). They often yield scaffolds characterized by irregular pore shapes, a broad or poorly controlled pore size distribution, and insufficient interconnectivity, thereby hindering uniform cell seeding and mass transfer efficiency throughout the implant bulk (Liao et al., 2012; Mathieu et al., 2005).

These pervasive limitations underscore the motivation for advancing solvent-free manufacturing techniques, establishing the utilization of $scCO_2$ foaming as a promising and technologically rational alternative. This methodology is inherently safer and more environmentally conscious because is nontoxic, chemically inert, inexpensive, and leaves behind no toxic residues in the final biomedical product (Carrascosa et al., 2024).

The scientific rationale relies on the unique physical properties of acting as a simultaneous solvent and plasticizer. When the polymer matrix is exposed to high-pressure , the gas readily dissolves into the polymer, dramatically weakening interchain forces (Valor et al., 2021). This action causes a notable depression of the $T_g$ and a reduction in viscosity, enabling the material to transition into a mobile, rubbery state at relatively mild, low temperatures (often near ambient body temperature).

This reduction in thermal demands is crucial, as it allows for the integration of thermolabile pharmaceutical agents and growth factors without compromising their biological activity, a significant advantage over high-temperature solvent evaporation and melt processing. The rapid depressurization that follows saturation initiates thermodynamic instability, causing the rapid nucleation and growth of gas bubbles, thereby generating the porous scaffold architecture (Carrascosa et al., 2024).

Ultimately, foaming offers the technological means to exert enhanced control over the resulting scaffold morphology, including controlling porosity, pore size distribution, and cell density characteristics, simply by modulating processing parameters such as pressure, temperature, and depressurization rate (Liao et al., 2012). The resulting structure is fixed upon vitrification (re-solidification of the polymer chains) as the $CO_2$ rapidly desorbs and the plasticizing effect dissipates, stabilizing the desired microstructure (Carrascosa et al., 2024). This control

minimizes the structural heterogeneity inherent in solvent-based methods and maximizes the functional utility of the resultant scaffolds.

## 2.2 Supercritical CO2 foaming fundamentals

### 2.2.1 Principles of Supercritical $CO_2$ ($scCO_2$)

The unique characteristics of $scCO_2$ underpin its growing significance as an indispensable tool for modifying biodegradable polymers like PLGA and facilitating solvent-free foaming processes. A substance achieves the supercritical fluid state (Figure 6) when both its temperature (*T*) and pressure (*P*) exceed their respective critical points ($T_c$ *and* $P_c$) (Liao et al., 2012). For $CO_2$, these conditions are easily accessible ($T_c$=*31.1C and* $P_c$=*7.38MPa*) (de Macedo Rooweder Lima, 2024). In this dense phase, exhibits properties intermediate between a gas and a liquid (Liao et al., 2012).

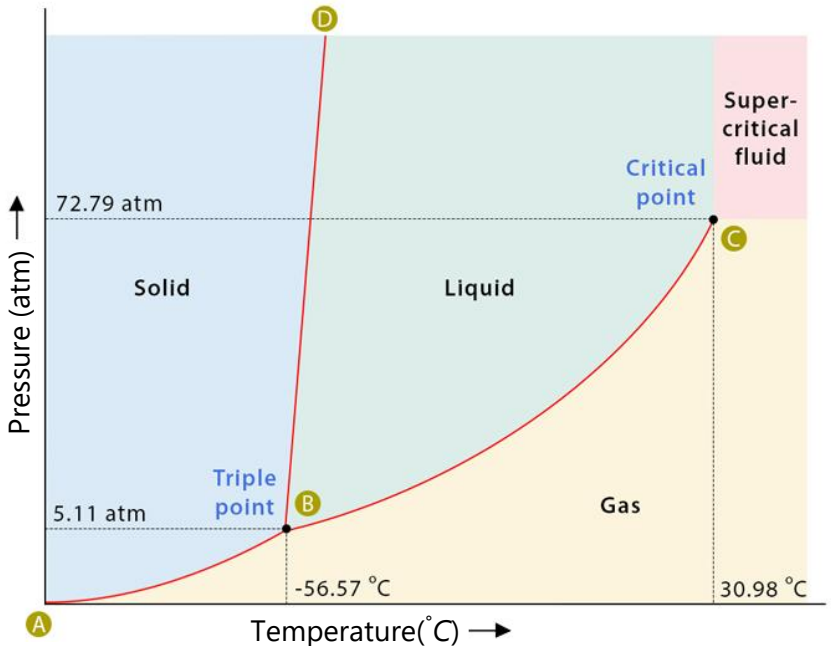


Figure 6. Phase diagram for $CO_2$ (Bhuyan, 2023).

The density of $scCO_2$ is highly responsive to marginal changes in temperature and pressure, particularly near the critical point, affording unique control over its properties. This tuneable density fundamentally dictates the fluid's capacity for solvation and diffusivity (Liao et al., 2012). By adjusting the density, the solvent power of $scCO_2$ can be modulated over a wide range to dissolve non-polar or weakly polar solutes (Machado et al., 2022). Simultaneously, $scCO_2$ maintains relatively high gas-like diffusivity (in the order of $10^{-3}\frac{cm^2}{s}$ range) and low viscosity (in the order of $10^{-4}\frac{g}{cm \cdot s}$ range), enabling rapid mass transfer and efficient liquid-like penetration into the polymer matrix (Liao et al., 2012).

The technological utility of $scCO_2$ is significantly enhanced by its substantial environmental and safety advantages, which position it as a superior alternative to traditional organic solvents (Carrascosa et al., 2024). $CO_2$ is an inert, non-toxic, and non-flammable substance (Liao et al., 2012). This characteristic permits the processing of biomedical-grade materials, such as PLGA scaffolds, without the introduction of toxic organic solvent residues (like dichloromethane or ethyl

acetate) that often necessitate lengthy and expensive post-purification steps in conventional techniques, thus circumventing critical biocompatibility concerns (Machado et al., 2022).

Furthermore, the low critical temperature of $CO_2$ allows processing to occur at mild, low temperatures, which is crucial for handling thermosensitive bioactive agents (such as encapsulated growth factors or complex therapeutic molecules) that would otherwise degrade or lose activity under the high temperatures required by conventional solvent-evaporation or melt-extrusion methods (Valor et al., 2021).

The adoption of $CO_2$ aligns strongly with green processing principles and the concept of a circular economy. $CO_2$ is readily available, non-corrosive, and relatively inexpensive (Liao et al., 2012). Most importantly, it can be efficiently separated from the polymer matrix simply by depressurization, and subsequently recovered and recycled within the process loop, minimizing waste generation and reducing the overall environmental footprint compared to the disposal of hazardous organic solvents (Machado et al., 2022).

These physicochemical attributes are crucial for polymer processing, notably through the phenomenon of plasticization. Supercritical $CO_2$ acts as an efficient plasticizing agent, substantially softening the polymer matrix (Valor et al., 2021). This action weakens the intrinsic polymer chain-chain interactions, functioning as a "molecular lubricant" that enhances polymer chain and segment mobility (Liao et al., 2012). The effectiveness of this plasticization, particularly in polyesters like PLGA , is attributed to the inherent affinity between $CO_2$ molecules and the carbonyl functional groups (C=O) within the polymer backbone via Lewis acid-base interactions (Mathieu et al., 2005).

At the macroscopic level, the physical interaction mechanisms between $scCO_2$ and the polymer result in polymer swelling and expansion of the internal free volume due to the diffusion and absorption of gas molecules (Liao et al., 2012). Critically, this enhanced chain mobility leads to a demonstrable reduction in the glass transition temperature ($T_g$) (Valor et al., 2021). For PLGA , this $T_g$ depression ensures that the polymer transitions from its rigid, glassy state to a mobile, rubbery state even at mild temperatures (often well below its ambient $T_g$) (Carrascosa et al., 2024). This effect is fundamental for enabling processing methods like high-pressure foaming (Valor et al., 2021).

The control over $T_g$ is paramount for regulating foam morphology. During the initial saturation stage, the polymer/$CO_2$ solution is metastable. Foaming is induced when rapid depressurization creates thermodynamic instability (supersaturation), initiating cell nucleation and growth. The subsequent rapid desorption of $CO_2$ abruptly reverses the plasticizing effect, causing the $T_g$ to increase rapidly (Carrascosa et al., 2024). This mechanism leads to vitrification (re-solidification into the glassy state), which effectively freezes and stabilizes the growing porous microstructure, preventing cell coalescence and collapse. This ability to precisely modulate the transition state of the polymer is key to tailoring the scaffold's internal architecture for applications like tissue engineering (Liao et al., 2012).

### 2.2.2 Mechanisms of Polymer Foaming

The fabrication of highly porous polymer structures, such as those utilized in controlled drug delivery and tissue engineering applications, fundamentally relies on the precise control of phase transitions inherent to the $scCO_2$ foaming process. This methodology is segmented into four sequential stages: (1) gas saturation of the polymer matrix, (2) bubble nucleation triggered by thermodynamic instability, (3) subsequent cell growth and expansion, and (4) the final stabilization of the porous structure, this process is depicted in the Figure 7 as part of the work of (Di Maio & Kiran, 2018). Supercritical $CO_2$ is preferentially employed due to its non-toxic, chemically inert properties and its capacity to facilitate solvent-free processing under relatively mild temperature conditions (Valor et al., 2021).

The process begins with the sorption or dissolution of $CO_2$ into the polymer matrix under high pressure and temperature to form a homogeneous polymer/gas solution (Di Maio & Kiran, 2018; Valor et al., 2021). This stage is defined by critical thermodynamic principles, most notably $CO_2$ induced plasticization. Carbon dioxide molecules interact with specific functional groups along the polymer backbone, weakening intermolecular chain-chain interactions (Di Maio & Kiran, 2018). For polyesters like PLGA, the strong affinity between $CO_2$ the and the polymer's carbonyl groups facilitates this molecular softening (Tai et al., 2010). This plasticization causes a measurable decrease in the $T_g$ and viscosity of the material, enhancing polymer chain and segment mobility (Di Maio & Kiran, 2018; Valor et al., 2021).

The decrease in $T_g$ moves the polymer from its rigid, glassy state into a softer, rubbery state, significantly increasing the free volume within the matrix. This increased mobility is essential, as it minimizes the energetic requirements for the subsequent phase of foam production. The saturation process continues until the amount of $CO_2$ absorbed reaches equilibrium under the given pressure and temperature conditions (Di Maio & Kiran, 2018).

The transition to the second stage, nucleation, is initiated by inducing thermodynamic instability, typically through a rapid reduction in pressure (pressure quench) or, less commonly, an increase in temperature (Di Maio & Kiran, 2018; Mathieu et al., 2005). This rapid change renders the polymer/gas solution supersaturated, serving as the essential driving force for the spontaneous formation of gaseous bubbles that act as “nucleation sites” (Chan et al., 2020; Valor et al., 2021).

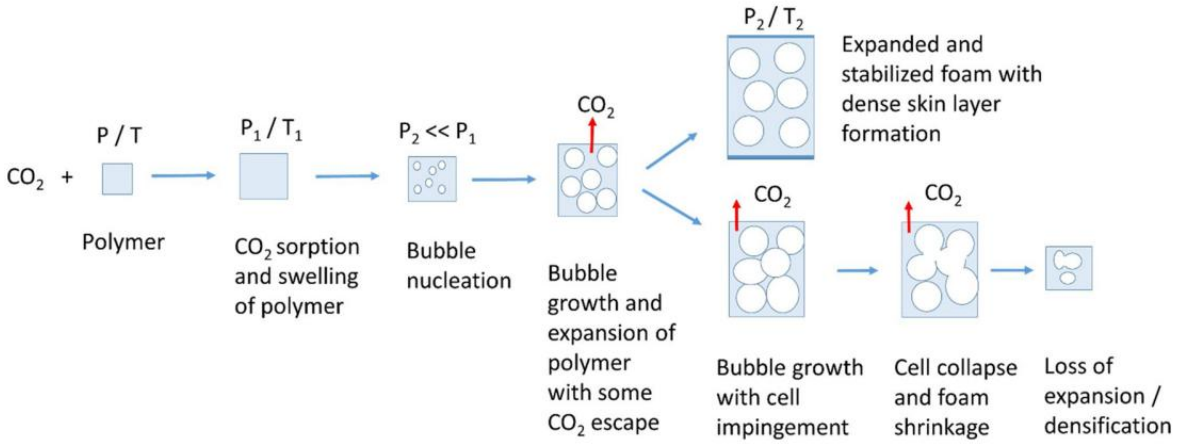


Figure 7. Schematic illustration of the foaming process with $CO_2$ demonstrating $CO_2$ sorption, followed by the cell growth and expansion (leading to initial formation of isolated pores), cell-impingement and cell-collapse (which, if can be controlled, may lead to interconnected pores, but if proceeds further, may lead to extensive cell collapse and densification). The outcomes depend on the sorption stage (pressure and temperature), decompression stage (rate of decompression), $CO_2$ diffusion coefficient under the prevailing *P*/*T* conditions, thermophysical state of the polymer system (the distance from and/or approach to the glass transition or melting temperature, i.e., whether glassy, rubbery or crystalline), and the dynamics of the changes in the rheological properties (viscosity, modulus) of the polymer (Di Maio & Kiran, 2018).

The principles governing this spontaneous process are framed by the Classical Nucleation Theory (CNT). According to CNT, a bubble nucleus forms only if its radius ($R$) surpasses a specific critical radius ($R^*$). The formation of a nucleus requires overcoming an energetic barrier to nucleation ($\Delta G^*$), which is fundamentally derived from two competing contributions: the volumetric free energy reduction associated with bubble creation ($\propto R^3$) and the energetic cost of forming the new surface area ($\propto R^2$) (Di Maio & Kiran, 2018).

The critical energetic barrier ($\Delta G^*$) and the required critical radius ($R^*$) are directly dependent on the pressure difference ($\Delta P$) experienced by the fluid (pressure quench) and the interfacial tension ($\gamma$) between the gas and the polymer solution. Mathematically, the critical radius is defined as:

$$R^* = 2\gamma/\Delta P \tag{1}$$

and the nucleation barrier $\Delta G^*$ is inversely proportional to the square of the pressure difference

$$\Delta G^* \propto 1/\Delta P^2 \tag{2}$$

Consequently, maximizing the pressure quench ($\Delta P$) results in a sharp reduction of the critical energetic barrier, leading directly to significantly higher nucleation rates (Di Maio & Kiran, 2018).

Crucially, nucleation can occur via two pathways: homogeneous nucleation, which occurs throughout the uniform phase, or heterogeneous nucleation, which is strongly favoured by introducing solid particles (nucleating agents) (Di Maio & Kiran, 2018). Mineral fillers, such as rice husk ash (RHA) containing amorphous silica, hydroxyapatite (HAp), or bentonite clay, act as heterogeneous nucleation sites (Carrascosa et al., 2024; Piperopoulos et al., 2022; Stefani et al.,

2006). These external surfaces partially contribute to the nucleus interface, effectively lowering the required free energy threshold for nucleation ($\Delta G^*_{Het}$) and thus promoting the formation of micro or nano cellular structures (Di Maio & Kiran, 2018).

Following nucleation, the third phase involves cell growth, wherein bubbles expand by mass transfer driven by the concentration gradient: $CO_2$ continues to diffuse from the supersaturated polymer solution into the nascent cells (Chan et al., 2020; Valor et al., 2021). This cell expansion is dynamically contested by the viscoelastic properties of the polymer matrix (Di Maio & Kiran, 2018). The polymer's viscosity must be maintained within a critical range: it must be low enough to permit sufficient bubble growth, yet simultaneously high enough to withstand the stress imposed by expansion and the negative internal pressure resulting from escaping from the matrix (Di Maio & Kiran, 2018).

If the melt viscosity is insufficient, excessive extensional deformation of the cell wall occurs, leading to detrimental cell coalescence and rupture, ultimately causing the collapse of the foam structure (Di Maio & Kiran, 2018). However, fillers can positively influence these dynamics; for instance, materials like polytetrafluoroethylene (PTFE) form entangled nanofiber networks that restrict excessive cell growth and merging, leading to reduced cell size and high cell density (Kang et al., 2025; Wang et al., 2024). Moreover, certain inorganic fillers, such as magnesium borate whisker, enhance the rigidity of the cell walls and act as a physical barrier, slowing down the desorption rate of $CO_2$ from the inside of the bubbles, which aids in mitigating foam shrinkage (Gao et al., 2022).

The final stage is stabilization, during which bubble expansion ceases and the newly formed microstructure is preserved (Di Maio & Kiran, 2018). For amorphous polymers such as the common PLGA 75:25 formulation, stabilization is achieved exclusively by vitrification, where the rapid desorption of the $CO_2$ reverses the plasticizing effect, causing the polymer chains to solidify abruptly back into a rigid, glassy state (Carrascosa et al., 2024; Mathieu et al., 2005). This vitrification process mechanically "freezes" the porous structure, restricting further molecular motion and preserving the desired pore morphology against subsequent coalescence or collapse (Di Maio & Kiran, 2018).

Consequently, in amorphous biodegradable polymers, the lack of intrinsic melt strength often results in cell coalescence and structural collapse during depressurization. This instability highlights the critical need for additional stabilization strategies, such as physical reinforcement or pre-foaming structural conditioning, to ensure scaffold integrity.

### 2.2.3 Processing Parameters and Morphological Control

The final cellular architecture and structural performance of PLGA foams prepared via supercritical carbon dioxide ($scCO_2$) foaming are meticulously controlled by the interplay of key processing variables and the resulting physicochemical state of the polymer matrix (Carrascosa et al., 2024; Di Maio & Kiran, 2018; Mathieu et al., 2005; Valor et al., 2021). The primary processing parameters governing foaming behaviour and cellular structure are saturation pressure (*P*), foaming temperature (*T*), and depressurization rate (*Dr*) (Di Maio & Kiran, 2018; Mathieu et al., 2005; Valor

et al., 2021). These parameters dictate the thermodynamic and kinetic mechanisms underlying nucleation, growth, and stabilization (Di Maio & Kiran, 2018).

The influence of these parameters is intrinsically linked to polymer-related effects, particularly the polymer's initial melt strength (viscosity), chain mobility, and $CO_2$ solubility (Di Maio & Kiran, 2018; Mathieu et al., 2005; Valor et al., 2021). Increasing the saturation pressure generally yields a higher concentration of dissolved $CO_2$ within the polymer matrix (Di Maio & Kiran, 2018; Mathieu et al., 2005; Valor et al., 2021). This rise in $CO_2$ solubility acts as an efficient plasticizer, significantly reducing the glass transition temperature ($T_g$) and viscosity of the polymer, thereby enhancing chain mobility and increasing the material's free volume (Di Maio & Kiran, 2018; Mathieu et al., 2005; Valor et al., 2021). For PLGA and similar amorphous polymers, this plasticization shifts the material into a rubbery state, which is necessary for the cell formation processes to occur efficiently, often below the material's ambient $T_g$ (Carrascosa et al., 2024).

The relationship between processing parameters and polymer properties is complex, often exhibiting competing effects (Di Maio & Kiran, 2018; Valor et al., 2021). For instance, increasing pressure generally results in higher $CO_2$ density and greater plasticization, enhancing the foaming effect and typically leading to a decrease in mean pore size and an increase in cell density (Carrascosa et al., 2024; Mathieu et al., 2005; Valor et al., 2021). This is because higher gas concentration provides more nucleation sites during the subsequent depressurization step (Carrascosa et al., 2024; Di Maio & Kiran, 2018; Valor et al., 2021). Conversely, increasing the foaming temperature tends to promote polymer chain mobility and gas diffusivity, accelerating bubble expansion and cell growth but often resulting in larger cell sizes and reduced cell density, partly because higher temperatures increase the rate of $CO_2$ desorption, which can lead to cell collapse or undesirable coalescence if melt strength is insufficient (Di Maio & Kiran, 2018; Valor et al., 2021).

The depressurization rate (*Dr*) is critically important for controlling the morphological outcomes, as the speed of pressure release dictates the degree of supersaturation achieved, which is the driving force for cell nucleation (Di Maio & Kiran, 2018; Mathieu et al., 2005). A rapid depressurization rate results in high supersaturation and subsequently promotes a higher cell density and smaller pore sizes (Carrascosa et al., 2024; Mathieu et al., 2005). In contrast, slower depressurization may allow a significant portion of the dissolved $CO_2$ to escape (diffuse out) before nucleation can effectively stabilize the structure, potentially leading to lower cell density and poorer foaming effects, as observed in some PLGA studies. However, high *Dr* can also induce pore collapse or coalescence due to the instantaneous, high expansion forces coupled with adiabatic cooling of $CO_2$ inside the vessel (Valor et al., 2021).

This highlights the critical importance of kinetic competition during the foam expansion and stabilization stages. Bubble growth is dictated by the kinetics of $CO_2$ diffusion from the polymer solution into the nascent cells, driven by the concentration gradient. This growth must occur rapidly enough to achieve the desired expansion ratio and interconnectedness, yet slowly enough for the polymer matrix to maintain structural integrity against bubble growth forces and prevent

coalescence. For successful scaffold fabrication, the $CO_2$ desorption rate and the polymer's viscosity must be precisely managed to ensure stabilization (Di Maio & Kiran, 2018).

The stabilization of the porous structure is achieved through polymer vitrification, where the rapid desorption of the $CO_2$ reverses the plasticizing effect, causing the $T_g$ to increase rapidly back above the foaming temperature (Carrascosa et al., 2024; Di Maio & Kiran, 2018). This transition effectively "freezes" the polymer chains into a rigid, glassy state, preserving the cellular architecture developed during cell growth (Carrascosa et al., 2024; Di Maio & Kiran, 2018; Mathieu et al., 2005). If the timing of this vitrification is poor, for instance, if it occurs too slowly, the melt strength of the matrix may be insufficient, leading to continued cell expansion, eventual rupture, and catastrophic coalescence and collapse of the foam structure (Di Maio & Kiran, 2018).

Thus, optimizing PLGA foaming parameters requires striking a delicate balance: maximizing gas solubility (high *P*) and diffusivity (moderate *T*) to ensure adequate nucleation (fast *Dr*), while controlling polymer viscosity and enabling prompt vitrification to stabilize the highly porous structure and achieve the desired cell density, pore size, and interconnectivity (Carrascosa et al., 2024; Di Maio & Kiran, 2018; Mathieu et al., 2005). The resultant structural uniformity and morphology ultimately determine the suitability of the PLGA scaffold for specific tissue engineering applications (Carrascosa et al., 2024).

The combined effects show a clear trend: parameters that lead to higher gas dissolution and rapid nucleation (high *P*, high *Dr*) generally yield scaffolds with higher mechanical strength due to reduced mean pore size. Conversely, conditions leading to high expansion ratios and large pores often compromise mechanical performance (Carrascosa et al., 2024). This interplay reflects the core challenge of $scCO_2$ foaming: continuously manipulating the polymer's viscoelastic state through precise temperature and pressure cycling to achieve a thermodynamically optimized yet kinetically stabilized cellular structure (Di Maio & Kiran, 2018; Mathieu et al., 2005).

### 2.2.4 Limitations and Opportunities

The widespread application of PLGA scaffolds fabricated via $scCO_2$ foaming is hindered primarily by challenges related to achieving reproducible microstructures and maintaining structural integrity throughout the rapid depressurization stage. The complex dynamics of this process, involving $CO_2$ sorption, nucleation, cell growth, and subsequent stabilization, are exquisitely sensitive to subtle variations in processing parameters such as saturation pressure (*P*), foaming temperature (*T*), and depressurization rate (*Dr*) (Carrascosa et al., 2024; Di Maio & Kiran, 2018; Mathieu et al., 2005; Valor et al., 2021). A fast depressurization rate, for instance, is necessary to achieve the supersaturation required for maximum nucleation sites (high cell density) but simultaneously promotes rapid volumetric expansion and often catastrophic foam collapse due to insufficient time for the material to vitrify and stabilize (Di Maio & Kiran, 2018; Valor et al., 2021). Consequently, reliably tailoring a scaffold’s properties to meet specific therapeutic requirements (e.g., target pore size and density for optimal cell growth) remains difficult without an a priori understanding of the material's response profile (Di Maio & Kiran, 2018).

This challenge is magnified when working with amorphous polymers such as common PLGA compositions (e.g., 75:25 or 50:50), which are typically amorphous across the key industrial processing windows (Nifant'ev et al., 2024). The lack of crystalline domains means that mass transfer, specifically $CO_2$ sorption, occurs readily throughout the matrix, resulting in profound $CO_2$-induced plasticization (Nifant'ev et al., 2024). This plasticizing effect dramatically lowers the polymer's glass transition temperature ($T_g$), shifting the material into a highly mobile, rubbery state necessary for foaming (Di Maio & Kiran, 2018). However, for amorphous PLGA, the resulting cellular architecture relies exclusively on vitrification (the instantaneous re-solidification of chains as $CO_2$ desorbs upon depressurization) for its final stabilization (Di Maio & Kiran, 2018; Nifant'ev et al., 2024). If the viscosity or melt strength of this highly plasticized state is inadequate, or if the timing of vitrification is delayed, the rapidly growing cells merge and rupture, leading to total structural collapse and the extreme difficulty in maintaining a fine, highly interconnected cell structure (Di Maio & Kiran, 2018; Mathieu et al., 2005).

To overcome these intrinsic material limitations and stability issues, an important technological opportunity lies in controlled material modification strategies. The inclusion of rigid inorganic mineral fillers is a highly effective strategy to counter high $CO_2$-induced plasticization and enhance foaming performance (Carrascosa et al., 2024). Particulate materials such as hydroxyapatite (HAp), magnesium hydroxide [$Mg(OH)_2$], or bentonite function effectively as heterogeneous nucleation sites, physically reducing the energetic barrier ($\Delta G^*$) required for bubble formation during depressurization (Carrascosa et al., 2024; Di Maio & Kiran, 2018). This enhanced nucleation efficiency drives the formation of smaller, denser cells and, crucially, the fillers increase the overall melt viscosity and stiffness of the polymer/gas solution (Piperopoulos et al., 2022).

The resulting increase in viscoelastic properties imparted by the fillers helps resist the destructive extensional forces exerted by growing bubbles, substantially limiting the rate of cell growth and mitigating the critical risk of coalescence and subsequent foam collapse inherent to amorphous PLGA (Piperopoulos et al., 2022). For instance, the addition of high-aspect-ratio fillers, such as fibrous $Mg(OH)_2$, enhances the rigidity of the cell walls, contributing to the foam's enhanced compressive mechanical strength and actively resisting foam shrinkage after stabilization (Gao et al., 2022; Jang et al., 2018). Studies have demonstrated that incorporating fillers like HAp can significantly improve compressive stress values in PLGA 75:25 scaffolds to levels comparable with native trabecular bone, thereby achieving the necessary mechanical performance while maintaining adequate porosity levels (Carrascosa et al., 2024).

Furthermore, alternative, solvent-free methods for modification, such as hydrothermal treatment, present non-filler-based opportunities to manipulate the polymer structure. Although demonstrated for polycaprolactone (PCL) as a similar biodegradable polyester, the principle may extend to other polymers: applying hydrothermal pre-treatment before $scCO_2$ foaming modifies the precursor's internal structure, promoting advantageous changes in viscosity and chain mobility during the subsequent foaming process. This technique can significantly enhance final scaffold properties, resulting in increased porosity, improved pore size distribution, and enhanced interconnectivity, without introducing foreign particulate matter. Critically, the sequence matters;

hydrothermal treatment applied after foaming typically results in structural degradation, pore collapse, and excessive mechanical fragility, underscoring that modifying the polymer precursor is key to successful foam architecture tuning (García-Jarana et al., 2025).

## 2.3 Hydrothermal treatment mechanisms

### 2.3.1 Definition and Processing Conditions

The utility of hydrothermal treatment (HT) in the modification of biodegradable polymers lies in its ability to induce controlled structural changes in precursor materials through a highly tuneable aqueous environment. HT is defined as a processing technique in which materials are exposed to liquid water or saturated water vapor at temperatures above the normal boiling point of water, under elevated pressure conditions. By employing water as both the processing medium and the reactive environment, HT enables physicochemical modifications that are difficult to achieve through conventional dry or solvent-based approaches. This distinctive feature makes HT particularly attractive for the sustainable modification of polymeric systems, especially those sensitive to thermal or chemical degradation (García-Jarana et al., 2025)

The operational parameters employed for achieving structural modification via HT are designed to exploit the reactivity and penetrating power of hot, pressurized water. Representative laboratory conditions for HT often involve temperatures ranging from *343K* to *373K* in some polymer studies, although protocols for processing inorganic fillers, such as bentonite, have used higher temperatures up to *120℃*. Corresponding pressure ranges typically fall between *10* and *30 bar* (e.g., *~17 bar*) to maintain the aqueous medium in a subcritical state or vapor phase saturation, The exposure medium may be either liquid water or saturated vapor, with treatment durations generally ranging from a minimum of 10 minutes up to several hours to achieve the desired effect (García-Jarana et al., 2025; Piperopoulos et al., 2022).

HT is particularly relevant for preparing precursors for $scCO_2$ foaming because it promotes desirable structural changes, specifically enhancing features such as scaffold porosity and interconnectivity. The utility of HT lies not in adding material to the matrix but in inducing internal structural modification of the polymer chains without relying on external cross-linking agents, thus offering an appealing strategy for optimizing material properties for applications like tissue engineering scaffolds (García-Jarana et al., 2025).

The fundamental physicochemical rationale behind HT's effect involves the high-energy penetration of the aqueous medium into the polymer matrix. Water molecules, energized by the elevated temperature and pressure, readily diffuse into the amorphous domains of the polymer, acting as a powerful plasticizer. This water penetration disrupts the native intermolecular forces, such as hydrogen bonds or weak van der Waals interactions between polymer chains (García-Jarana et al., 2025). This effect is pronounced in hydrophilic polyesters or copolymers like PLGA, promoting initial water uptake and chain separation Figure 8 describes this process graphically.

This disruption in the polymer structure leads directly to polymer chain relaxation and enhanced molecular mobility. Unlike simple heating, which requires reaching the polymer's glass

transition temperature ($T_g$) under ambient pressure to achieve significant mobility, HT leverages the plasticizing capacity of water to temporarily depress the $T_g$. This allows substantial structural adjustments, or structural reorganization, to occur at mild operating temperatures. Such internal modifications, achieved by HT, are critical for tuning the precursor material to facilitate optimal pore formation kinetics during subsequent $scCO_2$ foaming (García-Jarana et al., 2025).

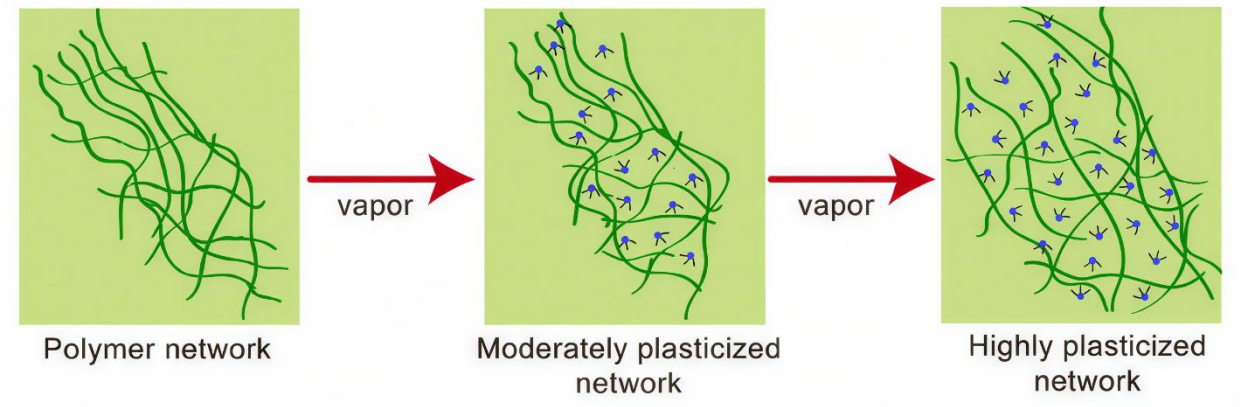


Figure 8. Schematic depiction of plasticization: solvent (vapor) absorption mediated swelling of the polymer network results in an increase in the effective free volume (Bhattacharya et al., 2013).

A primary advantage of HT lies in its inherent safety and environmental profile compared to traditional polymer processing techniques, such as solvent casting or thermally induced phase separation. These conventional methods necessitate the use of volatile and often toxic organic solvents, such as dichloromethane or ethyl acetate. The subsequent removal of these solvents requires costly and often high-temperature steps, leading to the high probability of residual solvent toxicity, which severely compromises the material's biocompatibility for medical applications (Álvarez et al., 2020; García-Jarana et al., 2025). HT, in contrast, utilizes water or steam, ensuring the final product remains solvent-free and minimally contaminated, aligning with green processing principles (García-Jarana et al., 2025).

When contrasted with thermal annealing or melt conditioning, HT offers a distinct mechanistic difference. Annealing typically involves heating the polymer below its melting point ($T_m$) or glass transition temperature ($T_g$) for long periods to induce crystallization or molecular reorganization, relying primarily on thermal energy and time (Anderson & Shive, 1997). HT introduces the element of pressurized water, which actively participates in the structural change by dramatically lowering the polymer's $T_g$ and enhancing chain mobility via plasticization, thereby facilitating the rearrangement process at lower temperatures than would be required otherwise (García-Jarana et al., 2025; Makadia & Siegel, 2011).

The role of HT is clearly demarcated by its timing within the fabrication process: applying the treatment before $scCO_2$ foaming (pre-treatment) successfully imparts the desired structural modification, optimizing the polymer's viscoelastic state for nucleation and bubble growth. Conversely, applying the HT after the porous scaffold has been formed (post-treatment) proved detrimental, leading to structural compromise, pore collapse, and excessive fragility, rendering the scaffolds unsuitable for mechanical applications (García-Jarana et al., 2025). This indicates that the goal of HT is strictly the initial structural optimization of the bulk material, providing a pathway

to tune the resulting foam architecture without relying on external, potentially compromising, chemical agents.

### 2.3.2 Effects on Polymer Structure and Properties

The modification of biodegradable polymers such as PLGA through hydrothermal treatment (HT) involves two interrelated mechanisms: an initial physical alteration of the polymer matrix followed by chemically driven degradation processes. These mechanisms do not occur independently; rather, the physical changes induced by HT directly govern the extent and kinetics of subsequent chemical transformations. Understanding this interaction is essential for modifying the polymer precursor prior to supercritical $CO_2$ foaming.

During HT, elevated temperature and pressure promote efficient penetration of the aqueous medium into the polymer matrix. The absorbed water acts as a temporary plasticizer, swelling polymer chains, increasing free volume, and enhancing chain mobility. This physical plasticization facilitates not only improved gas sorption in later foaming stages but also increases the accessibility of hydrolysable ester bonds within PLGA, thereby accelerating controlled hydrolytic degradation. In this sense, HT-induced plasticization serves as the enabling step that links structural relaxation with chemical modification. Similar plasticization effects have been reported for $CO_2$/polymer systems under supercritical conditions, highlighting a conceptual parallel between HT and $scCO_2$ processing (Machado et al., 2022; Valor et al., 2021).

This physical plasticization is immediately followed by profound structural changes within the polymer. The water penetration disrupts inter-chain forces, promoting relaxation of polymer chains and enhanced amorphous phase mobility. Since the thermal stability and mechanical response of polyesters rely heavily on their chain arrangement, the mobility facilitated by HT enables a structural reorganization toward a thermodynamically favourable state. This physical conditioning, particularly when employed as a pre-treatment prior to $scCO_2$ foaming, is intended to optimize the polymer's viscoelastic state. Such pre-conditioning is believed to maximize the potential for achieving high porosity and enhanced pore interconnectivity during the explosive depressurization phase of foaming (García-Jarana et al., 2025).

However, the presence of hot water inevitably initiates chemical effects, primarily through non-enzymatic hydrolytic processes that cleave the polymer’s ester bonds (Anderson & Shive, 1997). This ester bond scission occurs via random chain scission, initially targeting the amorphous regions and leading to a progressive reduction in the polymer's molecular weight ($M_\omega$) (Anderson & Shive, 1997; Makadia & Siegel, 2011). This phase of degradation, often termed the initial erosion stage, results in substantial $M_\omega$ loss before any noticeable mass erosion occurs (Nifant’ev et al., 2024). While polyesters primarily undergo hydrolysis, the potential for secondary oxidation pathways (such as the formation of peroxides and imides observed in polyamides like PA66 when exposed to moisture and heat) cannot be entirely disregarded, although hydrolysis dominates polyester breakdown kinetics (Gonçalves et al., 2007).

The efficacy of HT hinges on carefully managing the interplay between these mechanisms. While water plasticization (a physical effect) is necessary to unlock structural mobility, the

concurrent hydrolysis (a chemical effect) dictates the structural durability. If the reduction is too drastic, the material rapidly loses its mechanical strength, leading to embrittlement (Makadia & Siegel, 2011). In the case of PLGA/PCL processing, uncontrolled hydrolytic degradation accelerates mechanical failure, causing pore collapse and compromising scaffold integrity, a detrimental outcome demonstrated when the HT was performed after foaming (García-Jarana et al., 2025).

The goal of controlling $M_\omega$ loss during pre-treatment is to ensure that the beneficial structural reorganization (chain relaxation and controlled $T_g$ depression) occurs without compromising the material's ability to withstand subsequent shaping forces. The subsequent influence on thermal properties, such as the $T_g$, depends heavily on the extent of $M_\omega$ loss, as $T_g$ is directly influenced by molecular weight (Donati et al., 2023; Makadia & Siegel, 2011). For PLGA, the thermal stability (degradation onset temperature) is typically high (e.g., around *365℃*) , and controlled HT should aim to avoid initiating polymer decomposition prematurely.

Ultimately, controlled HT yields predictable property-level changes critical for optimal scaffold manufacturing. For scaffolds, the desirable outcome is enhanced porosity and improved interconnectivity (García-Jarana et al., 2025). Experimental results from analogous polyester studies show that when HT (e.g., at *373K* and *17.23bar*) is carefully applied before foaming, it successfully promotes significant enhancement in porosity (up to 51.88%) and improved pore architecture while preserving sufficient mechanical behaviour (compressive modulus) necessary for biomedical applications. This structural modification achieved through controlled physical-chemical conditioning is crucial, as the inherent lack of mechanical stability resulting from high porosity generally restricts the structural use of scaffolds (García-Jarana et al., 2025).

The effective use of HT, therefore, is analogous to precisely tensioning a spring: the physical penetration and plasticization introduce the necessary molecular mobility for structural refinement, while vigilant control over the accompanying chemical hydrolysis prevents the spring (the polymer chain) from breaking entirely, ensuring the material is perfectly conditioned for maximum and stable expansion during foam production.

### 2.3.3 Influence on Subsequent Foaming Behaviour

As discussed in the previous section, hydrothermal treatment induces controlled chain relaxation and molecular weight reduction, yielding a polymer precursor in an optimized viscoelastic state. This pre-conditioned structure directly governs the subsequent $scCO_2$ foaming behaviour.

The initial structure and condition of a polymer precursor significantly dictate the outcome of $scCO_2$ foaming, establishing the utility of Hydrothermal Treatment (HT) as a key pre-processing strategy to modulate polymer behaviour for optimal performance. HT is utilized specifically to condition the polymer matrix prior to gas saturation and nucleation, ensuring that the material is in the appropriate viscoelastic state to sustain controlled pore formation (García-Jarana et al., 2025).

This optimized precursor structure then directly dictates the expansion dynamics during rapid depressurization. The HT-induced reduction in internal resistance means that less energy is required to initiate cell nucleation and growth, allowing the polymer to expand uniformly under

supersaturation without fracturing prematurely. By optimizing the initial viscoelastic state, HT enables expansion dynamics that generate a finer, more numerous cell population, contrasting sharply with the often-heterogeneous results observed in unmodified bulk polymers (Carrascosa et al., 2024; Di Maio & Kiran, 2018).

The success observed in these semi-crystalline systems informs the mechanistic hypothesis regarding the applicability to amorphous PLGA. It is hypothesized that HT can systematically refine the precursor structure by maximizing chain mobility and increasing local free volume throughout the otherwise rigid glassy matrix.

In the context of foaming amorphous PLGA, which relies exclusively on rapid vitrification for structural stability (Di Maio & Kiran, 2018), this conditioning is vital. By promoting highly uniform $CO_2$ distribution and instantaneous plasticization throughout the precursor mass, HT minimizes the local concentration gradients that typically lead to erratic nucleation and subsequent cell coalescence (Anderson & Shive, 1997). Thus, HT is postulated to enhance foaming reproducibility in PLGA by ensuring that the material reaches the ideal, uniformly plasticized state necessary for homogeneous nucleation upon pressure release.

Further opportunities for morphological control lie in exploiting synergistic effects with mineral fillers. Inorganic additives serve the dual function of facilitating heterogeneous nucleation and controlling the viscoelastic behaviour (viscosity/melt strength) of the polymer/gas solution during expansion (Carrascosa et al., 2024; Li et al., 2018). Fillers such as hydroxyapatite (HAp) and magnesium hydroxide [$Mg(OH)_2$] significantly increase compressive strength and neutralize degradation byproducts, acting as physical reinforcement (Carrascosa et al., 2024).

When mineral fillers are combined with HT, the HT-induced chain relaxation likely enhances the interface quality between the stiff inorganic particles and the now more mobile polymer matrix. This superior coupling optimizes the fillers efficacy both as nucleation sites and as internal structural barriers (Carrascosa et al., 2024; Kang et al., 2025). For instance, particulate additives like amorphous silica found in rice husk ash (RHA) can retard desorption by interfering with gas diffusion kinetics (Sadykova et al., 2024), while the needle-like morphology of wollastonite provides crucial mechanical support, reinforcing the expanding pore walls during the high-mobility rubbery state necessary for maximal expansion (Chan et al., 2020; Hadal et al., 2004). This integrated approach, blending chemical/thermal pre-treatment with mineral reinforcement, offers a highly tuneable methodology to stabilize fine, highly interconnected pore architectures that are structurally stable enough for demanding tissue engineering applications.

From a mechanistic perspective, hydrothermal treatment is expected to modify chain mobility and free volume distribution in amorphous PLGA. By pre-relaxing the polymer chains, HT theoretically alters $CO_2$ solubility and nucleation kinetics during subsequent foaming, aiming to optimize the cellular architecture before vitrification sets in.

## 2.4 Role of mineral fillers

### 2.4.1 Classification and General Role in Polymer Composites

The development of composite materials incorporating biodegradable polymers, such as PLGA, and carefully selected inorganic fillers is a foundational strategy in biomedical engineering aimed at mitigating inherent limitations of polymer matrices, particularly inadequate mechanical stiffness. These composite systems rely on fundamental principles of polymer composite science, where the added mineral phase critically dictates the resulting material properties through microstructural, mechanical, and surface interactions.

In polymer composites, inorganic reinforcing agents are broadly classified based on size, typically distinguished as micro or nanofillers (Liao et al., 2012). Microfillers generally possess particle dimensions in the range of micrometres (*μm*), such as certain grades of bentonite or synthetic wollastonite, which has been studied with an average particle size of approximately *8μm* (Cloarec, 2015; Piperopoulos et al., 2022). Nanofillers, conversely, feature at least one dimension below *100nm*, exemplified by hydroxyapatite (HAp) nanoparticles used in orthopaedic applications, which are often less than *200nm* in diameter (Rodriguez et al., 2016).

Beyond size, the morphology and surface characteristics of the filler material are crucial determinants of their functional performance. Fillers exhibit varied shapes, including amorphous and porous forms (such as rice husk ash (RHA) containing amorphous silica (Sadykova et al., 2024; Stefani et al., 2006), layered or platy structures (like bentonite) (Piperopoulos et al., 2022), or acicular (needle-like) and fibrous shapes (such as wollastonite and specific magnesium hydroxide preparations) (Jang et al., 2018). For instance, synthetic wollastonite has been shown to form acicular-needle shaped crystals up to *8μm* long and *≈0.5μm* wide (Novembre et al., 2025). This morphology, alongside inherent surface energy, governs the filler's capacity to interact with the polymer matrix and enhances properties differently, thereby driving key structure-property relationships.

Mineral fillers reinforce the polymer matrix primarily through enhancing stiffness and strength via established composite mechanisms, making them indispensable components in applications like tissue engineering scaffolds (Hadal et al., 2004; Mathieu et al., 2005). A primary mechanism involves interfacial adhesion and load transfer efficiency (Pakeyangkoon et al., 2009). High-aspect-ratio fillers, such as fibrous $Mg(OH)_2$ or wollastonite, are particularly effective because their geometry maximizes the interfacial surface area available for bonding with the polymer chains, enabling efficient transfer of external stress from the softer polymer matrix to the stiffer inorganic phase (Pakeyangkoon et al., 2009). Studies involving hydroxyapatite demonstrate that its inclusion significantly increases the composite's compressive modulus (Rodriguez et al., 2016).

A second critical function involves interference with the matrix failure process, notably through crack deflection and bridging. When a crack propagates through the material, rigid whiskers or fibres intercept its path. This mechanism forces the crack front to deflect around the particle or requires additional energy to fracture the filler (crack bridging), thus dissipating stress and inhibiting catastrophic failure (Gao et al., 2022). This mechanism is vital not only for improving

ultimate mechanical performance but also for guaranteeing the structural integrity of highly porous materials, such as those produced by foaming. Fillers effectively increase the viscosity and melt strength of the polymer matrix, which critically hinders bubble coalescence and rupture during the expansion and stabilization stages of foaming, thereby controlling the final porous morphology (Piperopoulos et al., 2022).

The incorporation of mineral fillers profoundly affects the chemical, structural, and macroscopic properties of polymers, yielding composite materials with tailored functionalities.

Mechanically, fillers impart high stiffness (modulus) and strength, countering the relative softness of base biodegradable polymers like PLGA (Hadal et al., 2004). For biomedical applications, incorporating specific fillers such as hydroxyapatite (HAp) or magnesium hydroxide $Mg(OH)_2$ into PLGA scaffolds has successfully yielded compressive stresses comparable to native trabecular bone, addressing the critical need for initial structural support (Carrascosa et al., 2024; Mathieu et al., 2005). However, highly stiff fillers often reduce the overall toughness or ductility of the polymer matrix, meaning that while the composite is stronger, it may exhibit reduced elongation before brittle fracture (Hadal et al., 2004).

At the physical level, fillers frequently enhance crystallinity by acting as heterogeneous nucleation sites (Chen et al., 2024; Hadal et al., 2004). By providing surfaces for polymer chain alignment, they reduce the activation energy required for crystal formation, thereby increasing the rate of crystallization. This effect is noticeable in polyester foaming, where the accelerated formation of crystalline domains enhances the viscoelastic behaviour and melt strength of the matrix, which is essential for stabilizing the cellular architecture during high-strain expansion (Jiang et al., 2021; Wang et al., 2021).

Furthermore, fillers influence the material's barrier properties and fluid interactions. Particulate fillers confer improved diffusional barrier properties in polymers (Hadal et al., 2004). In the context of the current work, where $scCO_2$ is used for foaming, mineral fillers play a crucial role by resisting the extreme plasticization induced by the absorbed carbon dioxide. This resistance effectively stiffens the polymer under processing conditions, allowing reproducible generation of dense cellular structures. For example, specific modifications to PLGA co-monomers, such as utilizing methylglycolide, markedly improve gas ($O_2$) and moisture ($H_2O$ vapor) barrier properties in the resulting copolymer, demonstrating the strong link between microstructure and functional attributes in biodegradable polyesters (Nifant'ev et al., 2024).

The distinct morphologies of wollastonite (acicular), rice husk ash (porous), and bentonite (lamellar) suggest different nucleation efficiencies and gas-solid interfacial interactions during $scCO_2$ foaming. This necessitates a comparative analysis of their specific effects on stabilizing the PLGA foam structure.

### 2.4.2 Wollastonite (WLS)

Wollastonite ($CaSiO_3$) stands as a mineralogical analogue to established bio ceramic fillers, offering unique advantages due to its distinct acicular morphology and high intrinsic stiffness, which make it an excellent candidate for reinforcing biodegradable polymer matrices in tissue

engineering applications. As a naturally occurring calcium silicate (Figure 9), is structurally classified within the pyroxenoid group, characterized by repeating chains of silicon-oxygen tetrahedra ($SiO^{4-}$) (Novembre et al., 2025). The mineral typically presents in polymorphic forms, such as monoclinic Wollastonite, which is stable below *1150°C* (Novembre et al., 2024).

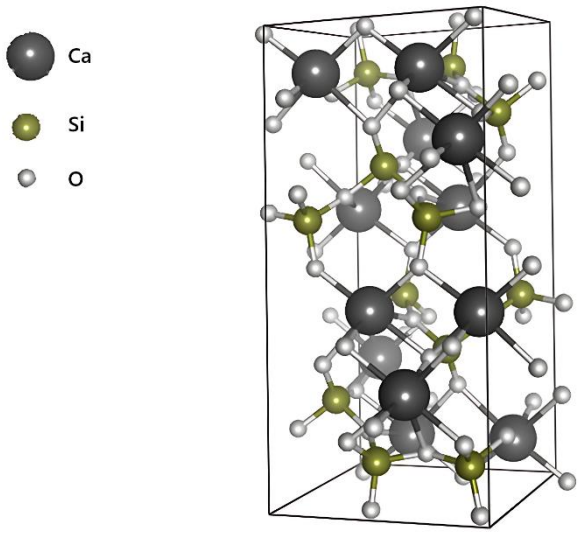


Figure 9. Wollastonite (Edrees et al., 2018)

The primary functional appeal of wollastonite in composites is derived from its acicular, or needle-like, crystal morphology (Hadal et al., 2004; Chan et al., 2020; Novembre et al., 2024). This fibrous geometry fundamentally governs its mechanical influence, allowing it to function effectively both as a reinforcement phase and as a nucleating agent during polymer processing. Importantly, wollastonite exhibits high biocompatibility and bioactivity, aligning with the stringent requirements for medical materials designed for applications such as artificial bones and orthotics (Chan et al., 2020; Novembre et al., 2024; Zenebe, 2022).

The remarkable reinforcement capacity provided by wollastonite is directly attributed to its high aspect ratio, often ranging from 10 to over 20 in synthetic nanofiber forms (Chan et al., 2020; Sasikumar & Ravy, 2015). This high aspect ratio maximizes the interfacial surface area between the filler and PLGA matrix, a geometric prerequisite for achieving optimal load transfer efficiency (Hadal et al., 2004; Piperopoulos et al., 2022). When external stress is applied, the extensive surface contact facilitates the efficient transfer of force from the compliant polymer chains to the stiffer inorganic crystals, leading to a demonstrable increase in the overall composite stiffness and tensile modulus (Hadal et al., 2004; Chan et al., 2020).

Mechanistically, the presence of wollastonite's rigid, acicular structure alters the intrinsic failure mechanisms within the polymeric phase. In comparative studies with other minerals, it has been observed that the stiff, rod-like inclusion of WLS promotes localized plastic deformation patterns, notably inducing micro-mechanisms such as wedge or ridge tearing (Hadal et al., 2004; Sadykova et al., 2004). This localized yielding absorbs energy and helps restrict the growth of larger cracks or flaws that would typically lead to catastrophic failure in unreinforced polymers, thereby enhancing the material's structural integrity (Hadal et al., 2004).

Beyond structural support, WLS acts as an efficient heterogeneous nucleating agent within the polymer matrix. By providing numerous large, high-energy surfaces, the filler successfully lowers the energy barrier required for nucleation. In polymer crystallization, WLS inclusion enhances the rate of crystal nucleation, contributing to a substantial increase in the bulk crystallinity of the final composite (Hadal et al., 2004; Hadal et al., 2004). This capability is highly analogous to the performance of other inorganic fillers like bentonite or talc, which exhibit enhanced nucleation effects in polyester systems.

In the specialized context of $scCO_2$ foaming, this nucleation propensity is critical, as WLS particles serve as preferred sites for the immediate nucleation of gas bubbles when the saturated polymer solution undergoes rapid depressurization (Carrascosa et al., 2024; Di Maio & Kiran, 2018). This proliferation of nucleation sites inherently leads to the formation of a higher cell density and a finer mean pore size in the resulting foam structure, both of which are desirable characteristics for high-performance biomedical scaffolds (Carrascosa et al., 2024).

The extent to which WLS successfully reinforces the polymer and modulates the foaming process is inherently dependent on optimal polymer-filler interactions at the interface. Because the $CaSiO_3$ surface is generally hydrophilic, achieving compatibility with hydrophobic biodegradable polyesters like PLGA often necessitates careful manipulation of the filler's surface chemistry (Piperopoulos et al., 2022). Strategies commonly employed for improving adhesion involve chemical modifications or surface activation treatments, allowing for better stress transfer and maximizing the mechanical contribution of the acicular particles (Sadykova et al., 2020).

Furthermore, by boosting the overall stiffness of the polymer/gas solution, the inclusion of WLS aids in stabilizing the delicate porous architecture generated during $scCO_2$ foaming (Carrascosa et al., 2024). The increased melt viscosity conferred by the filler assists the polymer matrix in withstanding the intense expansion forces of growing bubbles, effectively resisting phenomena such as cell coalescence and subsequent foam collapse (Stefani et al., 2006). This mechanism ensures that the enhanced cell nucleation translates into a structurally stable, dense cellular network, maximizing the potential functional uniformity of the porous scaffold (Piperopoulos et al., 2022).

While direct comparative data for wollastonite in $scCO_2$-foamed PLGA systems remain limited in recent literature, analogous studies involving its precursor, rice husk ash (RHA), and other polymer foams confirm its positive influence on structural outcomes and mechanical strength (Kopuru et al., 2025; Stefani et al., 2006). For example, mineral fillers like magnesium hydroxide [$Mg(OH)_2$] and HAp incorporated into PLGA via foaming resulted in composites with superior compressive stresses comparable to trabecular bone, highlighting the efficacy of incorporating similar stiff mineral reinforcement (Carrascosa et al., 2024). In one composite study, the addition of wollastonite to a polymer matrix reduced the average cell diameter and significantly increased the cell density compared to the neat polymer foam, confirming its robust effect on optimizing the foaming microstructure (Cloarec, 2015).

Thus, wollastonite's unique acicular morphology provides a superior platform for creating composite systems characterized by high stiffness and improved stability under the extreme conditions of $scCO_2$ foaming. The ability to increase both cell density and structural uniformity through heterogeneous nucleation positions WLS as a highly promising filler for the next generation of load bearing, porous biodegradable scaffolds designed for applications such as bone tissue engineering.

### 2.4.3 Rice Husk Ash (RHA)

The pivotal need to enhance the structural and processing characteristics of biodegradable polymers while simultaneously addressing global environmental concerns has positioned Rice Husk Ash (RHA) as a critically important mineral filler in advanced composite research. RHA is fundamentally an agricultural by-product derived from the thermal treatment or controlled combustion of rice husk, a lignocellulosic residue generated globally in massive volumes during rice processing (Sadykova et al., 2024).

The defining chemical feature of RHA is its high silica ($SiO_2$) content, exemplified by Figure 10, which typically accounts for over 85% and often exceeds 90% of its mass (Sadykova et al., 2024). Crucially, the production process, commonly involving combustion at controlled temperatures (e.g., up to *600°C*), yields a structure dominated by amorphous $SiO_2$, rather than crystalline forms (Stefani et al., 2006). This amorphous nature, confirmed by techniques like X-ray diffraction (XRD) analysis, which reveal a pronounced amorphous hump (Kopuru et al., 2025; Lei et al., 2025), is directly relevant to RHA's reactivity when incorporated into polymer matrices (Kopuru et al., 2025).

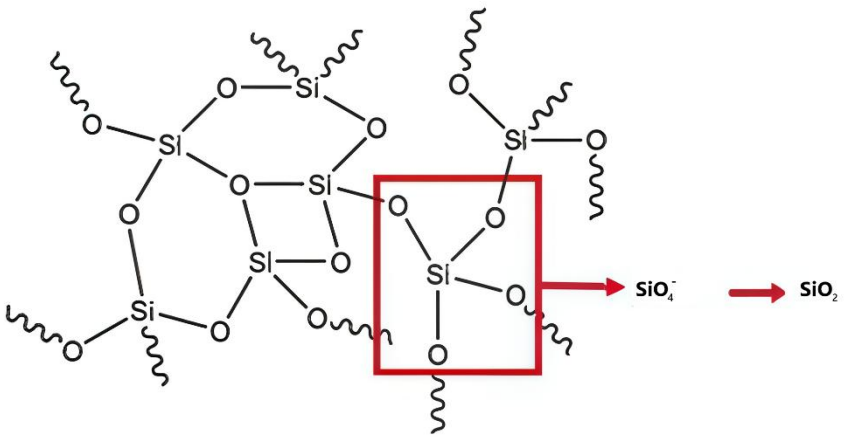


Figure 10. Amorphous Silica found as a main component of the Rice Husk Ash (Nzereogu et al., 2023).

The physical characteristics of particles often exhibit irregular, amorphous, and porous morphologies (Lei et al., 2025). Finely processed RHA powder may present as angular fragments or sometimes demonstrate a densely stacked lamellar structure (Du et al., 2024; Lei et al., 2025). Furthermore, the surfaces of these particles inherently possess silanol (Si-O-H) groups (Novembre et al., 2025; Sadykova et al., 2024). Although the silica component itself is regarded as primarily hydrophobic (Donati et al., 2023), the porous microstructure allows for significant water permeation and retention (Kopuru et al., 2025).

In the context of polymer processing, RHA functions effectively as a heterogeneous nucleating agent, a role critical for modifying the morphology generated during $scCO_2$ foaming (Du et al., 2024; Stefani et al., 2006). The inclusion of RHA particles promotes cell nucleation, leading to a concurrent decrease in the average cell size and an increase in the number of cells per volume unit (Donati et al., 2023; Stefani et al., 2006). This modification of the foam microstructure is a direct consequence of the physical filler surfaces providing multiple sites where the energetic barrier ($\Delta G^*$) required for bubble nucleation is substantially reduced under supersaturation conditions during depressurization (Stefani et al., 2006).

The effectiveness of RHA as a nucleating agent is intrinsically linked to its ability to accelerate the crystallization kinetics of semi-crystalline host polymers, such as Poly(lactic acid) (PLA), even though this effect is observed in the amorphous phase of many polymers. By increasing the rate of crystal nucleation, the mineral phase helps structure the material, confining the molecular chains and aiding in foam stabilization (Du et al., 2024). This beneficial mechanism directly influences the achieved foam architecture, leading to microstructures highly desired for applications requiring high cell density and structural uniformity.

However, controlling the interfacial interactions between RHA and the polymer matrix remains a key challenge, particularly for hydrophobic biodegradable polyesters like PLGA. The tendency of high silica content fillers to exhibit poor adhesion with organic matrices can introduce structural defects at the interface when incorporated at high concentrations (Donati et al., 2023). While fillers generally reduce the diffusion coefficients of plasticizers by partially retaining the liquid within their pores (Sadykova et al., 2024), the physical state of the filler and the polymer must be compatible to maintain melt strength during foaming. In $scCO_2$ processing, the presence of fine RHA particles notably increases the composite's overall specific surface area, thereby increasing the system's propensity for water absorption, which subsequently reduces paste fluidity and increases yield stress (Lei et al., 2025).

The incorporation of RHA yields quantifiable benefits in mechanical performance; for instance, laboratory studies have demonstrated that significantly increases the RHA specific modulus and compressive strength of polymer foams compared to unfilled controls (Stefani et al., 2006). However, the mechanical resilience of the composite systems is highly dependent on the filler loading; excessive RHA concentration can induce internal defects or agglomeration due to poor compatibility, which may ultimately compromise the material’s structural integrity (Donati et al., 2023).

Beyond structural benefits, the chemical nature of RHA's silica content may influence the degradation behaviour of the host polymer. In highly porous systems, the presence of accelerates the degradation rate of the polymer matrix, which may be attributed to the degradation process preferentially targeting the weakened filler-matrix interface (Donati et al., 2023). Furthermore, in certain composite systems (e.g., concrete reinforced with natural fibres), the $SiO_2$ in the RHA acts as a beneficial pozzolanic agent, reacting with calcium hydroxide [$Ca(OH)_2$] to mitigate local alkalinity, thereby protecting other embedded organic components from alkaline degradation

(Ma & Yan, 2025). This demonstrates a potential advantage for PLGA systems, whose degradation yields acidic by-products, suggesting RHA could help stabilize the local pH (Wang et al., 2024).

The valorisation of RHA aligns powerfully with the goals of sustainable materials design and the circular economy (Novembre et al., 2025; Sadykova et al., 2024). As a massive agricultural waste product whose disposal often presents a serious environmental and economic issue (Sadykova et al., 2024), incorporating RHA into biopolymer synthesis provides a sustainable alternative to conventional fossil-based fillers (Donati et al., 2023). This reuse increases the added value of the original rice husk material, transforming a problematic waste stream into a functional component for eco-friendly and biodegradable composites (Wang et al., 2024).

Thus, the critical challenge in successfully utilizing RHA within $scCO_2$-foamed biodegradable PLGA matrices is balancing the desirable enhancement of cell nucleation and density with maintaining optimal interfacial adhesion and material compatibility, ensuring that the necessary structural improvements and sustainability objectives are met without compromising the overall mechanical durability of the resulting scaffold.

### 2.4.4 Bentonite (BT)

Bentonite (BT) is a natural clay material belonging to the layered aluminosilicates group, renowned for its fundamental layered platelet morphology. This mineral structure typically consists of crystalline sheets, or layers, separated by galleries containing exchangeable ions and water molecules (Figure 11), a feature which imparts a high surface area and crucial ion-exchange capacity (Pakeyangkoon et al., 2009). These intrinsic structural characteristics position bentonite as an attractive, low-cost filler for application in polymer composite research (Piperopoulos et al., 2022).

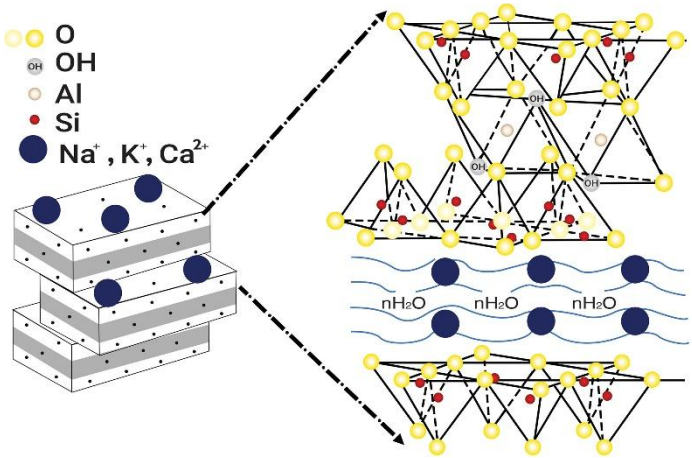


Figure 11. Structural geometry of bentonite ("Adsorbent," 2021)

The utility of BT in polymer nanocomposites fundamentally rests upon the achievement of fine dispersion, specifically the intercalated or exfoliated structural states, where the individual clay layers are either partially or fully separated within the polymer matrix. When successfully dispersed, layered silicates contribute substantially to reinforcement mechanisms that enhance the overall material performance. This reinforcement is directly related to the high aspect ratio of

the clay platelets, which facilitates the efficient transfer of stress from the softer polymer phase to the rigid inorganic filler (Pakeyangkoon et al., 2009).

Beyond enhancing intrinsic strength, BT incorporation yields measurable improvements in macroscopic mechanical performance. For instance, studies incorporating hybrid organic-inorganic porous clay heterostructures, which are derived from bentonite, into polymer foams demonstrated a maximum increase of up to 84% in compressive stress and a 137% enhancement in Young's modulus compared to unfilled systems. These mechanical improvements underscore the significance of utilizing the platelet morphology for enhanced load-bearing capacity (Pakeyangkoon et al., 2009).

However, the native structure of bentonite presents challenges related to its inherent hydrophilic nature, which results in poor compatibility and ineffective dispersion when blended directly into hydrophobic or biodegradable polyesters such as PLGA. This incompatibility typically leads to particle aggregation, severely limiting the potential reinforcement capacity of the filler (Pakeyangkoon et al., 2009). Consequently, efficient incorporation necessitates pre-processing via surface modification strategies (Pakeyangkoon et al., 2009; Piperopoulos et al., 2022).

The conventional strategy involves organo-modification, achieved primarily through ion exchange reactions with quaternary ammonium cations. This process substitutes the inorganic exchangeable cations found in the clay galleries with bulkier organic species, expanding the basal interlayer spacing of the clay structure. This modification lowers the clay's surface energy, improving its compatibility with the organic polymer phase and favouring the necessary intercalation and exfoliation upon melt compounding (Pakeyangkoon et al., 2009).

The effectiveness of this modification and the resulting dispersion quality are critical to maximizing mechanical gains. If the filler content is optimized and dispersion is high, the composite realizes superior performance; conversely, filler aggregation introduces microscopic defects that act as stress concentration points, leading to a detrimental reduction in the mechanical strength and structural stability of the material (Piperopoulos et al., 2022). For example, the maximum compressive strength in some bentonite-filled foams occurred at an optimal loading (*5 wt.%*), and exceeding this concentration led to agglomeration, consequently reversing the positive effect on mechanical properties (Pakeyangkoon et al., 2009).

In the context of $scCO_2$ foaming, the layered structure of bentonite profoundly influences the foaming behaviour, primarily through heterogeneous nucleation. The introduction of BT clay surfaces provides preferred sites for bubble formation, significantly reducing the energetic barrier to nucleation (Di Maio & Kiran, 2018). Bentonite acts as a nucleating agent, leading to a substantial increase in cell density and a corresponding reduction in bubble size in polymer foams. For example, in siloxane foams, the presence of bentonite favoured nucleation, resulting in higher compactness and smaller cell size compared to unfilled foams (Piperopoulos et al., 2022).

Furthermore, the layered filler influences cell growth dynamics by modifying the viscoelastic properties of the polymer/gas solution during the phase transition. The inclusion of BT markedly increases the viscosity of the compounded material. In $scCO_2$ systems, this elevated viscosity is a

crucial control mechanism, as it effectively hinders bubble flow and coalescence in the melt, thereby limiting excessive cell expansion during the pressure quench phase. This structural constraint, arising from the structure "processing" property relationship, is essential for stabilizing the fragile cellular architecture and achieving a high-density porous structure, minimizing the risk of foam collapse (Piperopoulos et al., 2022).

The precise control over foam microstructure afforded by bentonite translates into tailored morphological outcomes, vital for biomedical applications. Bentonite inclusion can lead to increased foam density and compactness. Moreover, the filler's inherent surface chemistry can be utilized: BT-filled composites exhibit hydrophobic interactions with non-polar liquids, enhancing the material's selective affinity for certain substances while rejecting others (Piperopoulos et al., 2022). This property is achieved because the bentonite addition helps to stabilize the surface polarity of the polymer matrix, a highly desirable characteristic for specific functional scaffolds (Piperopoulos et al., 2022). Although specific foaming research on PLGA incorporating BT is limited in the provided sources, the consistent mechanistic effects, enhanced viscosity, maximized nucleation sites, and subsequent microstructural control, are directly applicable for engineering advanced PLGA systems for precise biomedical applications (Pakeyangkoon et al., 2009).

### 2.4.5 Summary: Comparative Role of Fillers in $scCO_2$ Foaming

Table 1. Key characteristics and functional roles of mineral fillers used in $scCO_2$ foaming of PLGA scaffolds

| **Criteria** | WLS | RHA | BT | References |
|---|---|---|---|---|
| **Chemical composition & morphology** | Calcium silicate ($CaSiO_3$) with acicular (needle-like) morphology | Predominantly amorphous silica ($SiO_2$) with porous, irregular morphology | Layered aluminosilicate with platelet structure | Chan et al., 2020; Du et al., 2024; Hadal et al., 2004; Sadykova et al., 2024 |
| **Typical particle structure** | High-aspect-ratio needles (AR ≈10-20) | Micron-sized porous particles with high surface area | Platelet-like particles, effective at micro-nano scale | Li et al., 2018; Novembre et al., 2025; Stefani et al., 2006 |
| **Role in $scCO_2$ foaming (nucleation)** | Efficient heterogeneous nucleating agent | Highly effective heterogeneous nucleation, increasing cell density | Promotes heterogeneous nucleation and suppresses coalescence | Cloarec, 2015; Du et al., 2024; Piperopoulos et al., 2022 |
| **Mechanical reinforcement** | Increases stiffness and load transfer efficiency | Improves melt strength and compressive properties | Strong reinforcement; increases modulus and viscosity | Hadal et al., 2004; Pakeyangkoon et al., 2009; Stefani et al., 2006 |
| **Effect on $CO_2$ transport** | Limits excessive $CO_2$ plasticization | Alters diffusion/desorption due to porous structure | Increases viscosity, limiting bubble growth and coalescence | Carrascosa et al., 2024; Li et al., 2018 |
| **Compatibility with PLGA** | Hydrophilic; surface modification often required | Hydrophilic; prone to aggregation without modification | Requires organo-modification for good dispersion | Donati et al., 2023; Jang et al., 2018 |

| | | | | |
|---|---|---|---|---|
| **Effect on pore morphology** | Reduces pore size, increases cell density | Narrows pore size distribution, increases cell density | Produces compact foams with small, uniform pores | Du et al., 2024; Kang et al., 2025; Stefani et al., 2006 |
| **Sustainability relevance** | Can be synthesized from waste-derived sources | High sustainability (agricultural waste origin) | Abundant, low-cost natural mineral | Novembre et al., 2025; Sadykova et al., 2024 |

## 2.5 State of art

### 2.5.1 Overview of Current Research Trends

The application of $scCO_2$ foaming represents an important processing methodology for synthesizing porous scaffolds from biodegradable polymers including Poly(lactic acid) (PLA), Poly(lactic-co-glycolic acid) (PLGA), Polycaprolactone (PCL), and Polybutylene succinate (PBS) (Liao et al., 2012; Di Maio & Kiran, 2018; Zhou et al., 2023). This technology is favoured due to its inherent advantages over conventional solvent-based methods, specifically offering solvent-free processing and utilizing the plasticization effect of $scCO_2$ to reduce processing temperatures, thus enabling the incorporation of temperature-sensitive bioactive agents (Carrascosa et al., 2024; Valor et al., 2021). Despite these benefits, a fundamental and persistent challenge lies in the inherent physicochemical limitations of the polymers themselves. Specifically, amorphous polymers like common PLGA compositions are highly susceptible to $CO_2$-induced plasticization, requiring extreme sensitivity to processing parameters to ensure cell stability, as the matrix relies exclusively on rapid vitrification during depressurization to maintain its structural integrity (Nifant'ev et al., 2024; Di Maio & Kiran, 2018).

While it has been established that a minimum pore size of $\approx 100 \mu m$ is essential for successful bone regeneration, the reproducible adaptation of scaffolds to meet these requirements remains a significant hurdle when using conventional manufacturing techniques. These techniques often lack the ability to precisely control pore size, porosity, and interconnectivity independently, which has driven recent interest in the role of precise geometric design (such as pore curvature and shape) in stimulating tissue regeneration beyond simple material composition (Zadpoor, 2015). Research confirms that reliably dictating the final morphology, including pore size, density, and interconnectivity, is exquisitely sensitive to external variables such as saturation pressure ($P$), foaming temperature ($T$), and depressurization rate ($Dr$) (Mathieu et al., 2005; Valor et al., 2021). For instance, increasing the saturation pressure significantly enhances $CO_2$ concentration in the polymer, promoting heterogeneous nucleation and resulting in smaller, denser cells. Conversely, controlling the $Dr$ involves a critical trade-off: although a fast rate is required for high nucleation, it increases the risk of catastrophic foam collapse before the plasticized polymer can fully stabilize (Carrascosa et al., 2024; Valor et al., 2021).

To mitigate the instability inherent in polymer structure and the unpredictability of external processing controls, current trends heavily leverage material formulation, particularly the incorporation of inorganic fillers. Fillers such as hydroxyapatite (HAp), bentonite (BT), wollastonite (WLS), and rice husk ash (RHA) serve a dual function: acting as potent heterogeneous nucleation

sites to ensure the development of numerous, fine cells, and actively improving the mechanical and rheological stability of the polymer melt (Carrascosa et al., 2024; Piperopoulos et al., 2022). This nucleation effect leads directly to a smaller mean pore size and an increased cell density in the resulting scaffold (Chen et al., 2024; Wang et al., 2024). Furthermore, research exploring synergistic filler effects involves high-aspect-ratio phases, such as Poly(tetrafluoroethylene) (PTFE) nanofibers and Liquid Crystal Polymer (LCP), designed to enhance internal chain entanglement and overall viscoelastic properties to resist cell coalescence (Kang et al., 2025).

The development of strategies for enhancing mechanical performance is crucial, as the increased porosity required for biomedical function inherently compromises strength (Carrascosa et al., 2024). Filler incorporation is paramount: reinforcing agents such as $Mg(OH)_2$ and HAp have been successfully integrated into PLGA systems via melt-extrusion prior to foaming, demonstrably improving compressive stresses to levels comparable with native trabecular bone *(≈1.85MPa to ≈3.81MPa*) (Carrascosa et al., 2024). The morphology of the filler profoundly influences reinforcement; fibrous materials, like Whisker and Fiber shaped $Mg(OH)_2$ particles, enhance mechanical strength due to favourable interfacial interactions and structural reinforcement, exceeding the performance provided by plate-like alternatives (Jang et al., 2018).

Beyond structural reinforcement, controlling the internal mechanics of the polymer chains, through crystallinity control and chain mobility manipulation, is a vital strategy. Increasing the crystallization rate and bulk crystallinity (e.g., in semi-crystalline polyesters like PCL and PBS) strengthens the cell walls, directly resisting collapse and improving the structural integrity necessary for durable foams (Wang et al., 2021). Techniques such as incorporating chain extenders (e.g., in PBS) are specifically used to enhance melt viscoelasticity and melt strength, ultimately optimizing foam quality and mechanical resilience (Chen et al., 2024; Tian et al., 2025).

The newest trend emphasizes combined and sequential processing strategies, moving decisively away from single-parameter optimization toward integrated system design. A successful example is the increasing use of single-step foaming and supercritical impregnation, which allows for the solvent-free loading of bioactive agents (e.g., Rutin, Olive Leaf Extract) directly into the nascent scaffold structure (García-Casas et al., 2024; Valor et al., 2021). This approach offers a powerful method for precisely tuning drug release kinetics based on the tailored scaffold morphology (Valor et al., 2021).

Further critical advancements involve pre-treatment strategies such as Hydrothermal Treatment (HT) and annealing/pre-isothermal cold crystallization. Studies, typically focusing on PCL, show that applying HT prior to scCO exposure structurally conditions the polymer, resulting in scaffolds with substantially higher porosity, better pore size distribution, and enhanced interconnectivity compared to untreated material. Importantly, the sequence is definitive: applying the HT after foaming leads almost universally to detrimental pore collapse and excessive structural fragility, confirming that the treatment's primary function is to optimize the polymer precursor's state for the subsequent foaming process (García-Jarana et al., 2025). This integration of chemical and physical processing steps is characteristic of contemporary research efforts aimed

at systematically engineering high-performance porous structures to meet complex tissue demands.

### 2.5.2 Current Research Challenges

Despite significant research advancements in adapting biodegradable scaffolds using $scCO_2$ foaming, several challenges have limited the complete realization of highly reproducible and tuneable porous architectures, particularly for complex PLGA-based systems. A foundational challenge resides in the limited volume of studies dedicated specifically to amorphous PLGA copolymers, especially those with high glycolide content (e.g., 50:50 LA:GA), when compared to the extensive literature available for semi-crystalline polyesters like PLA and PCL (Di Maio & Kiran, 2018). The amorphous nature of PLGA makes it acutely susceptible to -induced plasticization, necessitating precise control over processing windows to ensure vitrification occurs rapidly enough to stabilize the nascent cellular structure during depressurization (Di Maio & Kiran, 2018; Nifant'ev et al., 2024). The relative dearth of fundamental data pertaining to the amorphous PLGA matrix fundamentally hinders the formulation of robust predictive models necessary for translating laboratory-scale observations into scalable industrial processes.

A further critical gap concerns the insufficient mechanistic understanding of how Hydrothermal Treatment (HT) modifies the key thermodynamic and transport properties of PLGA precursors, specifically $CO_2$ solubility and diffusivity, which ultimately govern the foaming efficacy. While existing research confirms that HT effectively alters the structural morphology and enhances porosity in semi-crystalline PCL scaffolds, achieving desirable interconnectivity (García-Jarana et al., 2025), the underlying physicochemical changes induced by water penetration and chain relaxation in amorphous PLGA remain unquantified in the context of $scCO_2$ processing. Without precisely characterizing the resultant changes in the polymer's viscoelastic state, melt strength, and absorption kinetics following HT, it is impossible to predictively tailor the $scCO_2$ saturation pressure and temperature required for optimal cell nucleation and growth in the modified PLGA system.

Moreover, the literature demonstrates a clear lack of systematic studies investigating the complex coupled interactions between inorganic fillers, the polymer matrix, and the gaseous $CO_2$ phase during the dynamic foaming process. Fillers such as bentonite, rice husk ash (RHA), and magnesium hydroxide [$Mg(OH)_2$] serve multiple, often simultaneous, roles by acting as heterogeneous nucleation sites, modifying melt viscosity, and influencing crystallization kinetics (Carrascosa et al., 2024). The successful incorporation and distribution of these fillers are highly complex; instances of non-uniform filler dispersion (e.g., Mg in polymers) demonstrate that achieving optimal bulk homogeneity is a significant hurdle that often leads to structural defects and compromises final mechanical performance (Carrascosa et al., 2024). To overcome this challenge, a comprehensive, multi-variable framework is required to definitively attribute observed morphological changes, such as reduced pore size or increased cellular density, to the individual or combined effects of the filler's nucleation efficiency, its impact on the polymer's viscoelasticity, and its interaction with the penetrating $CO_2$ molecules.

This scientific complexity culminates in the difficulty of decoupling the effects of polymer chemistry, filler characteristics, and processing parameters on final foam morphology and mechanical properties. The resultant foam architecture represents a convolution of these variables, yet current experimental designs frequently focus on optimizing one or two parameters in isolation (Di Maio & Kiran, 2018). The inability to fully isolate the contribution of each component, for example, differentiating the structural consequence of a pre-foaming thermal history (such as HT) versus the instantaneous pressure drop rate (*Dr*) applied during foaming, severely restricts the ability to establish universal structure/property relationships. Consequently, technological progression stalls, as material properties and porous structure remain difficult to reproduce consistently across batches, undermining the high standards of tunability and reliability required for clinical applications of biomedical scaffolds.

Despite extensive research on $scCO_2$ foaming and isolated pre-treatment strategies, the lack of integrated studies on hydrothermally conditioned, mineral-filled amorphous PLGA represents a critical barrier to predictive scaffold design. Addressing this interaction is necessary to transition from trial-and-error fabrication to engineered microstructural control, fully exploiting the synergistic potential of combining stiffness (mineral reinforcement) with structural refinement (HT).

### 2.5.3 Summary and Link to Present Study

Based on the reviewed literature, there is a clear lack of systematic studies examining the combined effects of hydrothermal pretreatment and supercritical $CO_2$ foaming on amorphous PLGA composites containing mineral fillers. The present research aims to address this gap by experimentally analysing how hydrothermal modification influences foaming behaviour, expansion, and microstructural evolution of PLGA 75:25 systems with wollastonite, rice husk ash, and bentonite. This work therefore contributes to a deeper understanding of solvent-free, tuneable fabrication routes for biodegradable porous materials.

# 3 MATERIALS AND METHODS

## 3.1 Materials

The polymer used in this study was Resomer® RG 753 S, Poly(D,L-lactid-co-glycolid), purchased from Sigma-Aldrich (Germany), with a lactic-to-glycolic acid molar ratio of 75:25 and CAS number 26780-50-7.

Three inorganic additives were selected for their potential as nucleating agents and structural reinforcements: wollastonite (WLS), supplied by Geokom (Russia); rice husk ash (RHA), obtained from SKF Biotech (India); and bentonite (BT), provided by Silmin Ibérica (Spain). Corresponding SEM images can be seen in Figure 12.

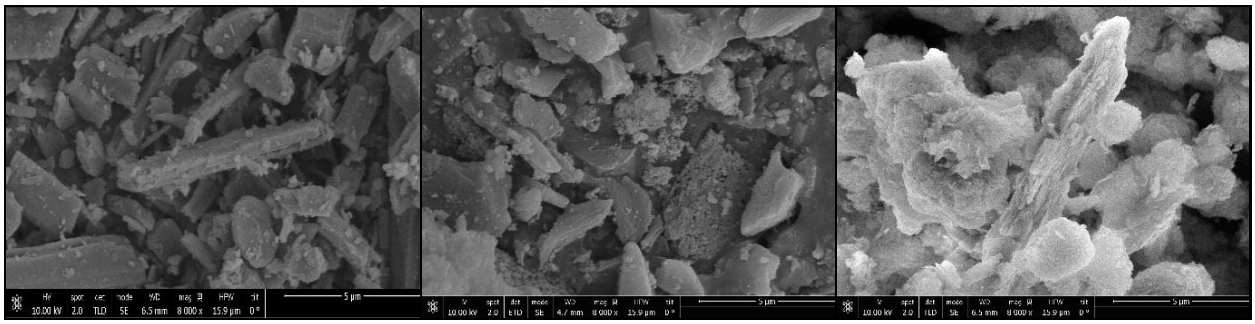

Figure 12. SEM images of the 3 additives (From left to right Wollastonite, Rice husk Ash and Bentonite)

## 3.2 Granulometric characterization

The particle size distributions of the inorganic additives: wollastonite (WLS), rice husk ash (RHA) and bentonite (BT) were characterized by laser diffraction using a Beckman Coulter LS I3 320 particle size analyser. Two independent measurements were performed for each material to ensure reproducibility. The results can be seen in Figure 13.

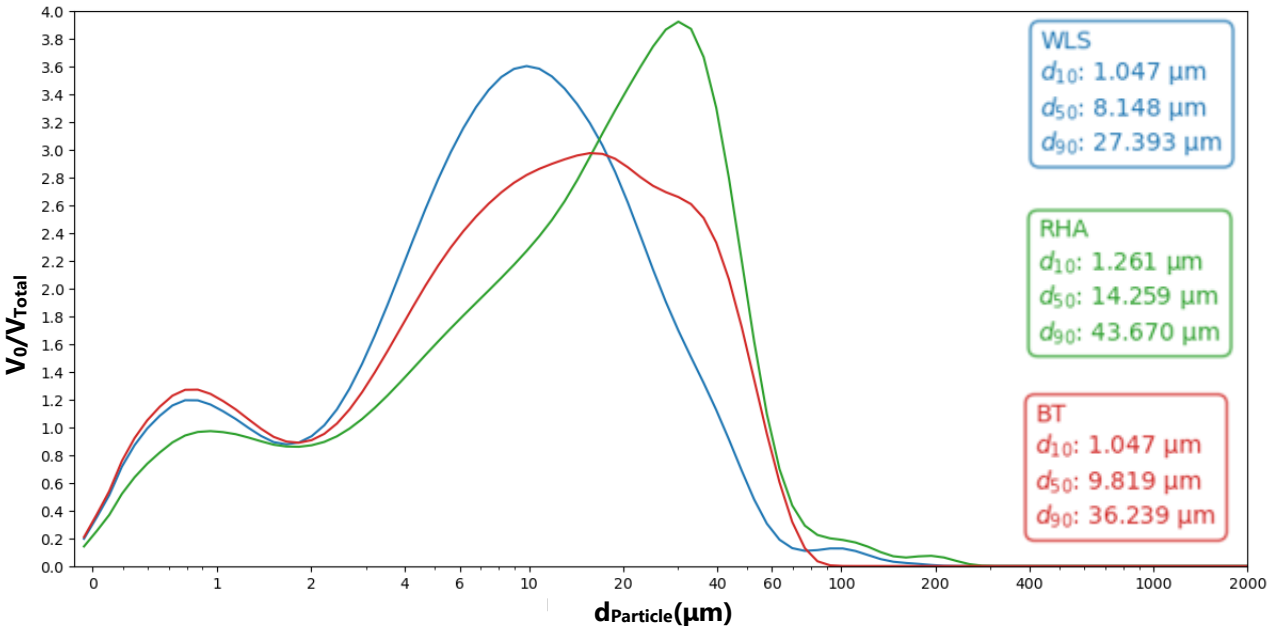


Figure 13. Particle size distribution of WLS, RHA and BT on a logarithmic scale. All additives display bimodal profiles, highlighting the coexistence of fine and coarse particle populations.

The resulting distributions were reported in terms of $d_{10}$, $d_{50}$ and $d_{90}$, corresponding to the particle diameters below which 10%, 50% and 90% of the sample volume falls, respectively. These parameters were later used to interpret the relationship between particle size, nucleation behaviour and foam morphology observed during supercritical $CO_2$ foaming.

## 3.3 Sample preparation

Mixtures were prepared manually to achieve visual homogeneity and then each sample was pressed into cylindrical pellets (approx. 7.6mm diameter × 1mm height) using a Qwik Handi Press (P/N 0016 125; Thermo Spectra Tech, Shelton, Connecticut, United States) and a 7 mm Die Set (P/N 0016 111; Thermo Spectra Tech, Shelton, Connecticut, United States) (Figure 14). Four

samples were produced per formulation. For each group, two samples were subjected to hydrothermal pretreatment followed by supercritical $CO_2$ foaming (HT + F), while the other two underwent foaming only (F).

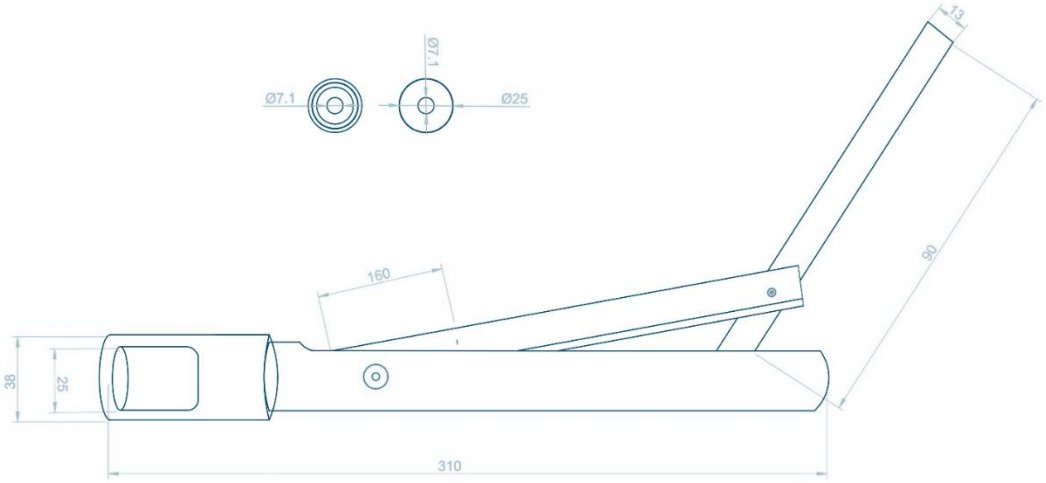


Figure 14. Schematic diagram of the pill pressing machine showing key components and dimensions.

## 3.4 Hydrothermal pretreatment (HT)

The hydrothermal treatment was conducted in a 316 stainless steel batch vessel (Parr 4570 series, *1084mL* capacity) equipped with a *2.3kW* PID-controlled electric furnace. For each trial, *750mL* of distilled water was added to the reactor (Figure 15). The PLGA pellets were individually sealed in stainless-steel mesh bags and fully submerged in the processing water. This ensures that the water reaches the entire polymer surface, avoiding direct contact with the reactor walls.

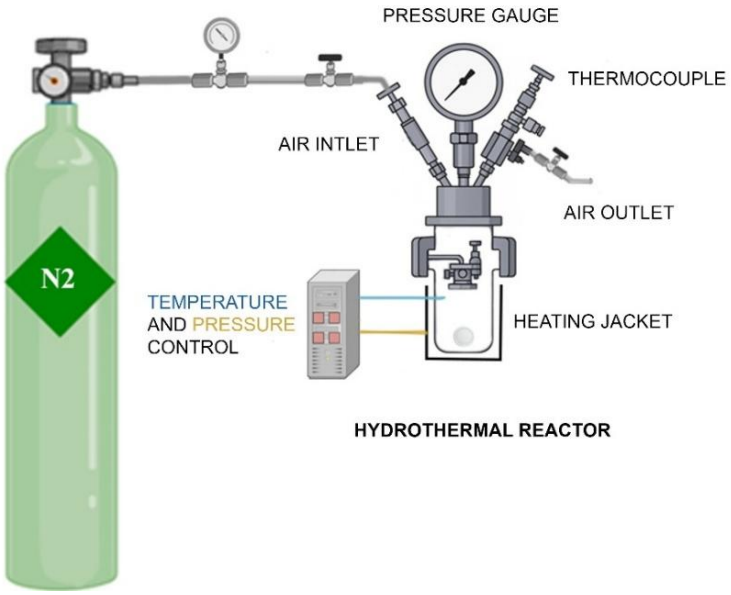


Figure 15. Schematic of the hydrothermal batch reactor system

Hydrothermal treatment was conducted at *25bar* $N_2$ pressure, *100* °C, and a duration of *10* minutes. These parameters were selected based on their proven effectiveness in the studies of (Terroba Parrado, 2025). The reactor was first purged with $N_2$. This was done to provide an inert atmosphere, mainly to avoid polymer degradation or oxidation reactions due to the oxygen

present in air. The reactor was then pressurised and heated to these target conditions. After treatment, the system was cooled to *25°C* and carefully depressurised before retrieving the samples and air-drying them.

## 3.5 Supercritical $CO_2$ foaming (F)

Following the methodology previously described in detail by (Montes et al., 2023), foaming was performed in a *257mL* stainless steel vessel of rapid expansion of supercritical solutions (RESS250; Thar Technologies®) (Figure 16) under the following conditions: *200bar* pressure (liquid $CO_2$), *45°C* and *30 minutes* processing time to achieve optimal gas dissolution in the polymer matrix.

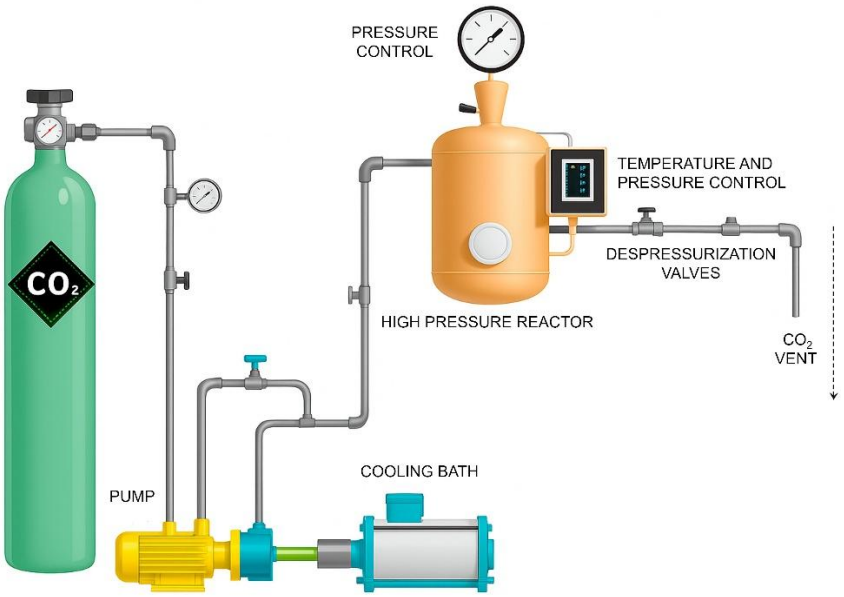


Figure 16. Schematic diagram of the foaming pilot plant.

Depressurisation was carried out rapidly (*150 bar/min*), inducing thermodynamic instability, $CO_2$ supersaturation and bubble nucleation. This resulted in pore formation and structural expansion of the polymer. Although the literature suggests that depressurization speed influences pore morphology (Di Maio & Kiran, 2018; Valor et al., 2021) , this effect was not investigated in this study. The experimental setup utilized manual depressurization valves, which limited the ability to reproducibly control variable rates. Therefore, a constant rapid rate was maintained for all trials to ensure consistency across the samples.

The following example summarizes the experimental setup that was used to conduct all the experiments.

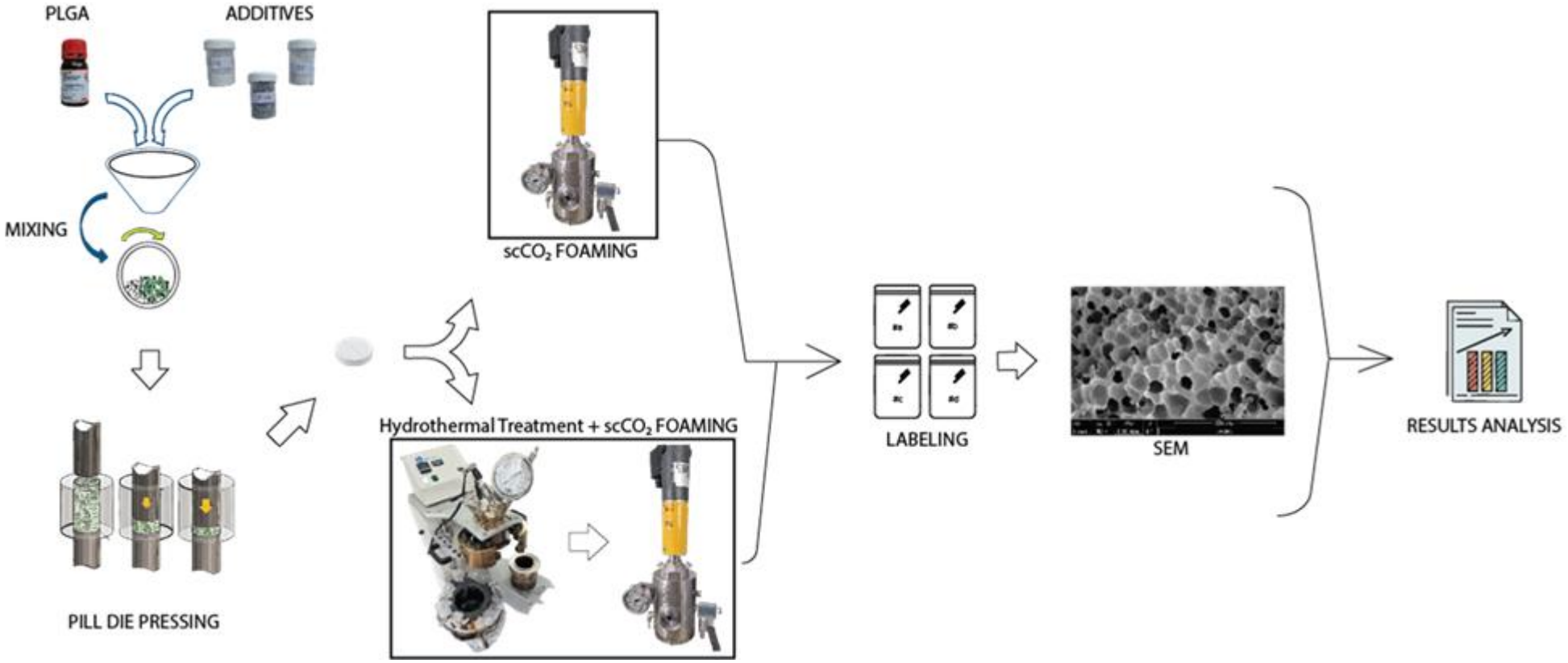


Figure 17. Experimental Setup

## 3.6 Expansion factor calculation

The expansion factor (*EF)* was estimated based on geometric volume calculations. Initially, it was assumed that the samples expanded uniformly after each processing step. This assumption was made in the absence of prior information regarding the final morphology of the foamed samples and due to the lack of alternative volume measurement techniques available at the time of the study.

The determination presented specific experimental challenges due to the small scale of the samples. The Archimedes principle (water displacement method) was initially attempted; however, it proved unfeasible due to the low mass of the samples (≈*30mg*). The buoyancy forces and surface tension prevented adequate submersion and accurate displacement readings. Consequently, a geometric approximation was adopted as the primary method.

This was calculated using Equation (3) and Equation (2), which compare the final ($V_f$) and initial ($V_i$) volumes of each sample based on cylindrical approximation, using diameter ($d$) and height ($h$) measurements obtained with a digital calliper.

$$V_{i,f} = \frac{\pi}{4} d^2 \cdot h \tag{3}$$

$$EF = V_f / V_i \tag{4}$$

Ideally, non-destructive imaging techniques such as X-ray Micro-Computed Tomography ($\mu CT$) or 3D scanning would provide the most accurate volumetric data for irregular morphologies. However, these methods were not available during the experimental phase, and subsequent analysis was not possible as most the samples underwent destructive testing for SEM characterization. Therefore, the volumes were calculated assuming a cylindrical geometry based on diameter and height measurements taken at the maximum extension points.

As a result, the calculated expansion factors should be regarded as approximate values and interpreted with caution, as they may not accurately represent the true volumetric expansion of the samples.

## 3.7 Microstructural characterisation

Selected samples were analysed using scanning electron microscopy (SEM) (FEI Nova NanoSEM 450) to evaluate surface and internal morphology. Prior to imaging the polymer samples were cryogenically fractured by immersion in liquid $N_2$ and cleaved with a blade to expose the internal structure. Each sample was then mounted to display both the cross-section and external surface. A 10nm gold layer was deposited onto the samples via cathodic sputtering (Cressington Sputter Coater 208HR) to enhance conductivity. The set of experiments is summarized in Tables 2-5 it lists the tested formulations along with their corresponding additive types, concentrations and processing methods. Each sample code indicates whether it was treated by foaming only or by

hydrothermal treatment followed by foaming. This coding system allows a clear allocation of the samples to their contents and treatment methods.

Table 2. Experimental design for PLGA without additive

| Additive Ratio | Treatment | HT-Parameters (T,P,t) | Foaming Parameters (T,P,t) | Analysis Type | Analysis Code |
|---|---|---|---|---|---|
| **0** | Foaming only | - | *45°C; 200bar; 30 min* | SEM | 0a |
| | | | | Duplicate | 0b |
| | HT + Foaming | *100°C; 25bar; 10 min* | | SEM | 0c |
| | | | | Duplicate | 0d |

Table 3. Experimental design for PLGA/Wollastonite (WLS) composites

| Additive Ratio | Treatment | HT-Parameters (T,P,t) | Foaming Parameters (T,P,t) | Analysis Type | Analysis Code |
|---|---|---|---|---|---|
| **25%** | Foaming only | - | *45°C; 200bar; 30 min* | SEM | 1a |
| | | | | Duplicate | 1b |
| | HT + Foaming | *100°C; 25bar; 10 min* | | SEM | 1c |
| | | | | Duplicate | 1d |
| **33.3%** | Foaming only | - | | SEM | 2a |
| | | | | Duplicate | 2b |
| | HT + Foaming | *100°C; 25bar; 10 min* | | SEM | 2c |
| | | | | Duplicate | 2d |

Table 4. Experimental design for PLGA/Rice Husk Ash (RHA) composites

| Additive Ratio | Treatment | HT-Parameters (T,P,t) | Foaming Parameters (T,P,t) | Analysis Type | Analysis Code |
|---|---|---|---|---|---|
| **25%** | Foaming only | - | *45°C; 200bar; 30 min* | SEM | 3a |
| | | | | Duplicate | 3b |
| | HT + Foaming | *100°C; 25bar; 10 min* | | SEM | 3c |
| | | | | Duplicate | 3d |
| **33.3%** | Foaming only | - | | SEM | 4a |
| | | | | Duplicate | 4b |
| | HT + Foaming | *100°C; 25bar; 10 min* | | SEM | 4c |
| | | | | Duplicate | 4d |

Table 5. Experimental design for PLGA/Bentonite (BT) composites

| Additive Ratio | Treatment | HT-Parameters (T,P,t) | Foaming Parameters (T,P,t) | Analysis Type | Analysis Code |
|---|---|---|---|---|---|
| **25%** | Foaming only | - | *45°C; 200bar; 30 min* | SEM | 5a |
| | | | | Duplicate | 5b |
| | HT + Foaming | *100°C; 25bar; 10 min* | | SEM | 5c |
| | | | | Duplicate | 5d |
| **33.3%** | Foaming only | - | | SEM | 6a |
| | | | | Duplicate | 6b |
| | HT + Foaming | *100°C; 25bar; 10 min* | | SEM | 6c |
| | | | | Duplicate | 6d |

The experimental design outlined in Tables 2-5 enables a systematic assessment of the effects of hydrothermal treatment and mineral fillers on the $scCO_2$ foaming behaviour of PLGA. By keeping foaming conditions constant, the influence of precursor conditioning and filler-induced nucleation on samples morphology can be directly evaluated.

## 3.8 Image Analysis and Morphological Evaluation

Due to budgetary and time constraints, the quantitative analysis of SEM images was performed on a representative subset of samples. The selected samples were chosen to include all additives (WLS, RHA, and BT) at *25* and *33.3 wt.%* ratios, processed either by foaming alone or by hydrothermal treatment followed by foaming (HT + Foaming), in order to enable a comparative assessment of the effects of additive type, additive content, and hydrothermal treatment on pore morphology and nucleation behaviour.

To quantify the cellular morphology of the foamed scaffolds, a computational image analysis approach was adopted instead of manual measurement. This method ensured statistical representativeness by processing the entire visible area of the SEM micrographs, thereby analysing hundreds of pores per sample to minimise operator bias.

The analysis was performed using a custom-developed algorithm in Python (utilising the *scikit-image* and *SciPy* libraries). The workflow consisted of the following stages:

1. Preprocessing: Raw SEM images were converted to grayscale and cropped to remove data bars. A Gaussian filter ($\sigma = 1.0$) was applied to reduce high-frequency noise while preserving pore edges.
2. Segmentation: The porous phase was distinguished from the solid PLGA matrix using Otsu's thresholding method, which automatically calculates the optimal intensity threshold to separate the foreground (pores) from the background.
3. Pore Separation: To accurately distinguish adjacent or touching pores, a Watershed algorithm was implemented based on the Euclidean distance transform. This step was critical to prevent the software from interpreting clusters of pores as single large voids.
4. Quantification: Detected features were filtered by eccentricity (<0.85) to exclude non-spherical artifacts or cracks. The area of each valid pore was measured and converted to an equivalent circular diameter ($D_{eq}$).

The resulting data were used to generate pore size distribution histograms (presented in Appendix) and the mean pore size for each sample group.

A summary of the samples, regions analysed, magnifications, treatments, and compositions considered in this evaluation is presented in Table 6.

Table 6. Selected samples, regions, and processing conditions used for SEM image analysis.

| Sample | Region | Magnification | Treatment | Additive | Wt. (%) | Justification |
|---|---|---|---|---|---|---|
| **Neat untreated** | External & Internal | 80x | None | — | — | Selected to include all three additives at 25 and 33.3 ratios, (both foaming and hydrothermal + foaming) to evaluate the effect of additive type/amount and hydrothermal treatment on internal morphology and pore nucleation. |
| **0a** | External & Internal | 40x | Foaming | None | — | |
| **0c** | External & Internal | 40x | HT + Foaming | None | — | |
| **1b** | Internal | 80x | Foaming | WLS | 25 | |
| **1c** | External | 80x | HT + Foaming | WLS | 25 | |
| **2a** | External | 40x | Foaming | WLS | 33.3 | |
| **2d** | Internal | 80x | HT + Foaming | WLS | 33.3 | |
| **3a** | External | 40x | Foaming | RHA | 25 | |
| **4b** | Internal | 80x | Foaming | RHA | 25 | |
| **4c** | External & Internal | 40x/80x | HT + Foaming | RHA | 33.3 | |
| **6b** | External & Internal | 40x/80x | Foaming | BT | 33.3 | |
| **6c** | External & Internal | 40x/80x | HT + Foaming | BT | 33.3 | |

# 4 RESULTS AND DISCUSSION

## 4.1 Morphological observations

Although the final geometry of the foamed samples often deviated from ideal cylindrical shapes this is evident as Figure 18 shows, frequently resembling discs, ovoids, or irregular morphologies, a cylindrical approximation was employed for volume estimation. While Di Maio & Kiran, (2018) describe the anisotropic nature of gas diffusion and expansion in polymer foaming, which inherently leads to irregular shapes, the use of a cylindrical approximation in this study serves as a simplified metric for relative comparison rather than an absolute morphological characterization. This approach allows for the consistent evaluation of expansion factors across different materials and processing conditions, acknowledging that precise density determination for irregular biodegradable foams often requires more advanced techniques like micro-computed tomography or water displacement methods when skin layers are intact.

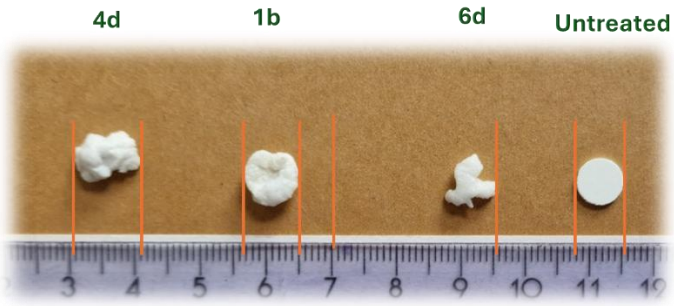


Figure 18. Final geometries of treated and untreated samples

Figure 19. presents SEM micrographs of neat PLGA (75:25) samples. In the absence of treatment, the neat PLGA exhibits a largely continuous and smooth external surface with no visible pores, consistent with findings by (Valor et al., 2021), who reported homogeneous structures with non-porous surfaces in raw PLGA prior to effective foaming optimization. While initial powder packing may influence thermal conductivity and gas diffusion pathways, the smooth surface is primarily indicative of a "solid skin" effect common in integral skin foams, where gas escapes from the surface layers before solidification.

As shown in Figure 20, neat PLGA exhibits an almost continuous and smooth external surface, with no visible pores or surface ruptures, even at higher magnifications. This observation is consistent with the formation of a solid skin layer often reported in $scCO_2$ foaming, where rapid diffusion of the blowing agent from the sample surface into the surroundings prevents stable pore nucleation at the interface (Valor et al., 2021; Zhou et al., 2024). While the bulk material expands, the depletion of $CO_2$ at the boundaries results in a non-porous exterior (Di Maio & Kiran, 2018). Consequently, a detailed analysis of these surface diffusion kinetics, rather than initial powder packing, would be required to fully characterize this skin effect, which lies beyond the scope of the present study.

Following hydrothermal pretreatment (Figure 20), morphological changes were observed. The external surface displayed increased texturing, characterized by localized protrusions and slight undulations, indicative of enhanced polymer deformation capabilities. Internally, the HT+F samples exhibited a more homogeneous porous structure with improved interconnectivity compared to the foaming-only condition. Mechanistically, this improvement aligns with the hypothesis that water uptake during HT acts as a plasticizer, increasing polymer chain mobility and free volume, thereby facilitating dissolution and diffusion. However, unlike semi-crystalline PCL, where García-Jarana et al., (2025) reported substantial porosity increases (up to 57%) due to HT-induced structural reorganization, the neat PLGA in this study showed only moderate improvements. This distinction is critical; PLGA is susceptible to hydrolytic degradation, which can reduce molecular weight and melt strength. If the melt strength drops excessively during HT, the polymer may fail to support high expansion ratios despite improved mobility.

Overall, the SEM observations indicate that while hydrothermal pretreatment improves internal pore uniformity in neat PLGA, it remains insufficient on its own to generate a fully developed, high-expansion cellular structure. This establishes a critical reference state: the significant enhancements in expansion and structural integrity observed in subsequent composite formulations likely arise from the synergistic interaction between HT and inorganic fillers. As noted

in the literature, fillers such as magnesium hydroxide or hydroxyapatite act as heterogeneous nucleation sites and rheological modifiers, counteracting the potential loss of melt strength from hydrolysis and stabilizing the cellular structure during expansion.

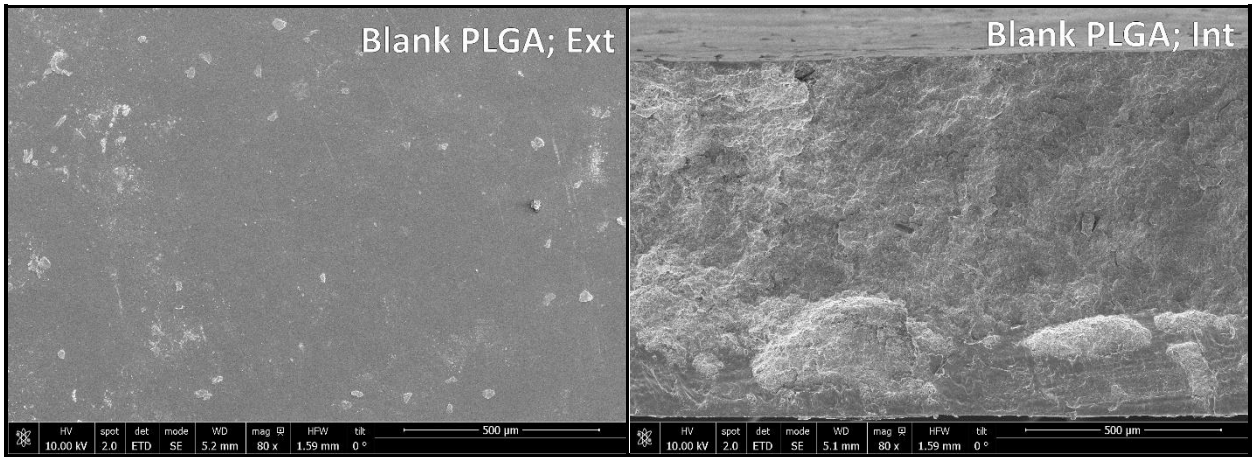


Figure 19. SEM micrographs of neat PLGA scaffolds without additive and without any processing treatment. The external surface, shown in the top left image (x80), exhibits a relatively smooth and continuous morphology with compact, rounded features and no evidence of pore formation or surface rupture. The corresponding internal micrograph, displayed in the top right image (x80), reveals a dense and homogeneous structure with the absence of a developed porous network, indicating that neither pore nucleation nor expansion occurs in the polymer matrix in the absence of foaming treatment and additives.

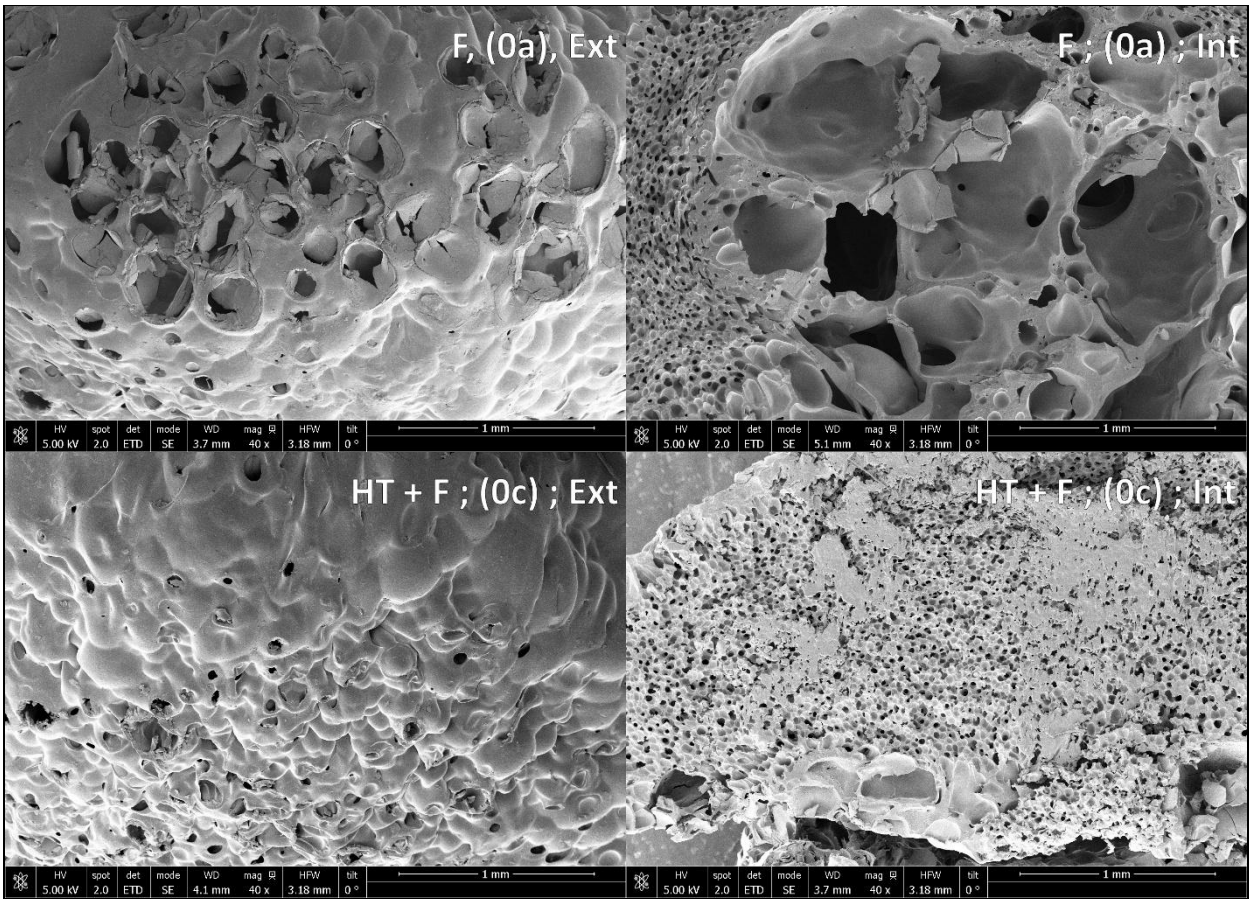


Figure 20. SEM micrographs of PLGA scaffolds processed with and without hydrothermal treatment (HT). The external surface of the non-treated sample (x40), shown in the top left image, exhibits a characteristic

"brain-like" morphology with rounded protrusions and localized ruptures, through which large surface pores (≈*250μm*) are exposed, while most of the surface remains intact. The corresponding internal micrograph, displayed in the top right image (x40), reveals a structure composed of massive, highly interconnected cavities *(800-1200μm*) linked by finer porosity, with folded or wrinkled pore walls indicative of partially developed bubbles. In contrast, the HT-treated scaffold, shown in the bottom left image (×40), presents a more compact external morphology with densely packed protrusions, reduced surface roughness, and only minor surface ruptures. The corresponding internal morphology, shown in the bottom right image (×40), displays a more homogeneous pore architecture with uniformly distributed pores (≈*36μm*), although approximately 20% of the observed area exhibits sealed or locally collapsed regions.

## 4.2 Effect of wollastonite (WLS) on expansion behaviour and pore morphology of PLGA composites

Wollastonite (WLS) exerted a significant influence on both the expansion behaviour and pore morphology of PLGA-based composites, with outcomes strongly dependent on filler concentration and the processing route (Table 7; Figures 22-23). All WLS-containing samples exhibited higher expansion factors than neat PLGA, confirming the role of wollastonite as an effective heterogeneous nucleating agent (Hadal et al., 2004). While WLS-based formulations showed moderate expansion under direct foaming conditions (F), the application of hydrothermal pretreatment prior to foaming (HT+F) resulted in a pronounced enhancement of expansion, particularly at lower filler loadings.

At 25 wt.% WLS, HT+F samples yielded the highest expansion factors among the composite systems, with sample 1c reaching a factor of 10.58. However, increasing the wollastonite content further to 33.3 wt.% resulted in a systematic reduction in expansion (e.g., samples 2c and 2d), indicating that excessive filler loading adversely affects foamability. This reduction is attributed to the interplay of several mechanisms reported in highly filled polymer foams. At elevated concentrations, mineral particles are prone to agglomeration, creating heterogeneous regions that locally restrict bubble growth (Donati et al., 2023; Mathieu et al., 2005). Furthermore, a high fraction of rigid fillers significantly increases melt stiffness and viscosity, physically constraining the ability of nucleated cells to expand (Chen et al., 2024; Kang et al., 2025). Concurrently, dense particle networks can act as physical barriers to gas transport, hindering $CO_2$ diffusion and absorption, thereby reducing the amount of blowing agent available for cell growth (Faba et al., 2024; Gao et al., 2022).

SEM observations provided further insight into the morphological effects of WLS and hydrothermal pretreatment (Figure 21). Samples processed under foaming-only conditions exhibited relatively smooth, undulating external surfaces with no visible open pores. Internally, however, these samples displayed a uniform, interconnected network with an average pore diameter of approximately 31*μm*. This structure suggests that the intrinsic acicular morphology of WLS fibres facilitated controlled heterogeneous nucleation (Chan et al., 2020), favouring the formation of evenly distributed cells.

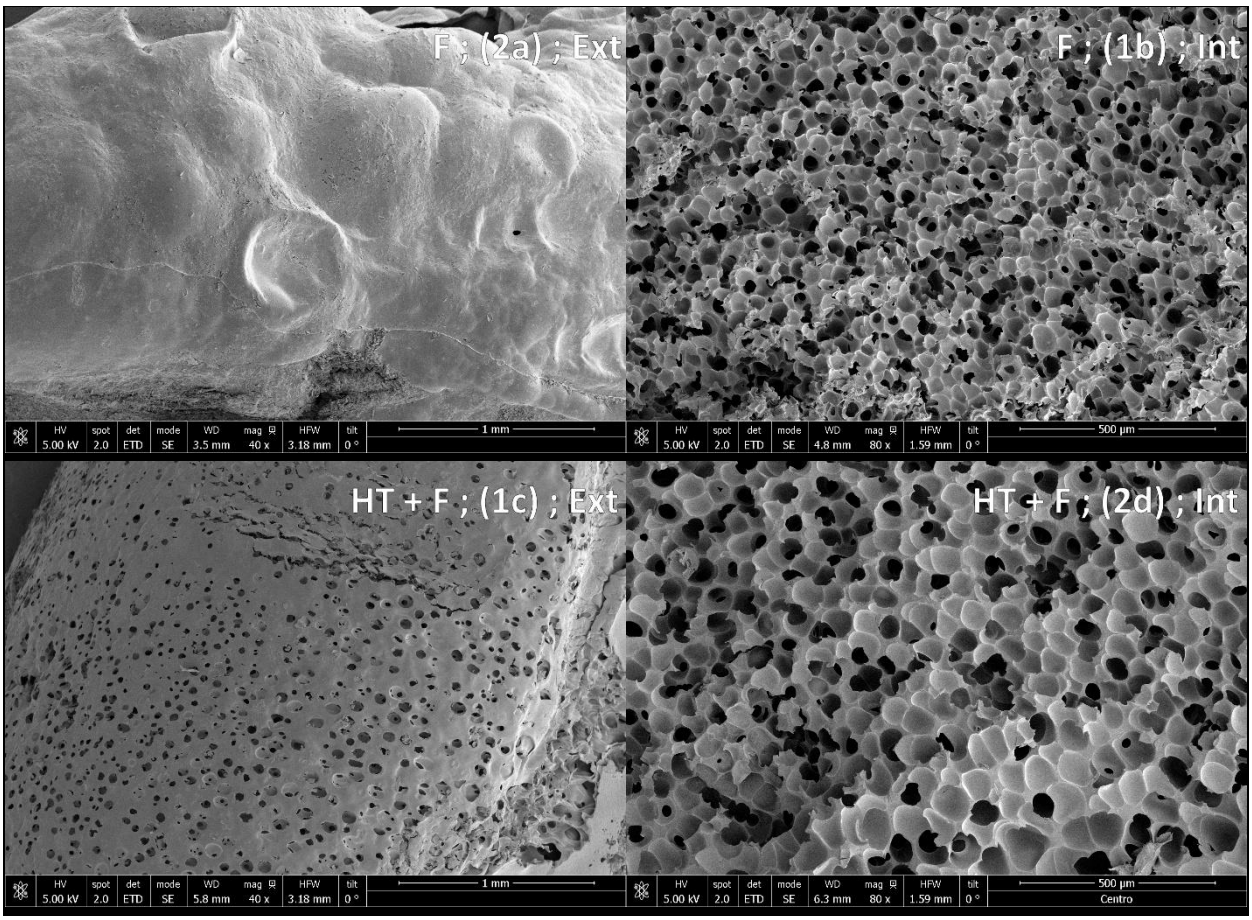


Figure 21. SEM micrographs of PLGA/WLS scaffolds processed with and without hydrothermal treatment (HT). The external surface of the non-treated sample (2a, x40), shown in the top left image, exhibits smoother protrusions with fewer surface ruptures and no visible open pores. The corresponding internal micrograph of the untreated scaffold (1b, x80), displayed in the top right image, reveals a homogeneous and well-interconnected porous network with an average pore size of approximately *30µm*, indicating moderate heterogeneous nucleation induced by wollastonite even in the absence of HT. In contrast, the HT-treated sample (1c, ×40), shown in the bottom left image, presents a smooth external surface with homogeneously distributed surface pores (≈*50µm*) and only minor, unruptured protrusions. The corresponding internal morphology (2d, ×80), shown in the bottom right image, is characterized by a highly uniform and well-interconnected pore architecture with larger pores (≈*75µm*), well-defined pore walls, and no evidence of structural collapse.

Hydrothermal pretreatment prior to foaming significantly enhanced the pore morphology. HT+F samples exhibited larger, more uniformly distributed internal pores (≈*48µm*) with mechanically stable pore walls. Notably, the external surfaces of HT+F samples displayed a homogeneous distribution of pores (≈*45µm*), contrasting with the non-porous skin observed in F-only samples. These features indicate that hydrothermal pretreatment promotes polymer chain relaxation and plasticization (García-Jarana et al., 2025), which, when combined with WLS reinforcement, enhances gas diffusion and stabilizes bubble growth, resulting in scaffolds with superior structural coherence.

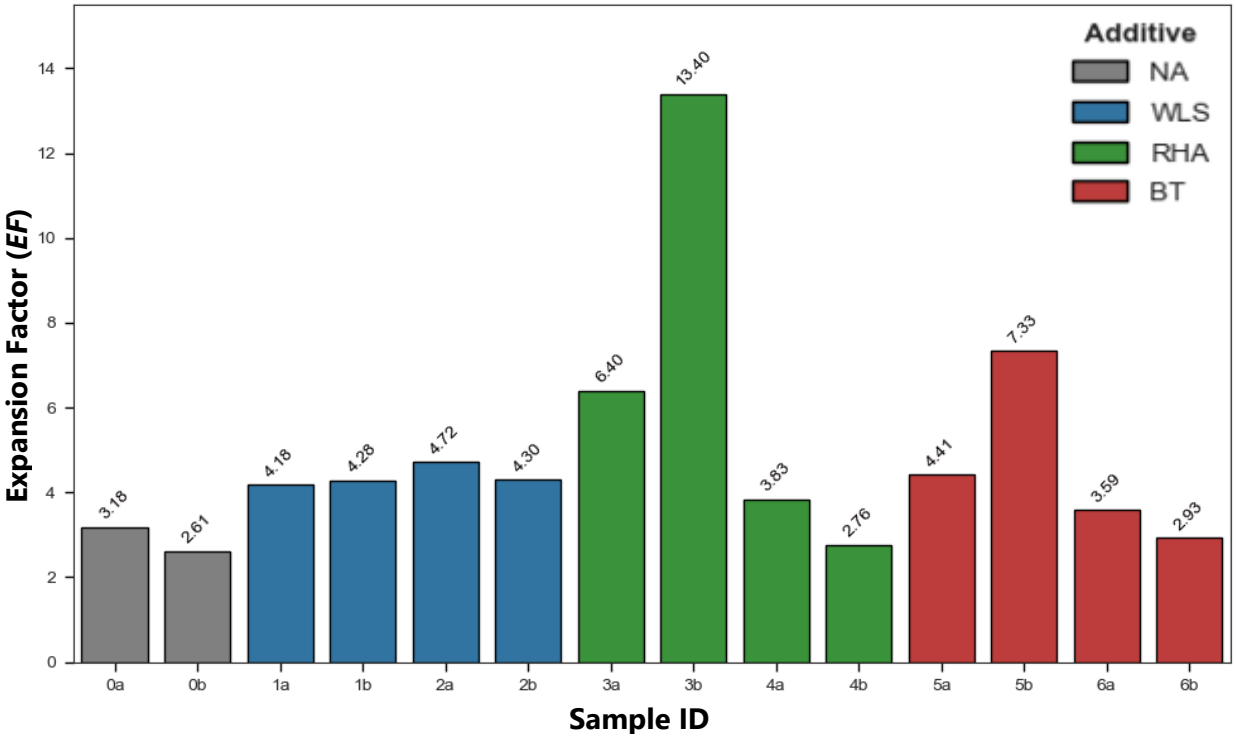


Figure 22. Comparison between expansion factors grouped by additive for foaming only.

The improvements observed can be attributed to several synergistic mechanisms. Wollastonite is widely recognized as an efficient heterogeneous nucleating agent, capable of reducing the activation energy required for bubble nucleation and promoting finer and denser cellular structures (Hadal et al., 2004). Additionally, its high aspect ratio enables WLS to function as a reinforcing filler, enhancing the mechanical stability of the polymer matrix and contributing to pore wall stabilization during bubble growth and expansion (Chan et al., 2020). These reinforcing effects appear particularly beneficial under HT+F conditions, where increased polymer chain mobility induced by plasticization could otherwise compromise foam integrity.

The beneficial role of hydrothermal pretreatment in WLS-based systems finds support in studies by Fiocco et al., (2016), who investigated wollastonite-containing glass-ceramic foams produced via $scCO_2$-assisted extrusion. They proposed a "double foaming agent" mechanism, whereby water vapour released from hydrated fillers acts synergistically with dissolved $CO_2$ to promote extensive foaming and uniform pore structures. A similar mechanism may be operative in the present study; although WLS is not a hydrated salt, it can retain moisture or possess surface hydroxyl groups arising from its synthesis and handling, potentially releasing water vapour during HT that assists the subsequent expansion.

It is hypothesized that interfacial interactions between the wollastonite filler and the polymer matrix constitute a critical determinant of final foam quality. Sadykova et al., (2024) demonstrated that surface-treated wollastonite in PVC composites improved compatibility by forming a boundary layer with restricted segmental mobility. Although no specific surface functionalization was applied to the PLGA/WLS system in the present study, it is postulated that the intrinsic acicular, needle-like morphology of the wollastonite crystals promotes physical anchoring or mechanical interlocking with the polymer chains. This mechanism is expected to facilitate filler

dispersion and reduce the energetic barrier for bubble formation, thereby enhancing nucleation efficiency, particularly when the polymer matrix undergoes chain relaxation during hydrothermal treatment.

While direct studies on hydrothermally treated PLGA/WLS systems remain limited, similar trends have been reported for other biodegradable polymers. The work of (García-Jarana et al., 2025) observed that hydrothermal pretreatment prior to $scCO_2$ foaming significantly improved pore morphology and interconnectivity in polycaprolactone (PCL) scaffolds, whereas post-foaming treatment was detrimental. These findings support the notion that hydrothermal pretreatment applied before foaming can favourably modify polymer/filler interactions and gas diffusion pathways, leading to an optimized foam architecture.

## 4.3 Effect of rice husk ash (RHA) on expansion behaviour and pore morphology of PLGA composites

The incorporation of rice husk ash (RHA) had a pronounced effect on the expansion behaviour and pore morphology of PLGA-based foams, with a strong dependence on both filler concentration and the processing route (Table 7; Figures 22-23). All RHA-containing formulations exhibited significantly higher expansion factors than neat PLGA, confirming the role of RHA as an effective heterogeneous nucleating agent during supercritical $CO_2$ foaming. Among all compositions investigated, sample 3b (25 wt.% RHA, F) exhibited the highest expansion factor of the entire study (*EF = 13.40*), highlighting the strong nucleation capability of this filler at moderate loadings.

The variability observed in the calculated expansion factors, particularly in samples such as RHA 25 wt.% (Samples 3a vs 3b), can be attributed to cumulative experimental factors. Firstly, variations in the initial volume ($V_i$) arose from the manual die-pressing process, where slight differences in applied compression force resulted in variations in initial pellet compactness and height.

Secondly, and most significantly, the anisotropic nature of the foaming process resulted in final geometries that deviated from the ideal cylinder. Since dimensions were measured at the widest points (maximum diameter and height) to apply Equation 3, the calculated volume represents a "bounding cylinder" rather than the true volume. For highly irregular samples, this method inherently overestimates the volume and amplifies differences between duplicates. Thus, the Expansion Factor should be interpreted as a relative index of foaming capacity rather than an absolute volumetric measurement.

Table 7. Summary of the sample identification codes, type and concentration of additive, treatment conditions, initial and final volume and its respective expansion factor for each formulation.

| Process | Additive | Additive-Content (wt.%) | $V_i$ ($mm^3$) | $V_f$ ($mm^3$) | Expansion Factor | Code |
|---|---|---|---|---|---|---|
| HT+F | NA | 0 | 35.87 | 103.54 | 2.89 | 0c |
| | | | 44.56 | 89.38 | 2.01 | 0d |
| | WLS | 25 | 31.23 | 330.41 | 10.58 | 1c |
| | | | 28.83 | 223.41 | 7.75 | 1d |
| | | 33.3 | 31.32 | 194.67 | 6.22 | 2c |
| | | | 30.77 | 131.95 | 4.29 | 2d |
| | RHA | 25 | 30.55 | 179.77 | 5.88 | 3c |
| | | | 26.95 | 328.72 | 12.20 | 3d |
| | | 33.3 | 24.22 | 141.67 | 5.85 | 4c |
| | | | 24.91 | 159.03 | 6.39 | 4d |
| | BT | 25 | 36.04 | 141.03 | 3.91 | 5c |
| | | | 33.35 | 135.62 | 4.07 | 5d |
| | | 33.3 | 28.58 | 110.36 | 3.86 | 6c |
| | | | 25.95 | 118.98 | 4.58 | 6d |
| F | NA | 0 | 40.01 | 127.36 | 3.18 | 0a |
| | | | 39.64 | 103.45 | 2.61 | 0b |
| | WLS | 25 | 36.84 | 153.88 | 4.18 | 1a |
| | | | 30.54 | 130.80 | 4.28 | 1b |
| | | 33.3 | 25.60 | 120.70 | 4.72 | 2a |
| | | | 34.63 | 149.01 | 4.30 | 2b |
| | RHA | 25 | 31.74 | 203.25 | 6.40 | 3a |
| | | | 10.33 | 136.09 | 13.40 | 3b |
| | | 33.3 | 32.60 | 124.93 | 3.83 | 4a |
| | | | 36.84 | 101.78 | 2.76 | 4b |
| | BT | 25 | 31.79 | 140.29 | 4.41 | 5a |
| | | | 31.85 | 233.43 | 7.33 | 5b |
| | | 33.3 | 32.52 | 116.66 | 3.59 | 6a |
| | | | 27.58 | 80.72 | 2.93 | 6b |

This behaviour is consistent with previous studies reporting that RHA particles promote bubble nucleation by providing energetically favourable sites for gas phase formation. Stefani et al., (2006) observed a similar nucleating effect in epoxy foams, where the incorporation of *6.8 wt.%* of white rice husk ash (WRHA) reduced the average bubble size from *258μm* (in pure epoxy) to *110μm*, effectively narrowing the size distribution. Likewise, Donati et al., (2023) reported that RHA (containing 93% silica) acted as an efficient nucleating agent in cassava starch foams, observing that filled samples exhibited smaller pores compared to unfilled ones due to RHA particles acting as nucleation sites. The high specific surface area and silica-rich composition of RHA, reported as high as *98.8 wt.%* $SiO_2$ in some studies, likely contribute to this behaviour by increasing the number of available nucleation sites during depressurisation.

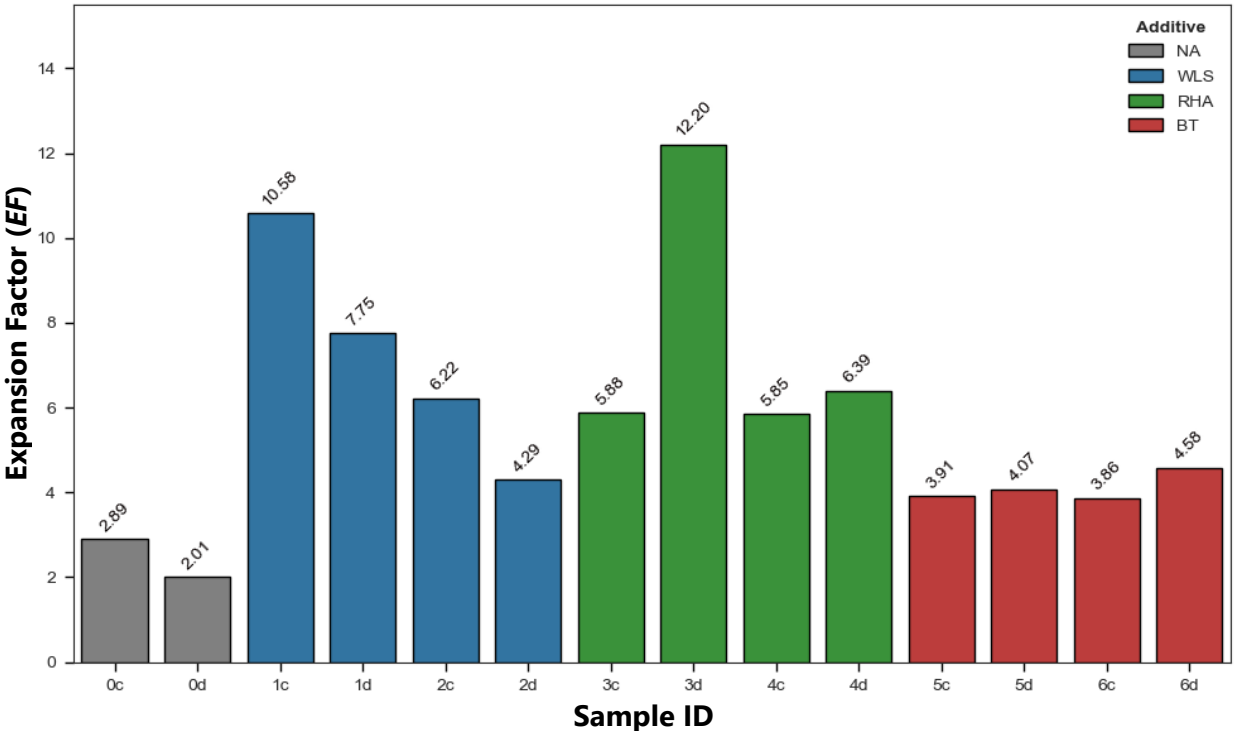


Figure 23. Comparison between expansion factors grouped by additive for HT+F

Despite its high expansion capability, SEM analysis (Figure 24) revealed notable structural instability in RHA-based foams, particularly when hydrothermal pretreatment was applied. Samples processed under foaming-only conditions exhibited relatively smoothly, cratered external surfaces with minimal surface ruptures and limited visible porosity. Internally, these samples displayed relatively uniform pore sizes (*≈30μm*); however, localized regions of collapsed or wrinkled pore walls were frequently observed, indicating uneven bubble growth and limited structural stability. In contrast, Hydrothermal Pretreatment + Supercritical $CO_2$ Foaming samples containing RHA showed markedly heterogeneous surface morphologies, characterized by irregular protrusions and very small surface pores *(≈5μm*). Internally, these samples presented irregularly sized, interconnected cavities with thin and partially collapsed pore walls, suggesting that hydrothermal pretreatment adversely affected bubble stabilization in this system. This response contrasts with the generally positive influence of hydrothermal or thermal pretreatments reported for other biodegradable polymer systems, such as PLA and PCL (Du et al., 2024; García-Jarana et al., 2025).

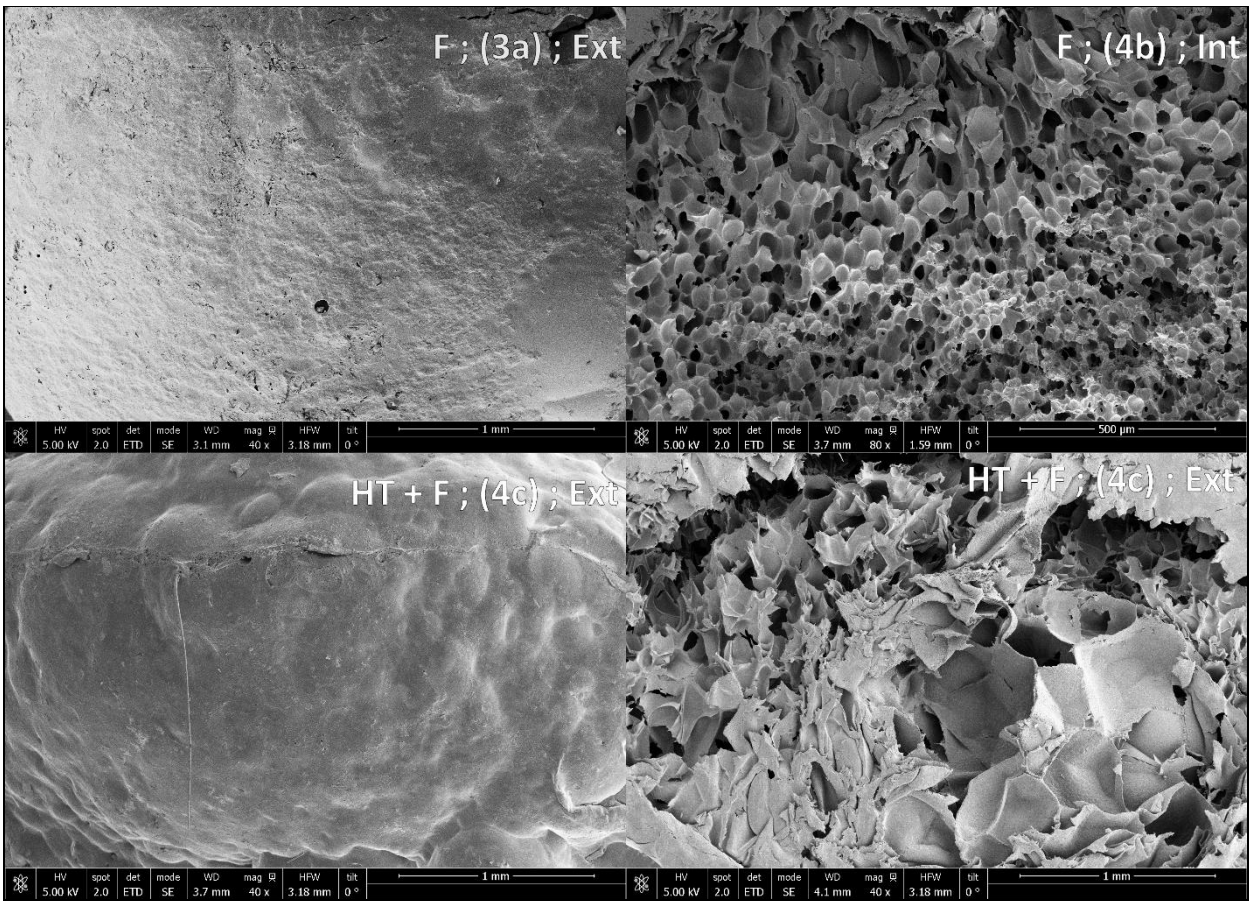


Figure 24. SEM micrographs of PLGA/RHA scaffolds processed under different conditions. External surface of sample 3a at x40 (top left) shows a relatively smooth, cratered morphology with few surface ruptures and no large open pores. Internal structure of sample 4b at x80 (top right) reveals uniformly distributed pores with an average diameter of approximately *30µm*, together with localized regions of pore collapse and folded, wax-like pore walls, likely associated with localized $CO_2$ accumulation. External surface of sample 4c at x40 (bottom left) displays non-clustered protrusions, while higher magnification (x800) highlights micropores (≈*5µm*) along seam-like regions. Internal morphology of sample 4c at ×40 (bottom right) exhibits an irregular, cavernous structure with thin, collapsed pore walls and erratically distributed voids.

In contrast, HT+F samples containing RHA showed markedly heterogeneous surface morphologies, characterized by irregular protrusions and very small surface pores (≈*5µm* at higher magnifications). Internally, these samples presented irregularly sized, interconnected cavities with thin and partially collapsed pore walls, suggesting that hydrothermal pretreatment adversely affected bubble stabilization in this system. This response contrasts with the generally positive influence of hydrothermal or thermal pretreatments reported for other biodegradable polymer systems, such as PLA and PCL (Du et al., 2024; García-Jarana et al., 2025).

A plausible explanation for this atypical behaviour lies in the interfacial incompatibility between the PLGA matrix and the silica-rich phase constituting RHA. While PLGA absorbs water and undergoes temporary plasticization during hydrothermal pretreatment, the predominantly silica-based RHA particles remain chemically inert toward the matrix, resulting in weak interfacial adhesion. Sadykova et al., 2024 reported similar behaviour in PVC/RHA composites, where microscopic analysis revealed voids surrounding RHA particles attributed to the absence of

effective physicochemical interactions. Under hydrothermal conditions, this incompatibility may be exacerbated by uneven moisture retention within the porous RHA or localized differential swelling at the interface, thereby compromising pore wall integrity during the rapid expansion of foaming.

The influence of RHA concentration further supports this interpretation. Increasing the filler content from *25wt.%* to *33.3wt.%* resulted in lower and more scattered expansion factors (samples 4a and 4b), accompanied by extensive pore collapse observed in SEM micrographs (Figure 24). Donati et al., (2023) similarly reported that excessive RHA loadings can weaken matrix-filler interactions, promote particle agglomeration, and generate internal defects. Such defects may act as stress concentration sites and increase water uptake, which, under hydrothermal pretreatment, can lead to heterogeneous moisture distribution, accelerated $CO_2$ desorption, and incomplete or uneven bubble growth.

Overall, while RHA demonstrated strong nucleation efficiency and expansion potential under direct foaming conditions, the application of hydrothermal pretreatment disrupted the balance between nucleation, interfacial adhesion, and bubble stabilization in the PLGA/RHA system. This resulted in highly expanded but structurally unstable foams, highlighting the sensitivity of RHA-filled PLGA composites to pretreatment conditions and underscoring the critical role of polymer-filler compatibility in achieving controlled and stable porous architectures.

## 4.4 Effect of bentonite (BT) on expansion behaviour and pore morphology of PLGA composites

Bentonite (BT) exhibited a markedly different foaming behaviour compared to wollastonite and rice husk ash, resulting in the lowest expansion factors among all the investigated formulations (Table 7; Figures 6-7). Both processing routes yielded limited expansion for BT-filled PLGA composites, with expansion factors remaining consistently lower than those obtained with WLS and RHA. This behaviour indicates that, under the conditions studied, bentonite is less effective as a nucleating agent for promoting volumetric expansion in PLGA foams.

Under BT-containing samples exhibited moderate to low expansion values (ranging from *2.93* to *4.41)*, with sample 5b (*25wt.%* BT, F) representing an outlier. Increasing the filler content from *25wt.%* to *33.3wt.%* resulted in a slight decrease in expansion (from *≈4.41* down to an average of *≈3.26*), indicating that filler concentration had a less decisive influence.

SEM analysis revealed pronounced differences in pore morphology between the two processing routes (Figure 25). Samples processed under F conditions exhibited external surfaces characterised by relatively regular, small protrusions containing numerous small pores. Internally, these foams displayed large and interconnected pores with sizes ranging from approximately *25µm* to *290µm*, accompanied by thick pore walls and partially collapsed regions. This heterogeneous morphology suggests unstable bubble growth and insufficient pore wall reinforcement, consistent with the limited expansion observed macroscopically.

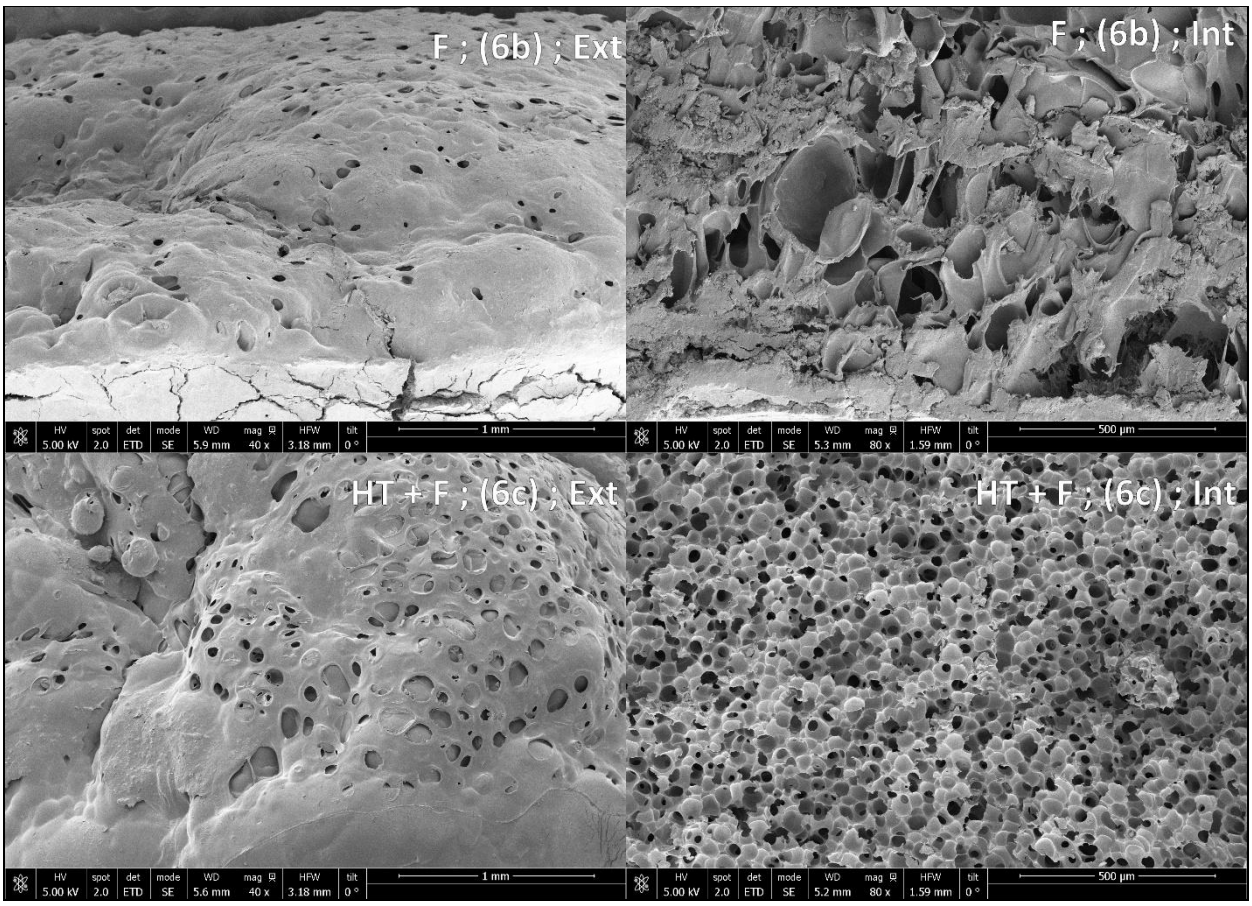


Figure 25. SEM micrographs of PLGA/BT scaffolds processed with and without hydrothermal treatment (HT). The external surface of the non-treated sample (6b, x40), shown in the top left image, exhibits a characteristic "brain-like" morphology with small, regularly spaced protrusions, along which small pores are observed. The corresponding internal micrograph (5b, x40), displayed in the top right image, reveals a cavernous structure with large pores (≈*250µm*), thick ridges, and residual collapsed membranes, resembling partially deflated cellular features. In contrast, the HT-treated scaffold, shown in the bottom left image (x40), presents an external surface characterized by surface pores of approximately *100µm* and leprous-like pits with limited interconnectivity, together with localized concave folding. The corresponding internal morphology, shown in the bottom right image (x80) (bottom right)), displays a uniform and well-interconnected pore network with an average pore size of approximately *50µm* and well-defined pore boundaries.

The limited expansion and morphological instability observed in BT-based foams can be attributed to the intrinsic characteristics of bentonite. Piperopoulos et al., (2022) reported that the incorporation of bentonite into PDMS foams increases the viscosity of the polymer-filler suspension, thereby hindering bubble flow, coalescence and growth. This increased viscosity restricts pore formation and promotes denser, more compact foam structures with reduced expansion. Additionally, high bentonite loadings may exacerbate structural heterogeneity and brittleness due to particle agglomeration and stress concentration effects.

In contrast, hydrothermal pretreatment prior to foaming led to a notable improvement in pore morphology for BT-containing samples, despite only modest changes in expansion factor. HT+F samples exhibited external surfaces with larger, more uniformly distributed pores (≈*45µm*) and only minor localised irregularities. Internally, these samples displayed a significantly more uniform

and interconnected pore structure with average pore sizes of approximately *31µm* and clearly defined, stable pore walls. This morphological improvement indicates enhanced bubble stabilisation and improved foam homogeneity resulting from hydrothermal pretreatment.

The positive influence of Hydrothermal Treatment (HT) on bentonite-based foams suggests that hydrothermal conditions optimize the interfacial coupling between the filler and the PLGA matrix primarily through polymer conditioning. While specific studies characterize bentonite as possessing a hydrophobic nature suitable for applications like oil absorption (Sadykova et al., 2024), achieving the structural benefits of exfoliation or intercalation in polymer composites typically requires prior chemical organo-modification (Pakeyangkoon et al., 2009). Therefore, rather than altering the filler's chemistry, exposure to elevated temperature and pressure likely drives plasticization and chain relaxation within the polymer matrix (García-Jarana et al., 2025). This enhanced macromolecular mobility may facilitate better wetting of the bentonite particles by the polymer chains, thereby mitigating the structural defects associated with particle agglomeration and improving pore wall stability.

Similar effects of surface treatment on foaming behaviour have been emphasized by de Macedo Rooweder Lima, (2024), who noted the importance of filler compatibility for dispersion and mechanical performance. In the context of PLGA/BT systems, HT appears to act as a physical processing aid that partially overcomes the limitations imposed by bentonite's inherent tendency to increase system viscosity and restrict bubble growth (Sadykova et al., 2024). Consequently, the observed improvements in pore morphology align with findings of García-Jarana et al., (2025), where pre-foaming hydrothermal treatment significantly enhanced pore uniformity and interconnectivity in biodegradable polyesters. These observations indicate that utilizing pretreatment protocols can effectively modulate the morphological development of composite scaffolds, facilitating the formation of interconnected cellular structures in systems processed via supercritical $CO_2$.

The incorporation of bentonite into the polymer matrix restricted overall cell expansion, likely due to an increase in system viscosity that hinders bubble flow and coalescence. However, the application of hydrothermal pretreatment prior to foaming significantly mitigated these limitations by modifying the resulting scaffold architecture. Consistent with findings reported by García-Jarana et al., (2025) for other biodegradable polyesters, the HT+F processing route successfully enhanced pore uniformity and interconnectivity in the PLGA/BT system. These observations indicate that, although bentonite remained the least effective filler in terms of expansion factor, the utilization of pretreatment protocols can effectively modulate the morphological development, enabling the formation of structurally homogeneous and interconnected cellular networks even in systems with high filler-induced viscosity.

# 5 CONCLUSIONS

Hydrothermal pretreatment (HT) prior to supercritical $CO_2$ foaming significantly influenced the foaming behaviour and pore morphology of PLGA-based systems. In neat PLGA, HT enhanced internal pore uniformity and interconnectivity; however, it was insufficient to generate high expansion ratios, likely due to the limited melt strength of the polymer and its susceptibility to hydrolytic degradation. Nevertheless, HT consistently promoted polymer chain mobility and gas diffusion, establishing favourable conditions for foam development when combined with reinforcing fillers. These findings confirm that HT functions primarily as a polymer-conditioning step rather than an independent foaming enhancer.

All mineral fillers acted as heterogeneous nucleating agents, yet their effectiveness was strongly dependent on filler type and concentration. Wollastonite (WLS) and Rice Husk Ash (RHA) promoted substantially higher expansion factors than bentonite (BT), confirming the critical role of filler morphology and interfacial compatibility in controlling foamability. At moderate loading (*25wt.%*), WLS and RHA exhibited optimal nucleation efficiency, whereas excessive filler contents (*33.3 wt.%*) generally reduced expansion. This reduction is attributed to particle agglomeration, excessive melt stiffness, and restricted gas transport mechanisms reported in highly filled composites (Donati et al., 2023; Mathieu et al., 2005).

Among the fillers investigated, wollastonite exhibited the most favourable synergy with hydrothermal pretreatment. The HT+F processing route yielded the highest expansion factors and the most mechanically stable pore structures. This success is attributed to the combined effects of HT-induced polymer chain relaxation and the acicular morphology of WLS, which facilitated effective heterogeneous nucleation and pore wall reinforcement (Chan et al., 2020; Hadal et al., 2004). These results demonstrate that HT can amplify the reinforcing functions of compatible mineral fillers, leading to scaffolds with superior structural coherence.

Conversely, while RHA displayed exceptional nucleation efficiency under direct foaming conditions, the application of hydrothermal pretreatment adversely affected pore stability. HT+F samples containing RHA exhibited heterogeneous morphologies and extensive pore collapse. This suggests that weak interfacial adhesion between the PLGA matrix and silica-rich RHA, combined with uneven moisture retention at the interface, undermines bubble stabilization during expansion (Sadykova et al., 2024). This finding highlights the sensitivity of RHA-filled systems to pretreatment conditions.

Finally, bentonite was the least effective filler regarding expansion factor, primarily due to its strong viscosity-enhancing effect which restricts bubble growth (Sadykova et al., 2024). However, hydrothermal pretreatment significantly improved pore uniformity and interconnectivity in BT-filled composites despite modest gains in expansion. This indicates that HT can partially mitigate rheological constraints by enhancing polymer wetting and interfacial coupling, enabling the formation of structurally homogeneous foams even in highly viscous systems.

## 5.1 Limitation and future perspective

A major technical limitation of the pilot equipment used was the manual operation of the depressurization valves. Although a rapid reference rate (*≈150 bar/min*) was established to induce effective nucleation in all samples, the lack of automated control prevented a systematic study of the influence of different depressurization rates (*Dr*) on cell morphology. Because manual operation makes it difficult to accurately and repetitively reproduce specific intermediate rates or gradients, this parameter was kept constant. Therefore, automation of the valve system is recommended for future research, as this would allow the kinetic effect of the pressure drop rate on pore size and cell density of PLGA scaffolds to be isolated and quantified.

# 6 REFERENCES


Adsorbent. (2021). In *Interface Science and Technology* (Vol. 33, pp. 71–210). Elsevier. https://doi.org/10.1016/B978-0-12-818805-7.00009-6

Álvarez, I., Gutiérrez, C., Rodríguez, J. F., de Lucas, A., & García, M. T. (2020). Production of biodegradable PLGA foams processed with high pressure CO2. *The Journal of Supercritical Fluids*, *164*, 104886. https://doi.org/10.1016/j.supflu.2020.104886

Anderson, J. M., & Shive, M. S. (1997). Biodegradation and biocompatibility of PLA and PLGA microspheres. *Advanced Drug Delivery Reviews, Biodegradable Microspheres/Therapeutic Peptide Delivery*, *28*(1), 5–24. https://doi.org/10.1016/S0169-409X(97)00048-3

Bhattacharya, S., Sharma, D., Saurabh, S., De, S., Sain, A., Nandi, A., & Chowdhury, A. (2013). Plasticization of Poly(vinylpyrrolidone) Thin Films under Ambient Humidity: Insight from Single-Molecule Tracer Diffusion Dynamics. *The Journal of Physical Chemistry. B*, *117*. https://doi.org/10.1021/jp401704e

Bhuyan, S. (2023, February 16). Carbon Dioxide (CO2) Phase Diagram. *Chemistry Learner*. https://www.chemistrylearner.com/co2-phase-diagram.html

Carrascosa, F., García, M. T., Ramos, M. J., García-Vargas, J. M., Rodríguez, J. F., & Gracia, I. (2024). Enhancing polymeric bone scaffolds mechanical characteristics using supercritical CO2 foaming and reinforcing agents. *Journal of the Taiwan Institute of Chemical Engineers*, *162*, 105619. https://doi.org/10.1016/j.jtice.2024.105619

Chan, J. X., Wong, J. F., Hassan, A., Shrivastava, N. K., Mohamad, Z., & Othman, N. (2020). Green hydrothermal synthesis of high aspect ratio wollastonite nanofibers: Effects of reaction medium, temperature and time. *Ceramics International*, *46*(14), 22624–22634. https://doi.org/10.1016/j.ceramint.2020.06.025

Chen, Z., Yin, X., Chen, H., Fu, X., Sun, Y., Chen, Q., Liu, W., & Shen, X. (2024). Mechanical, Crystallization, Rheological, and Supercritical CO2 Foaming Properties of Polybutylene Succinate Nanocomposites: Impact of Carbon Nanofiber Content. *Polymers*, *16*(1), Article 1. https://doi.org/10.3390/polym16010028

Cloarec, T. (2015, May). *Processing and Characterization of Polycarbonate Foams with Supercritical Co2 and 5-Phenyl-1H-tetrazole* [Thesis or Dissertation]. University of North Texas. UNT Digital Library. https://doi.org/10.12794/metadc799500

de Macedo Rooweder Lima, G. (2024). *Sustainable foaming using supercritical carbon dioxide and biopolymers*. University of Groningen. https://doi.org/10.33612/diss.1001496266

Di Maio, E., & Kiran, E. (2018). Foaming of polymers with supercritical fluids and perspectives on the current knowledge gaps and challenges. *The Journal of Supercritical Fluids, 30th Year Anniversary Issue of the Journal of Supercritical Fluids*, *134*, 157–166. https://doi.org/10.1016/j.supflu.2017.11.013

Donati, N., Spada, J. C., & Tessaro, I. C. (2023). Recycling rice husk ash as a filler on biodegradable cassava starch-based foams. *Polymer Bulletin*, *80*(9), 10231–10248. https://doi.org/10.1007/s00289-022-04557-9

Du, J., Yang, H., & Zhao, X. (2024). Preparation of tomato peel pomace powder/polylactic acid foams under supercritical CO2 conditions: Improvements in cell structure and foaming behavior. *International Journal of Biological Macromolecules*, *270*, 132480. https://doi.org/10.1016/j.ijbiomac.2024.132480

Edrees, S. J., Shukur, M. M., & Obeid, M. M. (2018). First-principle analysis of the structural, mechanical, optical and electronic properties of wollastonite monoclinic polymorph. *Computational Condensed Matter*, *14*, 20–26. https://doi.org/10.1016/j.cocom.2017.12.004

Faba, S., Agüero, Á., Arrieta, M. P., Martínez, S., Romero, J., Torres, A., & Galotto, M. J. (2024). Foaming of 3D-Printed PLA/CaCO3 Composites by Supercritical CO2 Process for Sustainable Food Contact Materials. *Polymers*, *16*(6), Article 6. https://doi.org/10.3390/polym16060798

Fiocco, L., Ferroni, L., Gardin, C., Zavan, B., Secco, M., Matthews, S., & Bernardo, E. (2016). Wollastonite-diopside glass-ceramic foams from supercritical carbon dioxide-assisted extrusion of a silicone resin and inorganic fillers. *Journal of Non-Crystalline Solids*, *443*, 33–38. https://doi.org/10.1016/j.jnoncrysol.2016.04.012

Gao, X., Chen, Y., Chen, P., Xu, Z., Zhao, L., & Hu, D. (2022). Supercritical CO2 foaming and shrinkage resistance of thermoplastic polyurethane/modified magnesium borate whisker composite. *Journal of CO2 Utilization*, *57*, 101887. https://doi.org/10.1016/j.jcou.2022.101887

García-Casas, I., Valor, D., Elayoubi, H., Montes, A., & Pereyra, C. (2024). Morphological 3D Analysis of PLGA/Chitosan Blend Polymer Scaffolds and Their Impregnation with Olive Pruning Residues via Supercritical CO2. *Polymers*, *16*(11), Article 11. https://doi.org/10.3390/polym16111451

García-Jarana, B., Valor*, D., García-Casas, I., Jezabel Sánchez-Oneto, Casimiro Mantell, Juan R. Portela, & Clara Pereyra. (2025). Hydrothermal treatment to enhance supercritical CO2 poly-3 caprolactone foaming processes for tissue engineering scaffolds. *Polymers*, *16*.

Gonçalves, E. S., Poulsen, L., & Ogilby, P. R. (2007). Mechanism of the temperature-dependent degradation of polyamide 66 films exposed to water. *Polymer Degradation and Stability*, *92*(11), 1977–1985. https://doi.org/10.1016/j.polymdegradstab.2007.08.007

Hadal, R. S., Dasari, A., Rohrmann, J., & Misra, R. D. K. (2004). Effect of wollastonite and talc on the micromechanisms of tensile deformation in polypropylene composites. *Materials Science and Engineering: A*, *372*(1), 296–315. https://doi.org/10.1016/j.msea.2004.01.003

Heller, J., Barr, J., Ng, S. Y., Shen, H.-R., Schwach-Abdellaoui, K., Emmahl, S., Rothen-Weinhold, A., & Gurny, R. (2000). Poly(ortho esters) – their development and some recent applications. *European Journal of Pharmaceutics and Biopharmaceutics*, *50*(1), 121–128. https://doi.org/10.1016/S0939-6411(00)00085-0

Jang, H. J., Park, S.-B., Bedair, T. M., Oh, M.-K., Ahn, D.-J., Park, W., Joung, Y. K., & Han, D. K. (2018). Effect of various shaped magnesium hydroxide particles on mechanical and biological properties of poly(lactic-*co*-glycolic acid) composites. *Journal of Industrial and Engineering Chemistry*, *59*, 266–276. https://doi.org/10.1016/j.jiec.2017.10.032

Jiang, C., Han, S., Chen, S., Zhou, H., & Wang, X. (2021). The role of PTFE in-situ fibrillation on PET microcellular foaming. *Polymer*, *212*, 123171. https://doi.org/10.1016/j.polymer.2020.123171

Kang, J., Liu, H., Bai, C., Liu, S., Chen, S., & Wang, X. (2025). Effect of simultaneous in-situ fibrillation of LCP and PTFE on PA12T composites and their supercritical CO2 foaming behavior. *Polymer*, *319*, 128070. https://doi.org/10.1016/j.polymer.2025.128070

Kopuru, V. N., Gayathri, J. R., & Vanama, R. K. (2025). Sustainable rice husk ash aggregates: Optimized production and performance for eco-efficient concrete. *Journal of Building Engineering*, *113*, 113999. https://doi.org/10.1016/j.jobe.2025.113999

Kreua-ongarjnukool, N., Soomherun, N., Niyomthai, S. T., Chumnanvej, S., Kreua-ongarjnukool, N., Soomherun, N., Niyomthai, S. T., & Chumnanvej, S. (2021). Aliphatic Polyester Nanoparticles for Drug Delivery Systems. In *Smart Drug Delivery*. IntechOpen. https://doi.org/10.5772/intechopen.100977

Lei, Z., Wang, E., Li, Z., & Shi, X. (2025). Ultrafine rice husk ash in alkali-activated slag systems: Synergistic modulation of *Si/Ca* and *Si/Al* ratios to improve mechanical performance and dimensional stability. *Construction and Building Materials*, *492*, 142969. https://doi.org/10.1016/j.conbuildmat.2025.142969

Li, C., Feng, L.-F., Gu, X.-P., Cao, K., & Zhang, C.-L. (2018). *In situ* visualization on formation mechanism of bi-modal foam *via* a two-step depressurization approach. *The Journal of Supercritical Fluids*, *135*, 8–16. https://doi.org/10.1016/j.supflu.2017.12.005

Liao, X., Zhang, H., & He, T. (2012). Preparation of Porous Biodegradable Polymer and Its Nanocomposites by Supercritical CO2 Foaming for Tissue Engineering. *Journal of Nanomaterials*, *2012*(1), 836394. https://doi.org/10.1155/2012/836394

Ma, W., & Yan, L. (2025). Mechanical and chemical effects of wet-dry cycling and UV exposure on flax textile reinforced recycled aggregate concrete: Role of rice husk ash. *Journal of Building Engineering*, *114*, 114177. https://doi.org/10.1016/j.jobe.2025.114177

Machado, N. D., Mosquera, J. E., Martini, R. E., Goñi, M. L., & Gañán, N. A. (2022). Supercritical CO2-assisted impregnation/deposition of polymeric materials with pharmaceutical, nutraceutical, and biomedical applications: A review (2015–2021). *The Journal of Supercritical Fluids*, *191*, 105763. https://doi.org/10.1016/j.supflu.2022.105763

Makadia, H. K., & Siegel, S. J. (2011). Poly Lactic-co-Glycolic Acid (PLGA) as Biodegradable Controlled Drug Delivery Carrier. *Polymers*, *3*(3), 1377–1397. https://doi.org/10.3390/polym3031377

Mathieu, L. M., Montjovent, M.-O., Bourban, P.-E., Pioletti, D. P., & Månson, J. -a. E. (2005). Bioresorbable composites prepared by supercritical fluid foaming. *Journal of Biomedical Materials Research Part A*, *75A*(1), 89–97. https://doi.org/10.1002/jbm.a.30385

Montes, A., Valor, D., Penabad, Y., Domínguez, M., Pereyra, C., & de la Ossa, E. M. (2023). Formation of PLGA–PEDOT: PSS Conductive Scaffolds by Supercritical Foaming. *Materials*, *16*(6), Article 6. https://doi.org/10.3390/ma16062441

Mukasheva, F., Adilova, L., Dyussenbinov, A., Yernaimanova, B., Abilev, M., & Akilbekova, D. (2024). Optimizing scaffold pore size for tissue engineering: Insights across various tissue types. *Frontiers in Bioengineering and Biotechnology*, *12*. https://doi.org/10.3389/fbioe.2024.1444986

Nifant'ev, I. E., Tavtorkin, A. N., Shlyakhtin, A. V., & Ivchenko, P. V. (2024a). Chemical features of the synthesis, degradation, molding and performance of poly(lactic-*co*-glycolic) acid (PLGA) and PLGA-based articles. *European Polymer Journal*, *215*, 113250. https://doi.org/10.1016/j.eurpolymj.2024.113250

Nifant'ev, I. E., Tavtorkin, A. N., Shlyakhtin, A. V., & Ivchenko, P. V. (2024b). Chemical features of the synthesis, degradation, molding and performance of poly(lactic-*co*-glycolic) acid (PLGA) and PLGA-based articles. *European Polymer Journal*, *215*, 113250. https://doi.org/10.1016/j.eurpolymj.2024.113250

Novembre, D., Gimeno, D., Marinangeli, L., Tangari, A. C., Rosatelli, G., Ciulla, M., di Profio, P., Rainone, M. L., & Calista, M. (2025). Single-step solid-state synthesis and characterization of Wollastonite-2M by rice husk ash. *Ceramics International*. https://doi.org/10.1016/j.ceramint.2025.09.458

Nzereogu, P. U., Omah, A. D., Ezema, F. I., Iwuoha, E. I., & Nwanya, A. C. (2023). Silica extraction from rice husk: Comprehensive review and applications. *Hybrid Advances*, *4*, 100111. https://doi.org/10.1016/j.hybadv.2023.100111

Pakeyangkoon, P., Magaraphan, R., Malakul, P., & Nithitanakul, M. (2009). Polymeric foam via polymerized high internal phase emulsion filled with organo-modified bentonite. *Journal of Applied Polymer Science*, *114*(5), 3041–3048. https://doi.org/10.1002/app.30091

Piperopoulos, E., Calabrese, L., Jovanovic, V. S., Nikolic, J., Ciric, S., Milone, C., & Proverbio, E. (2022). Bentonite-PDMS composite foams for oil spill recovery: Sorption performance and kinetics. *Journal of Applied Polymer Science*, *139*(41), e53003. https://doi.org/10.1002/app.53003

Rodriguez, D. E., Guiza-Arguello, V., Ochoa, O. O., Gharat, T., Sue, H. J., Lafdi, K., & Hahn, M. S. (2016). Development of a hydroxyapatite-poly(d,l-lactide-co-glycolide) infiltrated carbon foam for orthopedic applications. *Carbon*, *98*, 106–114. https://doi.org/10.1016/j.carbon.2015.10.086

Sadykova, D. F., Budylin, N. Yu., Nikulova, U. V., Shapagin, A. V., & Gotlib, E. M. (2024). Influence of rice husk ash and wollastonite on plasticizer migration in polyvinyl chloride system. *Journal of Applied Polymer Science*, *141*(1), e54748. https://doi.org/10.1002/app.54748

Shen, Y., Tu, T., Yi, B., Wang, X., Tang, H., Liu, W., & Zhang, Y. (2019). Electrospun acid-neutralizing fibers for the amelioration of inflammatory response. *Acta Biomaterialia*, *97*, 200–215. https://doi.org/10.1016/j.actbio.2019.08.014

Stefani, P. M., Cyras, V., Tejeira Barchi, A., & Vazquez, A. (2006). Mechanical properties and thermal stability of rice husk ash filled epoxy foams. *Journal of Applied Polymer Science*, *99*(6), 2957–2965. https://doi.org/10.1002/app.23001

Sun, F., Sun, X., Wang, H., Li, C., Zhao, Y., Tian, J., & Lin, Y. (2022). Application of 3D-Printed, PLGA-Based Scaffolds in Bone Tissue Engineering. *International Journal of Molecular Sciences*, *23*(10), 5831. https://doi.org/10.3390/ijms23105831

Tai, H., Upton, C. E., White, L. J., Pini, R., Storti, G., Mazzotti, M., Shakesheff, K. M., & Howdle, S. M. (2010). Studies on the interactions of CO2 with biodegradable poly(dl-lactic acid) and poly(lactic acid-*co*-glycolic acid) copolymers using high pressure ATR-IR and high pressure rheology. *Polymer*, *51*(6), 1425–1431. https://doi.org/10.1016/j.polymer.2010.01.065

Terroba Parrado, R. (2025). *Estudio del Pretratamiento Hidrotérmico de Polímeros para Mejorar su Uso en Aplicaciones Biomédicas* [Master thesis]. https://rodin.uca.es/handle/10498/36006

Tian, H., Wang, Zepeng, Yu, J., Zhao, Y., Pan, H., Bian, J., Yang, H., Wang, Zhibing, & Zhang, H. (2025). Preparation of high elastic bimodal cells biodegradable foam. *Polymer*, *318*, 127987. https://doi.org/10.1016/j.polymer.2024.127987

Valor, D., Montes, A., Monteiro, M., García-Casas, I., Pereyra, C., & Martínez de la Ossa, E. (2021). Determining the Optimal Conditions for the Production by Supercritical CO2 of Biodegradable PLGA Foams for the Controlled Release of Rutin as a Medical Treatment. *Polymers*, *13*(10), Article 10. https://doi.org/10.3390/polym13101645

Wang, X., Wang, C., Chu, C., Xue, F., Li, J., & Bai, J. (2024). Structure-function integrated biodegradable Mg/polymer composites: Design, manufacturing, properties, and biomedical applications. *Bioactive Materials*, *39*, 74–105. https://doi.org/10.1016/j.bioactmat.2024.05.024

Wang, Y., Mi, J., Du, Z., Chen, S., Zhang, C., & Wang, X. (2021). Peculiar micro and nano cell morphology of PBT/PTFE nanofibrillated composite foams of supercritical CO2 foaming induced by in-situ formed 3D PTFE nanofiber networks. *Polymer*, *232*, 124165. https://doi.org/10.1016/j.polymer.2021.124165

Zadpoor, A. A. (2015). Bone tissue regeneration: The role of scaffold geometry. *Biomaterials Science*, *3*(2), 231–245. https://doi.org/10.1039/C4BM00291A

Zhou, Y., Tian, Y., & Zhang, M. (2024). Technical development and application of supercritical CO2 foaming technology in PCL foam production. *Scientific Reports*, *14*(1), 6825. https://doi.org/10.1038/s41598-024-57545-6

# 7 APPENDIX

## Image Analysis

Pore size analysis for sample 0a

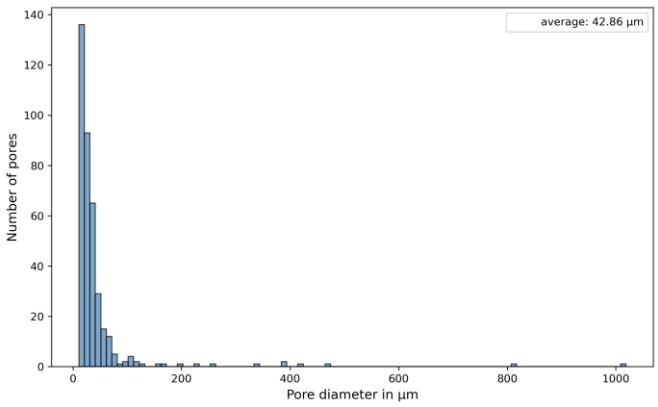


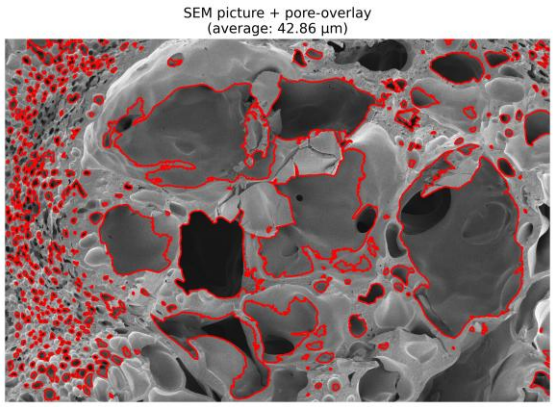


Pore size analysis for sample 0c

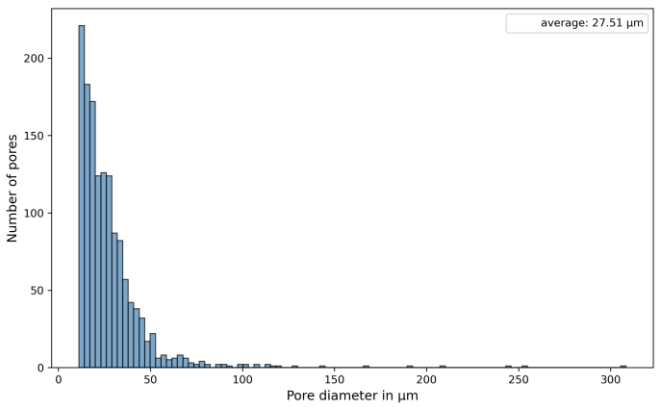


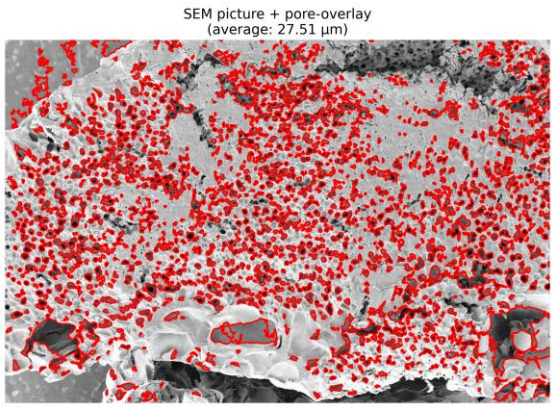

Pore size analysis for sample 1b

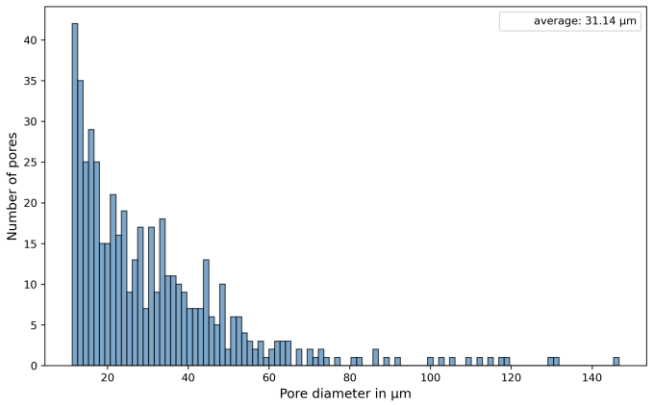


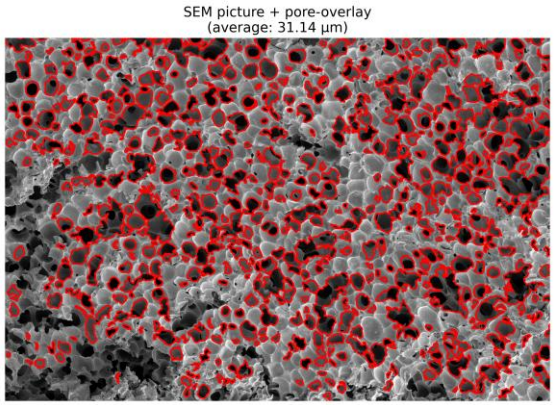


Pore size analysis for sample 2d

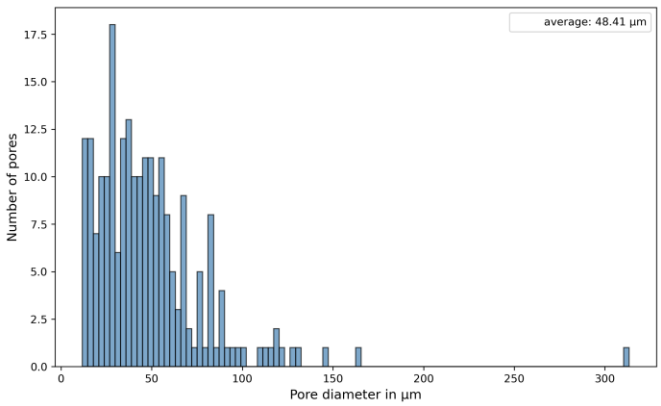


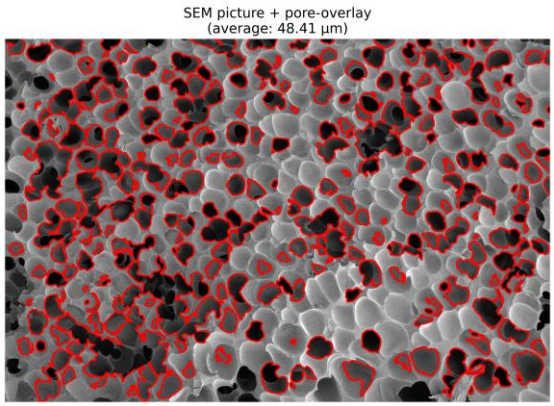


Pore size analysis for sample 4b

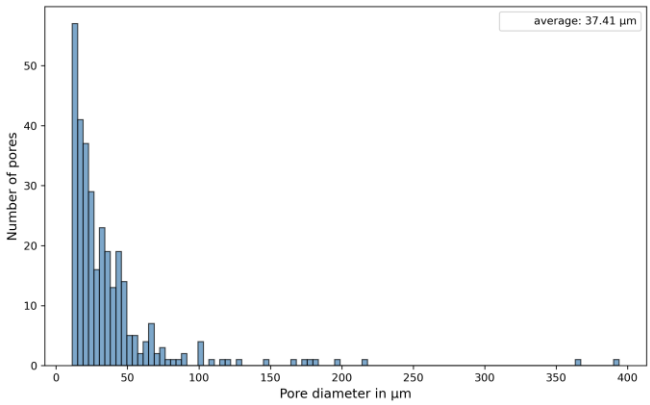


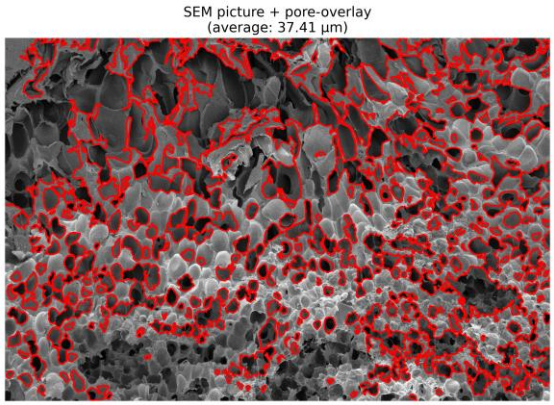

Pore size analysis for sample 6c

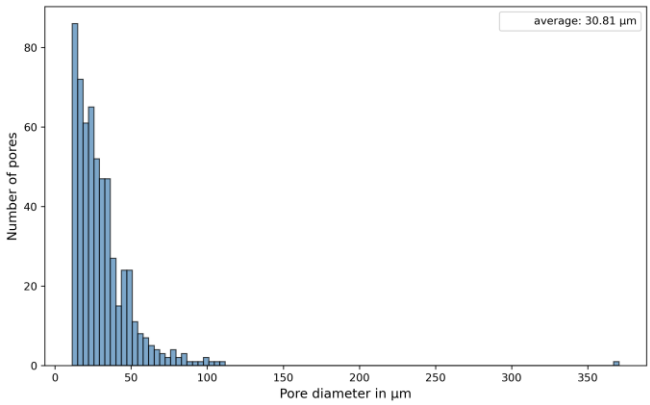


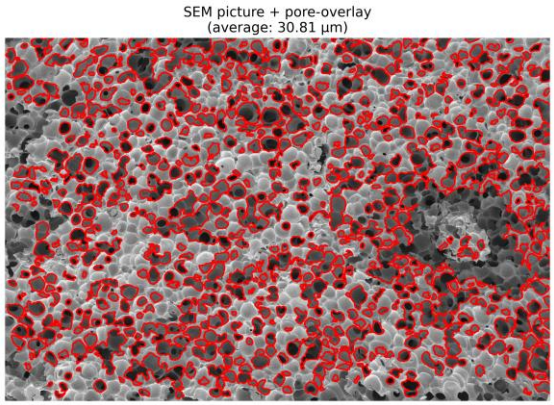


## Python Script

```
import numpy as np
import pandas as pd
import matplotlib.pyplot as plt
from skimage import io, color, filters, measure, morphology
from scipy import ndimage
from skimage.segmentation import watershed
import os
# ================================================
# Parameter
# ================================================
image_path = r"C:\Users\kilia\OneDrive\Dokumente\AAC_UCA\Foaming Paper\Coding\Particle size analysis\6c ext.tif"
pixel_size = 1000/484  # µm / Pixel
crop_height = 80  # Höhe des abzuschneidenden Bereichs unten (in Pixel)
output_dir = r"C:\Users\kilia\OneDrive\Dokumente\AAC_UCA\Foaming Paper\Coding\Particle size analysis\Export"
# ================================================
# Bild einlesen
# ================================================
image = io.imread(image_path)

# Bild unten abschneiden
image = image[:-crop_height, :]
# ================================================
# Export-Ordner erstellen
# ================================================
image_name = os.path.splitext(os.path.basename(image_path))[0]  # -> "1 int"
output_folder = os.path.join(output_dir, image_name)

# Ordner erstellen, falls nicht existiert
os.makedirs(output_folder, exist_ok=True)
# ================================================
# Vorverarbeitung
# ================================================
gray = color.rgb2gray(image) if image.ndim == 3 else image
blurred = filters.gaussian(gray, sigma=1.0)
# ================================================
# Segmentierung
```

```
# ================================================
thresh = filters.threshold_otsu(blurred)
binary = blurred < thresh
min_area_um2 = 100.0  # gewünsche Mindestfläche in µm²
min_size_pixels = min_area_um2 / (pixel_size**2)

cleaned = morphology.remove_small_objects(binary, min_size=int(min_size_pixels))
# ================================================
# Poren trennen
# ================================================
distance = ndimage.distance_transform_edt(cleaned)
markers = morphology.label(cleaned)
labels = watershed(-distance, markers, mask=cleaned)
# ================================================
# Eigenschaften extrahieren
# ================================================
props = measure.regionprops_table(labels, properties=['label', 'equivalent_diameter', 'eccentricity'])
df = pd.DataFrame(props)

df = pd.DataFrame(props)

# Nur runde Poren behalten:
df = df[df["eccentricity"] < 0.85]

# Durchmesser umrechnen
df["equivalent_diameter"] *= pixel_size
mean_diameter = df["equivalent_diameter"].mean()
print(f"\n🟢 average pore diameter: {mean_diameter:.2f} µm\n")
# ================================================
# Histogramm Werte
# ================================================
hist_values, bins = np.histogram(df["equivalent_diameter"], bins=100)

#print("Histogramm Werte (Anzahl Poren):")
#for i in range(len(hist_values)):
#    lower_bound = bins[i]
#    upper_bound = bins[i + 1]
#    count = hist_values[i]
#    print(f"{lower_bound:.2f}–{upper_bound:.2f} µm : {count}")
# ================================================
# Bild-Overlay
# ================================================
# Nur die gefilterten Labels
filtered_labels = df["label"].values

fig, ax = plt.subplots(figsize=(10, 10))
ax.imshow(image, cmap="gray")
boundaries = measure.find_contours(labels > 0, 0.5)

for boundary in boundaries:
    y, x = boundary[0]
    label_value = labels[int(y), int(x)]
    if label_value in filtered_labels:
        ax.plot(boundary[:, 1], boundary[:, 0], color='red', linewidth=1.5)
```

```
ax.set_title(f"SEM picture + pore-overlay\n(average: {mean_diameter:.2f} µm)", fontsize=14)
ax.axis("off")
plt.show()

# Overlay speichern
overlay_filename = "Poren_Overlay.png"
overlay_path = os.path.join(output_folder, overlay_filename)
fig.savefig(overlay_path, dpi=300, bbox_inches='tight')
print(f" Overlay gespeichert unter: {overlay_path}")

# ================================================
# Hochauflösendes Histogramm + Verlauf
# ================================================
plt.figure(figsize=(10, 6))
# Histogramm
count_values, bins, patches = plt.hist(df["equivalent_diameter"],
                                       bins=100,          # <-- mehr bins für feinere Auflösung
                                       edgecolor='black',
                                       color='steelblue',
                                       alpha=0.7)
# Durchschnittliche Porengröße
plt.axvline(mean_diameter, color='white', linestyle='', linewidth=2,
         label=f'average: {mean_diameter:.2f} µm')

# Verlauf (KDE) darüber legen
from scipy.stats import gaussian_kde
kde = gaussian_kde(df["equivalent_diameter"])
x_values = np.linspace(df["equivalent_diameter"].min(),
                       df["equivalent_diameter"].max(),
                       1000)  # feinere Auflösung
kde_values = kde(x_values)

# Anpassen an Höhe des Histogramms
kde_values = kde_values * max(count_values) / max(kde_values)

# Plotten
#plt.plot(x_values, kde_values, color='red', linewidth=2, label="KDE")

# Labels & Details
#plt.xscale("log")
plt.xlabel("Pore diameter in µm", fontsize=12)
plt.ylabel("Number of pores", fontsize=12)
#plt.title("Histogramm of the pore diameter", fontsize=14)
plt.legend()
plt.grid(False)
# Histogramm speichern
hist_filename = "Poren_Histogramm.png"
hist_path = os.path.join(output_folder, hist_filename)

# Speichern
plt.savefig(hist_path, dpi=300, bbox_inches='tight')
print(f" Histogramm gespeichert unter: {hist_path}")
plt.show()
```